universität wien

MASTERARBEIT / MASTER'S THESIS

Titel der Masterarbeit / Title of the Master's Thesis

Investigations into RTgill-W1 viability under various salinities, and evaluation of HPLC-QTOF-MS data of type C-prymnesins

verfasst von / submitted by

Romanos Argyriadis-Daras

angestrebter akademischer Grad / in partial fulfilment of the requirements for the degree of

Master of Science (MSc)

Wien, 2023 / Vienna 2023

Studienkennzahl lt. Studienblatt / degree programme code as it appears on the student record sheet:	**UA 066 863**
Studienrichtung lt. Studienblatt / degree programme as it appears on the student record sheet:	**Masterstudium Biologische Chemie**
Betreut von / Supervisor:	**Univ.-Prof. Dr. Doris Marko**

Acknowledgements

First and foremost, I would like to thank Univ.-Prof. Dr. Doris Marko for welcoming me into the Department of Food Chemistry and Toxicology and supervising my work for this master thesis. Thanks to her lectures and influence, I discovered my passion for toxicology so much so that it shaped the trajectory of my career.

Secondly, I would like to thank Dr. Elisabeth Varga, whose tutorage and co-supervision were instrumental in the creation of this work. Thanks to her experience and advice, I managed to hone my laboratory skills and evolve in ways I could never have on my own.

Furthermore, I would like to thank Hélène Christine Prause MSc for her kind support, helpful demeanor, and collegial spirit. Thanks to her and our discussions, I grew a deeper appreciation for the phenomenon of Harmful Algal Blooms.

I would be remiss if I did not express my deep gratitude for my colleagues “in the trenches” at the Department of Food Chemistry and Toxicology (most notable mentions: Carina Seidl, Cornelia Schmutz, Crepelle Plaza, Eszter Borsos, Dr. Francesco Crudo, Rebeka Früholz and many others) who welcomed me from the very first day with collegiality, cheerfulness and helpfulness and without whom my experience in the department would not be the same.

I would also like to personally thank all the friends and family who supported me not only during my work for the master thesis but the entire duration of my master studies. Most notably: Alexandros Skaribas, Alexia Tialiou, Andrea Pichler, Chrysoula Pipinis, Kleanthi Sifaki, Dimitris Kotasidis, Dr. Ioannis Kampatsikas, Julia Jürstel, Kanela Chatzimichail, Katharina Sigwald, Kostantinos Kanelopoulos, Kostantinos Chatzikyriakos, Margaret Rosenberg, Petros Spyridakis, Sofia Satanaki, and many others, who were with me through thick and thin and whose warm friendship, wise advice and generous support carried me through the challenges of these last years.

Special Thanks to:

Dipl. Eng. Athanasios Daras, my grandfather, who always inspired me by example to be a “homo universalis”.

In honor of my extraordinary mother: Dr. Phil. Vasiliki Dara

In memory of my loving Father: Dr. med. vet. Dimitrios Argyriadis

I would not be here without you all.

Table of contents

1 Introduction

In the last decades increasing attention has been drawn to the formation of Harmful Algal Blooms (HABs) and its environmental impact. HABs are a natural phenomenon in which one or a few algae in benthic waters form vast overgrowths with detrimental events to their local ecosystems, most notably massive fish kills. It has been clearly observed that HABs are increasing in both frequency and intensity so much so that both the scientific community and policy makers are called upon to combat this world-wide problem.

The "red/golden tides", as they are colloquially called, plague mostly near-shore marine waters, but also far-shore waters, rivers, and lakes. These events may result in massive fish kills, adverse economic effects, severe animal and human health hazards and even human deaths. Aquacultures of fish are especially vulnerable to HABs as the fish are enclosed and cannot escape to cleaner waters.

In fact, the consequences of the phenomenon can be so profound and far reaching, that Igarashi *et al.*, goes as far as to characterize HABs as a natural disaster equivalent to forest fires, earthquakes, and hurricanes. In contrast to such disasters though, HABs are clearly reinforced by what researchers' term as "cultural eutrophication". More worryingly, global warming is most likely to further exacerbate the problem and increase its frequency (Hallegraeff et al., 2004).

Notable examples would be the massive beaching of invertebrate species in 2016 in Cucao Bay in Chiloé island (Álvarez et al., 2019), and the most recent *Prymnesium parvum* (*P. parvum*) HAB in the river Oder in Poland/Germany in July/August 2022 (https://www.igb-berlin.de/news/verdacht-erhaertet-sich-algengift-einer-brackwasser-art-oderwasser-nachgewiesen).

It is very encouraging, that both the scientific community and policy makers recognize the severity of this problem and are investing time and resources to investigate the phenomenon and its causes, and research ways to prevent its occurrence and mitigate its effects on the environment and the communities. Furthermore, advances in science and engineering have allowed more sophisticated methods to be utilized in monitoring afflicted waters. The most notable example would be the use of satellite technologies.

Expanded empirical knowledge has contributed to wider knowledge of the problem and more coordinated efforts against it.

However, there are still many gaps in our understanding of the phenomenon. For instance, we do not fully comprehend the effect of stratification in the growth of HABs. Another elusive but nonetheless important factor are the effects of temperature to algae and their toxins. HABs are very site- and species-specific which complicates and often hinders the extrapolation of generalized theories. For example, toxins of one species might be photodegradable and toxins from another might be stable and capable of bioaccumulation. The required response to each situation would naturally vary significantly. Furthermore, all the different factors are interconnected making it impossible (or even erroneous) to study these factors in isolation. Despite the complicated and multifaceted nature of HABs, since they negatively affect their environment so profoundly, research efforts must be redoubled in order to fully elucidate the roots of this problem, its underlying mechanisms and most importantly, the most effective prevention and/or mitigation strategies.

2 Aims of the thesis

This master thesis, which was conducted as the culmination of studies at the University of Vienna for a master's degree in Biological Chemistry, took place within research efforts of the Department of Food Chemistry and Toxicology of the Faculty of Chemistry of the University of Vienna in HABs. The aim was firstly to successfully cultivate RTgill-W1 (fish gill cells from *Oncorhynchus mykiss*) in L-15 medium and secondly to investigate the effects of different salinities on the viability of RTgill-W1 cells as well as the viability of these cells in an L-15 medium completely free of chloride ions. Furthermore, as part of an overarching study in clade-specific toxins, a considerable part of this work was dedicated to the manual investigation of raw HPLC-QTOF-MS data provided from the institute.

The goal of the first part was to provide an L-15 medium for the RTgill-W1 cells which can be later used to study the effects of prymnesins (toxins created by *P. parvum*) and other toxins on these cells. Using cells like RTgill-W1 or others in toxicological assays is gaining more and more traction within the field as the scientific community decidedly tries to minimize the use of animal experiments. In essence, cells are used as proxies and substitutes for living organisms in adverse conditions. This line of experimentation has undeniably its limitations, as that which kills a cell is not necessarily that which kills an organism, but it is ideal for initial studies into the adverse effects of substances.

This data will in turn provide the basis for an L-15 medium for RTgill-W1 cells to which algal toxins will be added and investigated. Salinity, just like temperature, flow currents, and light intensity, is one of the factors which possibly affects HAB formation. Counterintuitively the conditions which support, or stress algae are not necessarily the same which support the formation of HABs or their toxicity. In fact, HAB formation and toxin production are most probably stress responses. Therefore, studying toxin effects in optimal or varying salinities could offer further insights into the underlying mechanisms.

Furthermore, since prymnesins and other toxins possibly interact with ion channels on the surfaces of the target cells, experimenting with media devoid of Cl ions could further be used to understand the mechanisms and modes of action of these toxins.

The goal of the manual investigation of the raw HPLC-QTOF-MS data was to establish, as reliably as possible, the presence or absence of slightly different prymnesins in extracts of *P. parvum*. Whilst originally only two prymnesins were discovered by Igarashi *et al.*, in the 90s, the actual chemical plurality of these toxins is extraordinary (Binzer et al., 2019; Igarashi et al., 1999; Rasmussen et al., 2016). This diversity of prymnesins is brought forth by minor alterations in the degrees of chlorination, saturation and number of sugar units whilst keeping the general profile of the prymnesins consistent. Interestingly, it seems that the toxins which the various subspecies of *P. parvum* create are clade-specific with each one creating only one specific type of prymnesin and never a combination of types (Binzer et al., 2019). Investigating the mixtures of prymnesins could provide insights into questions regarding what role evolutionary pressures had in the biosynthetic apparatus. Furthermore, a more practical application in the future could be the identification of subspecies of *P. parvum* based on the prymnesin content (chemotyping). Coastal resource managers could then identify more reliably and specifically what algae are forming the specific HAB they are dealing with and employ more suitable mitigation strategies.

In summary, this study aimed to provide insights into aspects relevant to HABs and the mode of action of their toxins as part of overarching research efforts into HABs through the lens of toxicology.

3 Theoretical background

3.1 Harmful algal blooms (HABs)

Harmful algal blooms could be defined as high biomass overgrowths of microalgal populations in marine, coastal, open ocean, brackish and fresh waters (Anderson et al., 2012; Marampouti et al., 2021). These events can often take place in relatively protected areas such as gulfs, but it is not uncommon to take place in far-shore waters. In fact, Wang *et al.*, collected HAB forming algae as far as 200 km away from the coast in the large golf of the yellow sea (Wang et al., 2021). These microalgae might be important parts of their respective ecosystems when held in balance, but under certain conditions, they proliferate excessively and form layers on the surface of waters. In such cases they might produce toxins, foams, or deplete the available oxygen by overconsumption. In this way they damage local ecosystems, aquatic and surrounding life, with massive fish-kills, shellfish-kills as the most notorious and characteristic negative effects. The mechanism underlying the formation of HABs are not always understood and are often species-specific, further complicating the unified study and extrapolation of mechanisms for this phenomenon (Anderson et al., 2012).

Colloquially, this phenomenon is called “red tides” or “golden tides” depending on the species of algae which form the HAB. This term however is an oversimplification since it includes cases of simple discoloration of water without necessarily the involvement of excreted toxins and relative harmlessness. In contrast the term HABs is more encompassing and has therefore been the chosen term to encompass the phenomenon (Anderson et al., 2012).

HABs can bring forth severe negative effects on local ecosystems, human health, and economies. The literature unanimously reports that the incidence of HAB outbreaks is becoming more frequent, more pronounced, and more persistent every year with some notable examples being exceptionally alarming (Table 1). The counterargument exists, that researchers and resource managers are far more interested and sensitive to the problem than previously and therefore more incidents are being detected and recorded. Also, our ability to monitor and track HABs is improving and becoming more sensitive.

Whichever the case, affirmative action must be taken in order to prevent or at least mitigate HABs and their consequences.

Table 1: List of historic examples

date	location	HAB forming species	consequences	reference
1974	Tvärminne Archipelago	*Chrysochromulina. birgeri*	no mortality reported	(Edvardsen and Paasche, 1998)
1987	Guatemala	*Gonyaulacoid dinoflagellates*	PSP outbreak:	(Manganelli, 2016)
1987	Canada	*Nitzschia pungens*	250 patients, 3 fatalities	(Manganelli, 2016)
1988	Skagerrak/Kattegat, Norway/Sweden	*Chrysochromulina polylepis*	High mortality of wide range of organisms	(Edvardsen and Paasche, 1998)
1991	Zealand Lake, Denmark	*Chrysochromulin parva*	fish kills	(Edvardsen and Paasche, 1998)
1992	Kirkfjärden Lake, Sweden	Chrysochromulin parva, *Prymnesium. parvum*	fish kills	(Edvardsen and Paasche, 1998)
2005	Genoa; Italy	*Ostreopsis. ovata*	200 patients after aerosol exposure	(Manganelli, 2016)
2006	Florida, USA	*Karenia brevis*	20 reported cases of NSP	(Arnich et al., 2021)
2007	Granbury Lake, Texas, USA	*Prymnesium parvum*	massive fish kills	(Brooks et al., 2011)
2016	Cucao Bay; Chiloé	*Alexandrium catanella*	Massive beaching of invertebrate species	(Álvarez et al., 2019)
2017	Thessaloniki; Greece	*Noctiluca scintillans*	Persistent red tide	https://greekreporter.com/2018/11/05/thessalonikis-infamous-red-tide-is-back-and-it-may-stay-awhile/
2022	River Oda; Germany	*Prymnesium parvum*	Massive fish kills	https://www.igb-berlin.de/news/verdacht-erhaertet-sich-algengift-einer-brackwasser-art-oderwasser-nachgewiesen

Depicted in the table are a few historic examples of HAB formation which could be recorded and which were consequential for their environment. Systematic recording of HAB occurrences has only begun in the last decades and depending on the location it might still be incomplete. A lot of historical data has been lost and to this author's knowledge no complete comprehensive list of world-wide HAB occurrences exists yet.

HAB forming microalgae could be organized according to whether they simply discolor the waters, actually form toxins or not and lastly whether they are harmful to humans even despite the biosynthesis of toxins (Hallegraeff et al., 2004). In cases in which

human health can be endangered, this can come to be either through direct skin contact, primary or secondary digestion or even inhalation of aerosols.

The key characteristic of HABs is that they, as Anderson *et al.*, 2012 formulate: "*a complex oceanographic phenomenon which requires multidisciplinary study*". It will require coordinated efforts in both local and international scales, from both scientific and municipal professionals to fully address and combat this phenomenon which more and more has impacts analog to natural disasters like earthquakes and floods.

3.2 Bloom dynamics of HABs

The formation and establishment of HABs is a multifactorial and complex problem (Anderson et al., 2012). Counterintuitively and even though eutrophication plays a key role in HAB development, HAB formations initiate as a response to stress factors (Granéli et al., 2012) alongside a plethora of environmental factors (Brooks et al., 2011). At first algal cells start proliferating much faster than they die and establish themselves in the ecosystem. These cells, have either been there from the start (hidden flora theory) or have been introduced into the ecosystem. Cyst formations, germination, and tides play key roles in impinging on new ecosystems. In addition to that, it is suspected that floating plastic also contributes to the expansion of HAB forming species (Marampouti et al., 2021).

There can be a multitude of causative factors determining the extent of HABs and their characteristics like biomass, toxicity etc. (Anderson et al., 2012). HABs are very site-specific as well as species-specific making it very challenging to establish commonalities and ubiquitous trends (Anderson et al., 2012).

The toxins which are associated with HAB-forming algae are also very wide-ranging and their effects can be severe both for the environment and for human health (Table 2). Collecting data on these toxins and their effects can be vital in understanding them. It is imperative that our understanding is expanded so that we may prevent and mitigate the effects of such toxins.

Table 2: Notable examples of HAB-associated toxins

Toxins	Microalgae	Effects
Azaspiracid (AZA) group	*Azadinium spinosum, Azadinium spp., Amphidoma spp.*	Azaspiracid shellfish poisoning (AZP)
Okadaic Acid (OA) group	*Dinophysis spp., Dinophysis fortii*	Diarrhetic shellfish poisoning (DSP)
Dinophysis toxins (DTXs)	*Prorocentrum lima*	
Pectenotoxin (PTX) group	*Dinophysis spp.*	Hepatotoxic (?)
Yessotoxin (YTX) group	*Protoceratium reticulatum, Lingulodinium polyedrum, Gonyaulax spinifera*	Cardiotoxic (?)
Saxitoxin (STX) group	*Alexandrium spp., Gymnodinium spp., Pyridinum spp.*	Paralytic shellfish poisoning (PSP)
Domoic acid (DA) group	*Pseudo-nitzschia spp.*	Amnesic shellfish poisoning (asp) or domoic acid poisoning (DAP)
Brevetoxin group	*Karenia brevis*	Neurotoxic shellfish poisoning (NSP)
Ciguatoxins	*Gambierdiscus toxicus*	Ciguatera fish poisoning (CFP)
Maitotoxins	*Gambierdiscus spp.*	
Cyclic imines	*Alexandrium ostenfeldii/peruvianum, Karenia selliformis, Vulcanodinium rugosum, Prorocentrum spp.*	Neurotoxic
Palytoxin (PlTX) group	*Ostreopsis cf. ovata*	Neurotoxic
Ovatoxin (OvTX) group	*Ostreopsis cf. ovata*	Unknown
Ostreocin (Ost)	*Ostreopsis siamensis*	Neurotoxic

This table depicts a few notable examples of HAB-forming algae, their associated toxins, and their effects primarily on human/animal health but is not all-encompassing as there are a myriad of HAB-forming algae and associated toxins (Manganelli, 2016).

Once a HAB has been initiated, its range is determined by physical controls like the temperature, currents, behavior of the fish, weather phenomena, degree of irradiance. Many key factors contribute to the extent of the duration of the HAB in an ecosystem. Sewage effluents is a prime example, as it has been shown that diversion of sewage distinctly decreased the perseverance of the HAB in the waters (Anderson et al., 2012).

Another interesting factor is the effect which bacteria can have on HABs and their toxicity. When it comes to the relationships between the HAB-forming algae and present bacteria, both mutualistic and impeding relationships have been observed depending on the species of the algae. In some cases, bacteria have been observed to control HABs and in others to support them and even increase their toxicity (Anderson et al., 2012; Tang et al., 2015). This is a prime example regarding the species-specificity of the phenomenon.

HABs finally decline once again through a combination of multiple factors, like introduction of fresh water from currents. In general, the mechanisms which underly the formation of HABs still need further research to be elucidated.

3.3 Bloom dynamics *P. parvum*

The mechanisms behind bloom growth of *P. parvum*, are still a matter of intense research and not fully elucidated. Understanding the links between events is hindered by facts which might seem contradictory. Furthermore *P. parvum* tends to bloom in locations which in themselves are hard to adequately monitor and observe (Brooks et al., 2011).

Contrary to what one would expect, *P. parvum* blooms occur under conditions which are not optimal for reproductive growth of the alga and on the contrary actually stress the cells. This in turn promotes the production of toxins from *P. parvum* which impede competitor species and hinder grazers (Granéli et al., 2012). This results in a characteristic situation in which surrounding populations drop whilst *P. parvum* perseveres. To add to this, at this stage, fish kills are maximized, and possible nourishment sources are becoming available. Furthermore *P. parvum* is a mixotrophic organism with two chloroplasts per cell and capable of photosynthesis. Its quality as a

mixotrophic organism (aka capable of photosynthesis and osmotrophy) provides it with a strong competitive advantage (Granéli et al., 2012).

In this series of events, in which more nutrients are becoming obtainable by means of "killing the competition", the HAB event is ultimately being propagated by self-sustaining circles and this is one explanation as to why this phenomenon can last for months. It is also noteworthy that the abundance of nutrients is in itself a stress-inducing parameter which causes *P. parvum* to create its toxins, which are collectively known as prymnesins. It has been theorized, that the production of prymnesins, these large ladder-like polyethers, is one way of storing excess carbon (Granéli et al., 2012).

Eventually the bloom declines. Regrettably the reasons are still not understood completely and in typical fashion to this phenomenon, the data can be contradictory. One possible solution and explanation are the water flows. Another is the depletion of nutrients and eventual death of *P. parvum* cells. The next steps in HABs research will require a detail-oriented and possibly in real-time collection of data relative to the bloom.(Brooks et al., 2011; Granéli et al., 2012)

3.4 Nutrient imbalance and eutrophication

Perhaps the most obvious factor for the increased occurrence of HABs is human-driven eutrophication. There is clear indication that HAB formation is being supported by eutrophication. Chronic or episodic eutrophication changes nutrient ratios in the ecosystems and thus favor certain species of algae over other which then severely outgrow their competitors (Hallegraeff et al., 2004; Ignatiades and Gotsis-Skretas, 2010).

It is important to mention that originally the term eutrophication described the natural phenomenon of increase in nutrient capacity in bodies of water but now mostly refers to the human-driven aka cultural eutrophication. Bodies of water like lakes, rivers, near-shore waters may receive large quantities of agricultural, industrial, and sewage effluents providing far more nutrients to an ecosystem than it needs to stay balanced and thus HAB formation may increase progressively with nutrification (Hallegraeff et al., 2004).

Interestingly though, the relation between eutrophication and HAB formation and toxicity is more complicated than one might intuit. Whilst eutrophication is a driving factor behind the phenomenon, research shows that it is nutrient imbalance, predominantly N and P, which drives the formation and toxicity of HABs (Davidson et al., 2012). More specifically, the proportional availability of nutrients to the algae together with dynamic factors like competition, grazers and hydraulics shape the extent of the phenomenon (Anderson et al., 2012).

One key aspect is the effect of sewage effluents. Mixotrophic species, like *P. parvum,* which employ allelochemical toxins, can make use of both the organic and the inorganic parts of sewage nutrients to grow. Research has shown that removing the addition of sewage effluents drastically curbed the formation of HABs (Lindehoff et al., 2009).

For this study's algae of interest, *P. parvum,* there seems to be an interesting phenomenon regarding eutrophication which Brooks *et al.,* 2011 fittingly termed "the nutrient supply paradox". According to research, even moderate eutrophication can support the overgrowth of a *P. parvum* bloom which is controlled by the supply of critical nutrients like P and N as well as the salinity of the waters and the hydraulics. When the critical nutrients have been depleted it is then that *P. parvum* HABs increase in toxicity (Figure 1). Thus, by killing competitors they can reach nutrients unencumbered by competition or even prey on other organisms (algae, bacteria and even fish) to sustain their growth. It is for this reason, that, counterintuitively treatment of affected areas with ammonium has shown to decrease the toxicity of the *P. parvum* HAB enough for other algae to regain hold in the ecosystem and start bringing it back to a balanced state (Brooks et al., 2011).

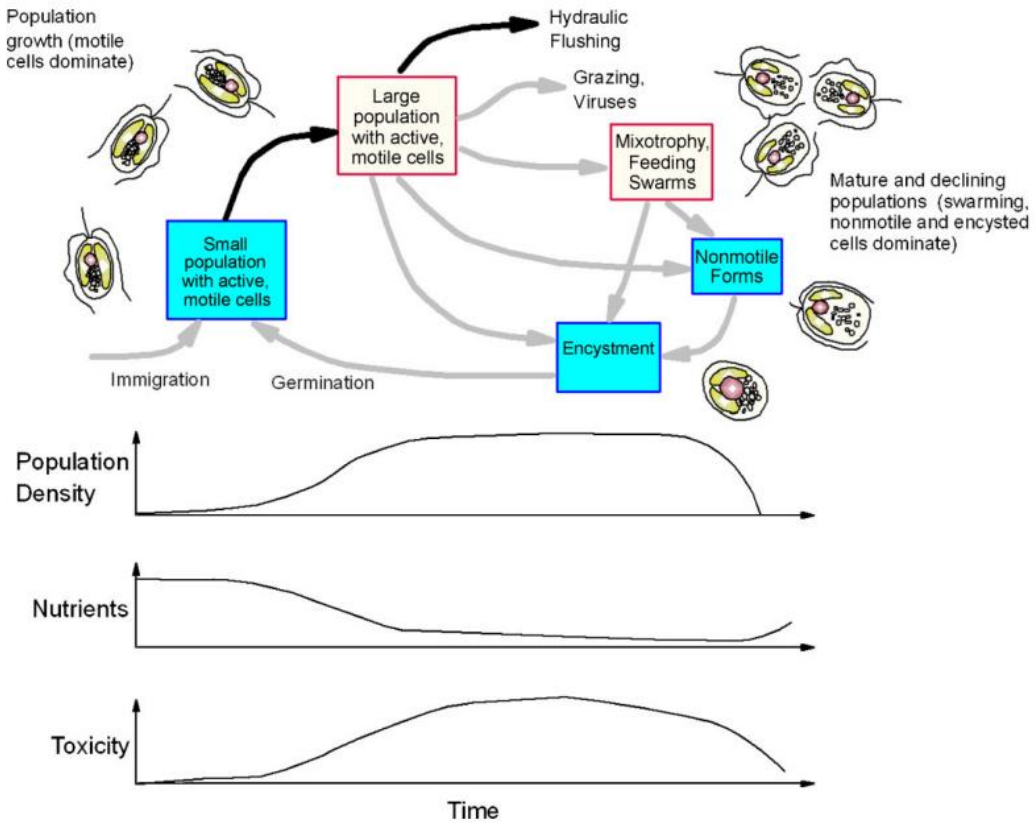

Figure 1: Depiction of bloom dynamics of *Prymnesium parvum* HAB
General representation of the life cycle of *P. parvum.* The red boxes indicate toxic stages while the blue boxes indicate non-toxic stages. The black arrows signify important transitions within the life cycle which are important to the toxicity of the bloom. Gray arrows indicate transitions which are still less understood. Drawn cell forms on the left depict motile individual cells which are typical of growing populations. Drawn cell forms on the right depict more stationary and mixotrophic forms. The graphs depict the dynamics of population density, nutrient availability, and HAB-mediated toxicity during a typical fish killing bloom (Brooks et al., 2011).

This highlights the intricacy and multifactorial nature of the problem. Even more due to the species-specificity mitigation strategies like the one described might not work for other species or even for *P. parvum* under different conditions of nutrient availability. This underlines the need for a deeper understanding of the inner workings of the mechanisms and the interplay of all factors.

3.5 Economic consequences

HABs can severely impact local economies, especially those which are dependent on marine resources and tourism (e.g., island communities). It is projected that HAB events can cause losses in the millions of dollars in multiple ways (Anderson et al., 2000; Brooks et al., 2011; Nikolaidis et al., 2005).

These economic losses can be summarily grouped into four general categories: 1) Public health impacts, 2) commercial fishery impacts (including shellfish), 3) recreation and tourism impacts, 4) monitoring and management costs (Anderson et al., 2000). These four categories are not encompassing on the entirety of the negative effects on the environment, as it could be argued that the consequences of these would exceptionally far reaching and intricately complex to adequately foresee. Accordingly, it must be stressed that there is an ethical responsibility to not turn a blind eye to all consequences which are not human-centric and actively explore them.

Starting with the economic impact due to public health it must be taken into account that no estimate will ever adequately depict the discomfort caused by adverse health effects or even the heart ache caused by loss of life. Both of these can occur in cases of HABs as the latter can release dangerous toxins which impact human health. There are toxins which can cause skin irritation by simple contact or even be inhaled in the form of aerosols carried by onshore winds. An example of such a case are brevetoxins (Pierce et al., 2005) which are lipophilic marine biotoxins produced by the dinoflagellate *Karenia brevis* (Arnich et al., 2021). Poisonings can also occur with the consumption of fish/shellfish carrying toxins, which is called “secondary poisoning”. One parameter which should also be considered are the workhours due to sick absence compounded by the costs of hospitalization and care (Anderson et al., 2000).

The most characteristic and prevalent is the damage done to aquaculture. In the case of caged fishes cultivated for nourishment, the fish cannot swim away from toxic waters in contrast to their wild counterparts (Hallegraeff et al., 2004). In this case the fish either die or even worse the toxins are eaten by the consumers to catastrophic results. Similar to fish are the shellfish-farms which can suffer similar fates (Theodorou et al., 2020). In both cases investments of capital and many labor hours are irrevocably lost. Even industries which rely on wild fish or natural, pockets of shellfish are harmed by HABs because fewer locations can be used and untapped, potential ones are lost (Anderson et al., 2000).

Tourism, recreational activities, sea sports, etc., are also negatively impacted by HABs. For some areas and some communities these might by the primary or even singular sources of income. Taking away or damaging the aesthetics of these places might be catastrophic for the people living there.

Perhaps the most interesting economic burden is the cost for monitoring and managing HAB activities. Considering that the frequency and potency of HAB events steadily increases (Hallegraeff et al., 2004; Igarashi et al., 1999), the costs and needs for monitoring this problem will only increase in value and importance. Interestingly though, expenses made in this category diminish the costs of the other categories (Anderson et al., 2000) since they help prevent or mitigate the adverse effects of HABs and their toxins. As our understanding of the phenomenon increases, these methods will naturally become more cost-effective, reliable, and finally ubiquitous.

As mentioned, there are several challenges for the correct and accurate estimation of economic losses caused by HABs. Even more, up until recently, coastal resource managers were not always prepared to create accurate estimates about economic losses. Therefore, there is a clear lack of historic data in this regard and moving forward more emphasis should be placed on the accurate collection of quantitative data about such losses (Anderson et al., 2000). It is also noteworthy that just as the frequency of HABs has increased, so too has the attention of scientists and policy makers. It very possible, that more HABs are being detected because communities are more interested and more capable in detecting them (Anderson et al., 2012).

Lastly it is this authors belief that although many aspects can and should be quantitated, it is also not really feasible to "place a dollar sign" on quality of life. A good anecdotal example is that in the city of Thessaloniki in Greece, a port city within a natural gulf, less than two generations ago it was considered the most natural and everyday thing to swim in the waters of the harbor. At the moment the situation has been reversed, as it is commonplace thinking that one never steps into these same waters out of health concerns. In the span of less than 100 years, a major quality of life asset has been denied to a community in ways that could never be calculated. This phenomenon is obviously not unique to Thessaloniki, but it underlines the need to elucidate the underlying mechanisms of the problem and create prevention and mitigation strategies.

3.6 *Prymnesium parvum*

Prymnesium parvum is an alga belonging to the division of Haptophyta (Granéli et al., 2012; Lassus et al., 2016). It was first described in England in 1937 by Carter *et al.*, (Lutz-Carrillo et al., 2010) and it is one of the most important allelopathic microalgae associated with fish kills worldwide and quite possibly one of the best studied (Binzer et al., 2019; Medić et al., 2022). The cells of this species have a length of 8-16 µm and a width of 4-10 µm, they are covered with two layers plate-like organic scales which are considered species-specific and are therefore used for species identification (Granéli et al., 2012). Observation of the scales under an electron microscope reveals that the scales have a radial pattern on their proximal face, concentric rings on their distal face and a broad and inflexed rim of the scales in the inner layer (Larsen and Medlin, 1997). Characteristically *P. parvum* has two flagella which are inserted subapically (Larsen and Medlin, 1997) and a haptonema which these single-celled algae use to attach themselves on surfaces or aid them in the capture of food particles (Granéli et al., 2012).

P. parvum contains two brown chloroplast thanks to which HABs of *P. parvum* have a characteristic brown appearance (Figure 2). It is a mixotrophic species (Granéli et al., 2012), which means, that it can both photosynthesize as well as use surrounding nutrients as a food source. This makes it an exceptionally resilient alga and HABs of *P. parvum* can be exceptionally persistent. Additionally, in contrast to some other HAB-forming species, *P. parvum* blooms are exceptionally hard to predict (Brooks et al., 2011). HAB events from *P. parvum* are associated with massive fish kills in large part due to the toxins they create and excrete in their surroundings (la Claire et al., 2015).

Figure 2: Phase contrast microscope image of *Prymnesium parvum*. *P. parvum* as shown in the picture is a single-celled, planktonic eukaryote with ellipsoid shape. Its length ranges from 8 to 16 µm and its width ranges from 4 to 10 µm. It possesses two chloroplast which give it the characteristic brown/golden color. It is bi-flagellated and the prominent haptonema is a hallmark characteristic of the taxa which belongs to the class Haptophyceae.(Roelke et al., 2016)

3.7 Prymnesins

The special toxins produced by the haptophyte *P. parvum* are collectively known as prymnesins. These are large ladder-frame polyethers (Binzer et al., 2019). Prymnesins are very potent hemolytic toxins which have allelopathic (killing of other algae) and ichthyotoxic (killing of fish) effects so severe as to cause massive fish kills (Binzer et al., 2019; Manning and La Claire, 2013). Igarashi *et al.*, characterize them as nothing less than a "natural catastrophe (Igarashi et al., 1999). Unlike other toxins, which might target specific biological structures, like for instance the nerve system, prymnesins have a non-specific membrane action causing lysis which is what gives them their allelopathic function (Edvardsen and Paasche, 1998). In the case of fish, prymnesins function as "gill irritants" They increase the permeability of the gills they come in contact further increasing their vulnerability to subsequent toxin exposure. The cells of the gills are lysed, and the gills are destroyed and/or clogged (Svendsen et al., 2018). It is suspected that the primary amine in the hydrophobic part of the prymnesin plays a key role in the mechanism of action of the toxin (James et al., 2011). Additionally anti-coagulant properties have also been proposed for the action of prymnesins. The fish suffer irrevocable gill damage which results in respiratory failure and death. Characteristically, fish exposed to prymnesins rapidly show symptoms and distressing behavior (increased coughing ratio, up-side-down-swimming) and try to swim to clean waters (Svendsen et al., 2018).

Originally, only two prymnesins, named prymnesin-1 and prymnesin-2 (PRM1, PRM2), (Figure 3, Table 3) were isolated and their structures elucidated by Igarashi *et al.*, (Igarashi et al., 1999, 1996). At the time isolating these toxins was very arduous due to their complexity and small concentration in culture samples (which was nonetheless toxicologically relevant). Isolation and enrichment procured two pale yellow substances, which were hard to resolubilize and therefore further complicated investigations (like NMR). Igarashi *et al.*, succeeded in explicating their chemical structures by a combination of several methods like, mass spectrometry, chemical tests (ninhydrin test), and most notably: multiple NMR experiments in different solutions. Cultivating *P. parvum* in the presence of $Na_2{}^{13}CO_3$ facilitated the C-NMR studies with great success. The use of X-Ray analysis was also key because it confirmed the

presence of chloride and nitrogen atoms in the structure which was an unusual find in phytotoxins (Igarashi et al., 1999).

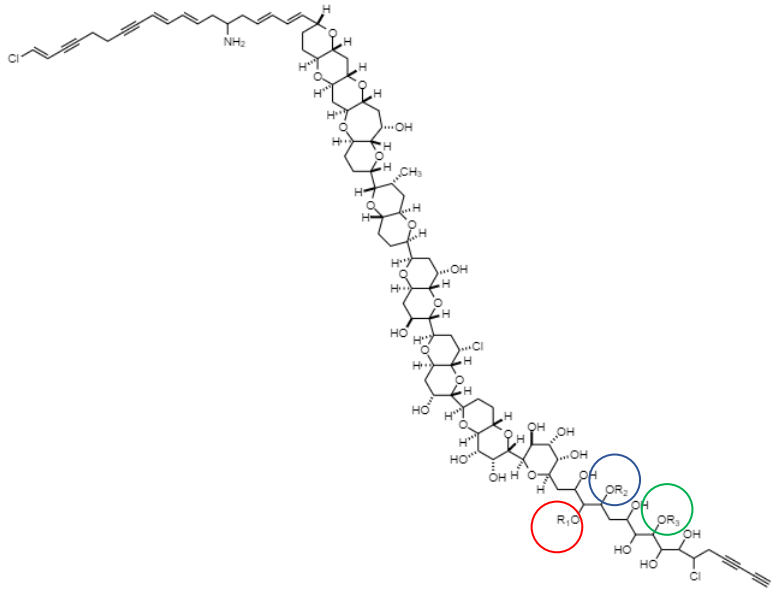

Figure 3: Prymnesin-1/2 structures (Igarashi et al., 1999, 1996).
Chemical structure of prymnesin 1 & 2 as discovered by (Igarashi et al., 1999). The two prymnesins differentiate in the substitution groups R1, R2 and R3 which in each case are different sugar rings. In the original research it was considered that these were the only two kinds of prymnesins, but it was later discovered that the prymnesins were a far more plural group of toxins.

Table 3: Prymnesin 1 & 2 side-groups (Igarashi et al., 1999, 1996).

Prymnesin 1	Prymnesin 2
R1 = α-D-ribofuranose 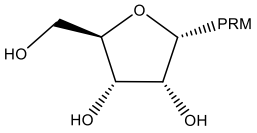	R1 = α-L-xylofuranose 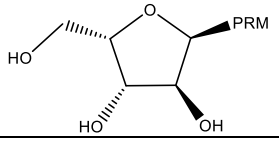
R2 = α-L-arabinopyranose 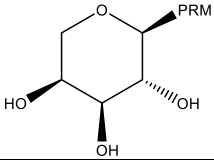	R2 = H
R3 = β-D-galactofuranose 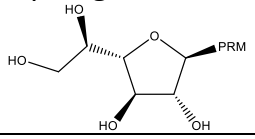	R3 = H

On the left of the table are depictions of the three sugar rings which are present in the formula of prymnesin-1 and on the right is the sugar ring present in prymnesin-2. PRM indicates the main body of prymnesin The R1 position is in fact the same for both prymnesins and the sugar ring is what differentiates them. Interestingly, the molecular formula of the R1 substitute is the same for both prymnesin-1 and prymnesin-2 but the difference lies in their stereochemistry. The consistency of this minor differentiation raises interesting questions regarding the biosynthesis of these toxins inside the cells as well as the evolutionary history behind them.

It became clear that there were more prymnesins than the two originally proposed (James et al., 2011), and after two decades, Rasmussen *et al.*, discovered that the chemical diversity of the prymnesins was in fact much larger than anticipated and after a series of investigations concluded that there are no less than three distinct groups of prymnesins based on the length of their backbone structure. NMR studies were instrumental in investigating the structures of the three types of prymnesin backbones (Rasmussen et al., 2016). Phylogenetic studies based on internal transcriber sequences (ITS) also revealed an extraordinary plurality of subspecies (Figure 4). It could also be confirmed that each subspecies of *P. parvum* can only produce prymnesins of one type (A-, B-, or C-) and never a combination of them (Binzer et al., 2019).

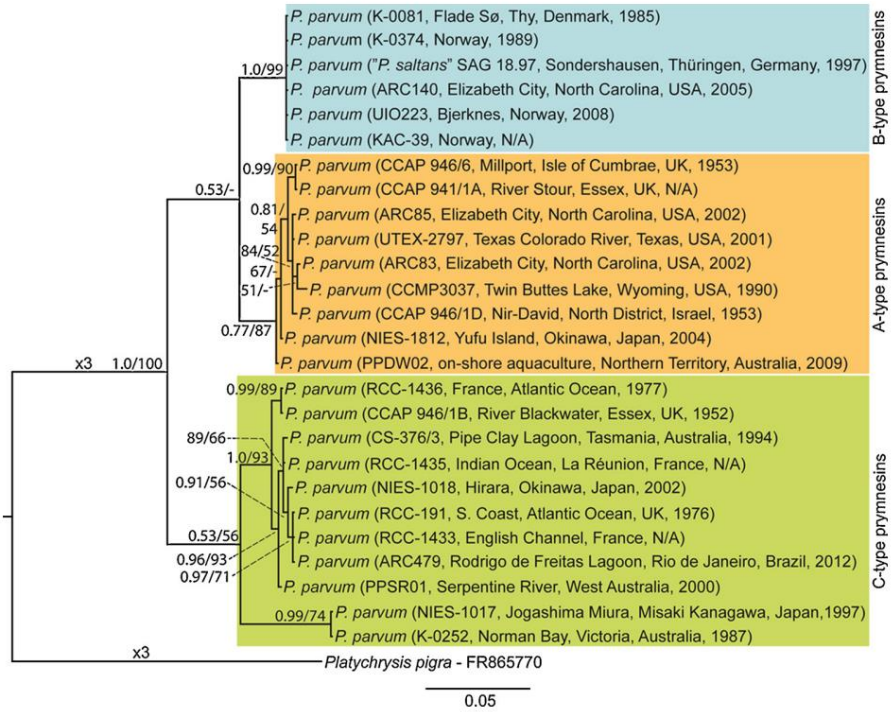

Figure 4: Phylogenetic tree of *P. parvum* strains.
The phylogenetic relationships were elucidated based on the internal transcribed spacer regions (ITS-1 and ITS-2) of the nuclear ribosomal cistron. These are characterized by high sequence variability and are therefore prime markers for analyses of closely related taxa. In this depiction the branch in blue color are the strains producing exclusively B-type prymnesins, while the orange and green branches are the ones producing A- and C- type prymnesins respectively. In the part concerning the manual investigation of HPLC-QTOF-MS raw data in the present thesis the strains belong to the green branch (Binzer et al., 2019).

In all afore mentioned studies and experiments, the biggest and as of date still unresolved problem is the absence of commercially available standards (Svenssen et al., 2019). Absence of standards hems efforts to reliably measure prymnesin

concentrations and this in turn deters more complex investigations (e.g., toxicity of prymnesin degradation products). So far prymnesin concentrations could only be measured either semi-quantitatively or at best indirectly by tagging the primary amine with fluorescent substances (Svenssen et al., 2019).

One very interesting question is the effect of sunlight on the stability of prymnesins. James *et al.,* 2011 conducted experiments with prymnesin filtrates (solutions free of algae). They observed that filtrates exposed to sunlight lost their toxicity to fish while filtrates kept in the dark maintained it. James *et al.,* 2011 explain that when structures feature double bonds and aromatic systems, these are vulnerable to photodegradation because their internal energy states correspond to the energy levels from the incoming light. Furthermore James *et al.,* 2011 distinguish between direct and indirect photolysis. In direct photolysis photons interact with molecular bonds and break them, whereas in indirect photolysis photons are absorbed by dissolved organic matter (DOM) which in turn form reactive species and these degrade the toxins. The filtrate experiments point towards the former mechanism but James *et al.,* 2011 could not definitively prove one over the other. Elucidating photodegradation for prymnesins is of crucial importance because it can become the cornerstone for mitigation strategies against *P. parvum* HABs (Granéli et al., 2012; Taylor et al., 2021).

This extraordinary diversity of the prymnesins raises interesting questions about their evolutionary history and what drove the alterations of the biosynthetic machinery. Furthermore, these molecules bear a definite resemblance to toxins produced from other algae. Although conventional wisdom would expect for the algae to be taxed in creating these supersized molecules, experiments have actually shown the opposite (Binzer et al., 2020). This would support the theory that prymnesins are in fact a way for the algal cell to store excess amounts of carbon (Granéli et al., 2012). The subject harbors many complexities which co-occur to give in the end the catastrophic results HABs and massive fish kills. Untangling all these factors will require further and deeper research but is nonetheless crucial in order to combat this problem.

3.8 Chemotaxonomy

Chemotaxonomy is defined as "the classification of plants and animals based on similarities and differences in biochemical composition" (taken from https://www.merriam-webster.com/dictionary/chemotaxonomy).

Within the context of HAB studies and mitigation, this could be applied by collecting water samples from locations of interest and endeavoring to identify the algae by the toxins or by-products it produces and releases in its environment. Considering the very expanded chemical diversities in minute differences in the chemical structure of the toxins (see prymnesins part of this study) a unique identification method arises. By pairing the exact chemical structure with the known algae, this could be later followed in reverse to establish the identity of an algae by analyzing the substances it has excreted.

As already mentioned, the phenomenon of HAB formation and its associated toxins is an extremely species-specific event. It follows that mitigation strategies and water treatment practices will be equally specific and often counter-intuitive (as is the case of introducing nutrients to decrease the algae-mediated toxicity). Therefore, rapid, and reliable identification of the main algae which cause the HAB event is of outmost importance.

In this avenue, chemotaxonomy can assume a key position in identifying the consistency of a particular HAB faster and more cost-effectively than traditional methods. Thanks to the increasing sensitivity of the analyzers, it might even be possible to make fingerprint identifications leading to highly tailored and better optimized mitigation strategies. Furthermore, as many researchers underline in the literature, there is a remarkably high need for on-line monitoring of near-shore waters (Anderson et al., 2012; Hallegraeff et al., 2004; Wang et al., 2021). Methods which identify HABs by analyzing the toxins they excrete in their surrounding are uniquely suitable for this role more so than identification based on genetics or microscopy.

Even more, chemotaxonomic methods are far less likely to make mistakes of false identification as might be the case with microscopic methods. In the words of Anderson *et al.*, 2012: "looking alike does not necessarily mean genetically identical and looking

different does not mean genetically isolated" (Anderson et al., 2012). Therefore, chemotaxonomic methods can be more reliable.

Lastly, chemotaxonomic methods are more practical and approachable. Marine resource managers could more readily conduct or outsource an investigation which is based on chemical properties and could be conducted with e.g., a HPLC-MS rather than the more tedious and expertise-intensive genetic of microscopic analyses.

3.9 Adverse outcome pathway (AOP)

As already mentioned, there is a definite push towards more ethically clean research methods which sacrifice less animals and resources (the three Rs principle). Within the scientific community there are voices like Bradbury *et al.*, who make the argument for a more expanded use of computational and molecular approaches (Bradbury et al., 2004). In service to this, the systematic use of AOPs could help scientists approach research questions in a more targeted way. AOPs were first strongly advocated for by Ankley *et al*. (2018) to be used in the field of toxicological risk assessment. AOPs are frameworks, in essence mental tools, which help summarize our collected knowledge on a toxicological scenario and succinctly represent the causative links between the observed events.

Ankley *et al*. (2018), define AOPs as: "A conceptual construct that portrays existing knowledge concerning the linkage between a direct molecular initiating event (e.g., a molecular interaction between a xenobiotic and a specific biomolecule) and an adverse outcome at a biological level of organization relevant to risk assessment." Importantly, these events may span multiple levels of organization, from the cellular to the organismal and then to the population level. Ankley *et al.*, (2018) considered an important distinction between the definition of AOP, the mechanism of action, and the mode of action. With the latter two to be respectively: "a complete and detailed understanding of each and every step in the sequence of events that leads to a toxic outcome" and "a common set of biochemical, physiological, or behavioral responses that characterize an adverse biological response where major, but not necessarily all, linkages between a direct initiating event and an adverse outcome are understood". Mechanism and mode of action are indisputably key concepts in their own rights but

can be limiting when one tries to give a complete picture of a toxicological scenario or when events which have been observed are not yet clear as to their causative relationship to the other events. AOPs provide a flexible framework which encompasses mechanism and mode of action and allows for adaptability to new data (Ankley and Edwards, 2018).

The AOP is constructed by setting two events as anchors. The first is the molecular initiating event (MIE). The MIE is the first step in the series of events in the toxicological scenario and can be a ligand-receptor interaction, binding proteins, binding to nucleic acids, etc. The site of action for each MIE is crucial as it defines the nature of the AOP. The second anchor is the apical toxicological endpoint and could be for example the death of the organism. Last comes the labeling of key events and placing them between the two anchors connected with causality links. This step is crucial as it needs to balance a degree of simplifications without omitting key events (Vinken, 2013).

AOPs offer a clear-cut overview of the toxicological event, in which newly discovered data, evidence or linkages can be easily added without significant effort or complications to the existing schemes. Most importantly, they can span multiple levels of biological organization. Starting from the interacting molecules to the cell, then to the organism and finally to a population (Vinken, 2013). Often, constructing a sound AOP does not require complete elucidation of all the involved mechanisms and causality links which in turn can help focus research efforts (Ankley and Edwards, 2018; Vinken, 2013).

On the other hand, AOPs have some distinctive disadvantages. The reductionist view they provide is often criticized that it cannot fully portray the complexities and interactions of the underlying mechanisms. The arrows and links which connect the labeled events are limited when it comes to multifactorial and dosage-dependent mechanisms (Vinken, 2013). The latter is holding a very special value for any toxicological assessment. In the words of the father of toxicology, Paracelsus: "*Sola dosis facit venenum*" (The dose alone make the poison) and naturally no study of adverse effects of chemicals on health would be complete without a comprehensive investigation into effects of different dosages.

Interestingly, the disadvantages of the AOPs often stem from the same characteristics which form the base of their advantages, namely simplicity and reductionism. It is therefore important to keep in mind that they are one mental tool which should support a research effort without neglecting to take their limitations into account. Furthermore, sound mathematical constructs and algorithms, can further enrich the linkages between the observed events lending further credence to their applicability (Kramer et al., 2011). Indeed, as technologies progress we are becoming more capable to set up and utilize AOPs (Ankley and Edwards, 2018).

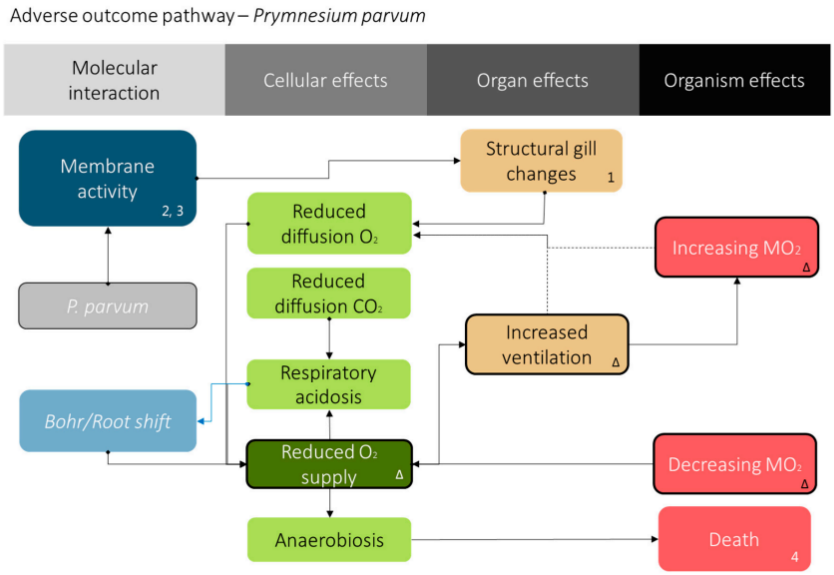

Figure 5: AOP of mode of action of *P. parvum.*(Svendsen et al., 2018)
Adverse Outcome Pathway created by (Svendsen et al., 2018) based on existing literature at the time and the findings of the research. The AOP itself follows norms discussed in previous literature (Ankley et al., 2010; Ankley and Edwards, 2018; Hutchinson et al., 2013; Kramer et al., 2011; Vinken, 2013). The AOP is divided into four stages from the molecular interaction level up to the organism effects level and thusly depicts the series of causality. Within each stage, the events/effects are depicted in boxes and number indicate the source of the information. 1: (Ulitzur, 1973), 2: (Binford et al., 1973), (Yariv and Hestrin, 1961), (ULITZUR and SHILO, 1966). The Greek letter Δ denotes findings which were discovered during the research efforts of the same paper (Svendsen et al., 2018). It could be observed during this research that *P. parvum* possessed membrane activity capable of causing gill damage which in turn alternated oxygen consumption and increased ventilation rate.

Svendsen *et al.*, 2018 constructed an AOP for *P. parvum* (Figure 5) and focused on the effects of prymnesins in the respiration of fishes and the observed symptoms (Svendsen et al., 2018). It is important to mention that different species of *P. parvum* produce different kinds of prymnesins and their MIE still needs further research. Yet as already mentioned, one key advantage of AOPs is their ability to seamlessly incorporate new

research findings into their structure and it would be interesting to see how the present AOP for prymnesins will expand over time.

Finally, there is a noteworthy convergence of opinions. Kramer *et al.* (2011) supports promoting studies of natural history and species demographics to strengthen AOP models. Interestingly, this point war reverberated by Shumway *et al* (2018) for the goal of strengthening HAB research (Kramer et al., 2011; Shumway et al., 2018).

4 Materials and methods

4.1 Machinery

Autoclave systec DX-150	Bartelt GmbH, Graz, AT
Balance	KERN & SOHN GmbH, Balingen, DE
Laminar flow hood	Thermo Fisher Scientific, Waltham, MA, US
Microbalance	DeltaRange® XP26, Mettler Toledo, Greifensee, CH
pH meter	Dostmann electronic GmbH, Wertheim, DE
Plate reader	Synergy H1 microplate reader, BioTek, Winooski, VT, US Software: Gen5, Version 3.08.01
	Victor3V, 1420 Multilabel Counter, Perkin Elmer, Waltham, MA, US Software: Wallac 1420 Workstation Software, Version 3.00
Centrifuge Rotina 420 R	Hettich Zentrifugen, Tuttlingen, DE
Centrifuge Z 326 K Hermle	Labortechnik GmbH, Wehingen, DE
Microbalance	Mettler Toledo, Colombus, OH, US
Inverse microscope Axiovert 40C	Carl Zeiss Microscopy GmbH, Jena, DE
Vortexer lab dancer S40	VWR, Vienna, AT
Water bath	Grant GD100, Grant Instruments, Cambridge, UK

4.2 Chemicals

Acetic acid	Fisher Chemical, Loughborough, UK
Calciumchlorid-dihydrat	Merck, Darmstadt, DE
Calciumsulfat dihydrat	Carl Roth GmbH & Co. KG, Karlsruhe, DE
Cell Titer Blue®	Promega Corporation Madison, Fitchburg, WI, US
Crystal violet (CV)	Fluka Chemika CH
D-(+)-galactose	Sigma-Aldrich, St. Louis, MO, US
Di-natriumhydrogenphosphate	Carl Roth GmbH & Co. KG, Karlsruhe, DE
Ethanol	Fisher Scientific, Loughborough, UK
Foetal bovine serum (FBS)	Thermo Fisher Scientific, Waltham, USA
Gibco Leibovitz's L-15 medium	Thermo Fisher Scientific, Waltham, MA, US
Gibco trypsin	Thermo Fisher Scientific, Waltham, MA, US
Gibco Leibovitz's L-15 medium	Thermo Fisher Scientific, Waltham, MA, US
Gibco penicillin streptomycin (P/S)	Thermo Fisher Scientific, Waltham, MA, US

Magnesium chloride	Sigma-Aldrich, St. Louis, MO, US
Magnesium sulfate	Merck, Darmstadt, DE
Natrium chloride	Merck, Darmstadt, DE
Natrium sulfate	Carl Roth GmbH & Co. KG, Karlsruhe, DE
Potassium chloride	VWR, Vienna, AT
Potassium dihydrogen phosphate	Carl Roth GmbH & Co. KG, Karlsruhe, DE
Potassium gluconate	Sigma-Aldrich, St. Louis, MO, US
Trypan blue	Sigma-Aldrich, St. Louis, MO, US
Triton-X 100	Sigma-Aldrich, St. Louis, MO, US
Triton-X 100	Carl Roth GmbH & Co. KG, Karlsruhe, DE
Gibco Versene	Thermo Fisher Scientific, Waltham, MA, US

4.3 Equipment

96-well black plate	Sarstedt AG & Co, Nümbrecht, DE
96-well clear plate	Sarstedt AG & Co, Nümbrecht, DE
Cell culture bottles	Sarstedt AG & Co, Nümbrecht, DE
Counting chamber: Neubauer	Paul Marienfeld GmbH & Co. KG, Lauda-Königshofen, DE
	Sarstedt AG & Co, Nümbrecht, DE
Dispenser-tips: 2.5 mL	Ratiolab GmbH, Dreieich, DE
Eppendorf tubes	Eppendorf GmbH, Vienna, Austria
Microtest Plate: 96 wells,	Sarstedt AG & Co, Nümbrecht, DE
Multichannel pipette	Eppendorf GmbH, Vienna, AT
Multistepper pipette	Dlab, Ontario, CA, US
pH meter	Dostmann electronic GmbH, Wertheim, DE
Pipettes	Eppendorf GmbH, Vienna, AT
Pipette tips (10µL, 20 µL, 200 µL, 1000 µL, 5000 µL)	Sarstedt AG & Co, Nümbrecht, DE
Pipetting device: Pipetus® Akku	Hirschmann Laborgeräte, Eberstadt, DE
Reagent reservoir	BIOLOGIX EUROPE GmbH, Niderzier, DE
Serological pipette (10 mL, 25 mL)	Sarstedt AG & Co, Nümbrecht, DE
TC flask vented (red cap) 75/175 cm^2	Sarstedt AG & Co, Nümbrecht, DE
TC plate (96 wells)	96 wells, sterile, standard, Sarstedt AG & Co, Nümbrecht, DE

4.4 *P. parvum* strains

For the purposes of the HPLC-QTOF-MS and the manual investigation, six strains of *P. parvum* were selected (Table 4), cultivated and had their toxins extracted. Each strain was cultivated in triplicates in 9 and 30 practical salinity units (psu) (Binzer et al., 2019). The raw data were kindly provided by Dr. Elisabeth Varga.

Table 4: Overview of the six *Prymnesium parvum* strains used in this study.

strain	origin	isolation year	isolator	obtained from
K-0252	Norman Bay, Victoria, Australia	1987	N/A	UIO
NIES-1017	Jogashima Miiura, Misaki Kanagawa, Japan	1997	N/A	NIES
NIES-1018	Hirara, Okinawa, Japan	2002	Moriya M.	NIES
PPSR-01	Serpentine river, Australia	2000	N/A	Hallegraeff, G.
RCC-1436	Atlantic ocean, France	1977	N/A	RCC
CCAP946/1B	River Blackwater, Essex, United Kingdom	1952	Butcher	CCAP

Listed are the six strains which provided the raw HPLC-QTOF-MS data for this study. N/A: not available. CCAP: Culture Collection of Algae and Protozoa (https://www.ccap.ac.uk/our-cultures.htm), NIES: National Institute for Environmental Studies Collection (http://mcc.nies.go.jp/), UIO: University of Oslo, RCC: Roscoff Culture Collection (http://roscoff-culture-collection.org/). Data provided from: (Binzer et al., 2019).

4.5 Test solutions

In order to achieve the goals of this study and investigate the effects of chloride-free medium on the RTgill-W1 cells, test solutions were prepared to facilitate that goal. Additionally, in order to study the effects of different salinities on the same cells, test solutions of varying salinity concentrations were also prepared and tested. These were prepared by following established protocols which were also used by this study's predecessors (Hochmayr, 2021; Riepl, 2019).

4.5.1 Chloride free normal external solution (NES Cl^-)

The center point of this study was to create and test a medium which would be compatible with RTgill-W1 cells and completely free of chloride ions (Table 5). This medium would act as platform for future studies endeavoring to elucidate the role of chloride ions in the mechanism of action of prymnesins.

Final volume 100 mL, pH= 7.3, adjusted with NaOH

Table 5: Chloride-free NES

substances	required (g)	actual (g)	M (g/mol)	moles (mmol)	C (mmol/mL)
Na_2SO_4	0.994	0.9729	142.04	6.849	0.0685
K-gluconate	0.058	0.1251	234.25	0.534	0.0053
$MgSO_4 \cdot 7H_2O$	0.020	0.0221	246.48	0.090	0.0009
$CaSO_4 \cdot 2H_2O$	0.043	0.0174	172.17	0.101	0.0010
$KHPO_4$	0.006	0.0073	136.10	0.054	0.0005
$Na_2HPO_4 \cdot 2H_2O$	0.019	0.0022	177.99	0.012	0.0001
D(+)Galactose	0.090	0.0909	180.16	0.505	0.0050

Depicted on the first column are the substances which were used in the creation of the chloride-free medium. In the second column are the values of the theoretically needed masses (g) while in the third are the masses which were actually weighted (g) and used in the solution. The fourth column (M) depicts the molecular weights (g/mol) of the corresponding substances (including the extra H_2O when present). The fifth column (mol) is created by dividing the values of the third column (actual) by the values of the fourth column (M) and depicts the values in mmol. Lastly the sixth column (c) depicts the final concentrations of the corresponding substances within the chloride-free medium by dividing the values of the fifth column by the final volume of the solution 100 mL and depicting the values in mmol/mL.

4.5.2. Normal external solution (NES)

The normal external solution (NES) which was used throughout the entirety of the experimental procedure was prepared and kingly provided by Helene-Christine Prause BSc, MSc (Table 6). This test solution, together with the L-15 medium acted as point of reference for the chloride-free medium. Interestingly, the experiments showed that the metabolic activity of the cells in NES surpassed the metabolic activity of the cells in L-15 medium. It is theorized by this author that this might be a phenomenon of "Hormesis" (Calabrese and Baldwin, 2002).

Final volume 100 mL, pH = 7.6 adjusted with NaOH

Table 6: Overview of NES

substances	**required (g)**	**actual (g)**	**M (g/mol)**	**moles (mmol)**	**C (mmol/mL)**
NaCl	0.800	0.8020	58.44	13.723	0.13723
KCl	0.040	0.0412	74.55	0.553	0.00553
$CaCl_2$	0.014	0.0139	110.98	0.125	0.00125
$MgCl_2$	0.009	0.0104	95.21	0.109	0.00109
$MgSO_4 \cdot 7H_2O$	0.020	0.0204	246.48	0.083	0.00083
KH_2PO4	0.006	0.0062	136.09	0.046	0.00046
$Na_2HPO_4 \cdot 2H_2O$	0.024	0.0250	177.99	0.140	0.00140
D(+)Galactose	0.090	0.0960	180.16	0.533	0.00533

Depicted are the substances which were used for the creation of the normal external solution (NES). This solution was produced and kindly provided by Helene-Christine Prause BSc, MSc. In the first column are the substances which were used. On the second column are the theoretically calculated masses which are needed for the creation of NES. On the third column are the masses which were actually weighted and used in the solution. In the fourth column (M) are the molecular weight of the corresponding substances, while on the fifth are the moles which are calculated by dividing the values of the third column (actual) by the values of the fourth column (M). Lastly, the sixth column (C) depicts the concentrations (mmol/mL) of the corresponding substances in the solutions and were calculated by dividing the values of the fifth column (moles) by the end-volume of the solution (100 mL).

4.5.3 Older chloride-free normal external solution (NES Cl^- "old")

NES Cl^- "old" was provided by the LMC institute as a means of more thoroughly exploring the behavior of the RTgill-W1 cells. It was created by this author's predecessor (Riepl, 2019) before the creation of NES described in 4.5.2. It was also used by (Hochmayr, 2021). In this study it will be referred to as "NES Cl^- old" (Table 7)

pH adjusted to 7.3 with NaOH

Table 7: Concentrations of substances in "NES Cl^- old" as created by M. Riepl.

Substance	**Concentration (mM)**	**1000 mL H_2O (g)**
Na_2SO_4	140.0	9.94
K-gluconate	2.5	0.58
$MgSO_4$ X $7H_2O$	1.0	0.25
EGTA	2.0	0.76
$CaSO_4$ X $2H_2O$	2.0	0.43
Glucose	10.0	1.80

4.5.4 Salinity test solutions (psu solutions)

Batch α stock solution (Table 8) final volume 105 mL, pH=7.6

Table 8: Batch α stock solution overview

substances	required (g)	weighted (g)	M (g/mol)	moles (mmol)	C (mmol/mL)
NaCl	0.80	0.80	58.44	13.70	0.1370
KCl	0.04	0.05	74.55	0.65	0.0065
$CaCl_2 \cdot 2H_2O$	0.02	0.01	147.01	0.10	0.0010
$MgCl_2$	0.01	0.01	95.21	0.10	0.0010
$MgSO_4 \cdot 7H_2O$	0.02	0.02	246.48	0.09	0.0009
KH_2PO_4	0.01	0.01	136.09	0.04	0.0004
Na_2HPO_4 $2H_2O$	0.02	0.02	177.99	0.11	0.0011
D(+)Galactose	0.09	0.09	180.16	0.51	0.0051

Listed in this table are the substances which were used to create the stock solution which in turn were used to prepare test solutions of varying salinities. The latter ones were referred to as "psu solutions". The column "required" depicts the masses (g) which were theoretically needed to create the stock solution, whereas the column "weighted" depicts the masses (g) which were actually used. The column "M" depicts the corresponding molar masses, including the molecular weight of water in the cases of $CaCl_2 \cdot 2H_2O$, $MgSO_4 \cdot 7H_2O$ and Na_2HPO_4 $2H_2O$. The column "moles" depicts the content of the corresponding substances in mmol by dividing the actual mass weighted by the corresponding molecular weight. Finally, the column "C" depicts the concentration of each substance in the solution. The stock solution of batch α had a final volume of 105 mL (after pH adjusting). Consequently, the concentration of each substance was calculated by dividing each mole content by 105 mL. It can be observed that the final concentrations of the substances in the stock solution are exceptionally low, and it might have been a source of errors during the experiments since minor handling errors were more consequential for such miniscule concentrations.

Batch α test solutions after division of stock solution, addition of required NaCl and filtration with 0.2 μm pore filters (Table 9):

Table 9: Batch α, psu solutions overview

Substances	psu 30	psu 35	psu 40	psu 45	psu 50
NaCl	0.284 (g)	0.587 (g)	0.683 (g)	0.725 (g)	0.880 (g)
KCl	0.010 (g)	0.010 (g)	0.010 (g)	0.010 (g)	0.010 (g)
$CaCl_2 \cdot 2H_2O$	0.003 (g)	0.003 (g)	0.003 (g)	0.003 (g)	0.003 (g)
$MgCl_2$	0.002 (g)	0.002 (g)	0.002 (g)	0.002 (g)	0.002 (g)
$MgSO_4 \cdot 7H_2O$	0.004 (g)	0.004 (g)	0.004 (g)	0.004 (g)	0.004 (g)
KH_2PO_4	0.001 (g)	0.001 (g)	0.001 (g)	0.001 (g)	0.001 (g)
$Na_2HPO_4 \cdot 2H_2O$	0.004 (g)	0.004 (g)	0.004 (g)	0.004 (g)	0.004 (g)
D-(+)-Galactose	0.018 (g)	0.018 (g)	0.018 (g)	0.018 (g)	0.018 (g)

After creating the stock solution, it was divided in five equal parts and a predetermined amount of NaCl was added to each one in order to reach the desired salt concentration (salinity). After this, each psu solution was filtered with 0.2 μm pore filters under the laminar in order of ascending salinity concentration. Each column after the first, depicts the mass content of each substance within the specified test solution (referred to as psu solution). This first ensemble of five test solutions, named "batch α", was created to have test solutions whose salinity increased incrementally and provided an overview of the effects of rising salinity to the metabolic activity of RTgill-W1 cells.

Batch β stock solution (Table 10) final volume 100 mL, pH=7.6

Table 10: Batch β stock solution overview

Substances	required (g)	weighted (g)	M (g/mol)	moles (mmol)	C (mmol/mL)
NaCl	0.8000	0.8137	58.44	13.924	0.1392
KCl_2	0.0400	*0.4094	74.55	5.492	0.0549
$CaCl_2 \cdot 2H_2O$	0.0185	0.0192	147.01	0.131	0.0013
$MgCl_2$	0.0094	0.0092	95.21	0.097	0.0010
$MgSO_4 \cdot 7H_2O$	0.0200	0.0204	246.48	0.083	0.0008
KH_2PO_4	0.0060	0.0085	136.09	0.062	0.0006
$Na_2HPO_4 \cdot 2H_2O$	0.0238	0.0243	177.99	0.137	0.0014
D(+)Galactose	0.0900	0.0908	180.16	0.504	0.0050

Similarly, to batch α, a second stock solution was created for the next series of salinity test solutions. This was called "batch β". The first column of the table lists the necessary substances for the creation of the stock solution. The second column lists under "required" the masses in (g)

needed for each of the corresponding substances while the third column lists under "weighted" the actual masses which were used in the stock solution. The fourth column lists the molecular weights of the corresponding substances while the fourth, depicts the mol of the actual substances in the stock solution. The sixth column, "C" lists the concentrations which are derived from dividing the mols of each substance by 100 mL. The asterisked value in the third column notes an error which occurred during the creation of this stock solution and was only much later discovered after completion of the experiments. During the weighing of KCl an error caused the wrong mass to be used for the solution. This could be a possible explanation for the highly irregular results of batch β.

Batch β test solutions after division of stock solution, addition of required NaCl and filtration with 0.2 μm pore filters (Table 11):

Table 11: Batch β stock solution overview

substances	**psu 31**	**psu 32**	**psu 33**	**psu 34**	**psu 40**
NaCl	0.6047 g	0.6262 g	0.6483 g	0.6680 g	0.7931 g
KCl	0.0819 g	0.0819 g	0.0819 g	0.0819 g	0.0819 g
$CaCl_2 \cdot 2H_2O$	0.0038 g	0.0038 g	0.0038 g	0.0038 g	0.0038 g
$MgCl_2$	0.0018 g	0.0018 g	0.0018 g	0.0018 g	0.0018 g
MgSO4 7H2O	0.0041 g	0.0041 g	0.0041 g	0.0041 g	0.0041 g
KH2PO4	0.0017 g	0.0017 g	0.0017 g	0.0017 g	0.0017 g
Na2HPO4 2H2O	0.0049 g	0.0049 g	0.0049 g	0.0049 g	0.0049 g
D(+)Galactose	0.0182 g	0.0182 g	0.0182 g	0.0182 g	0.0182 g

After creating the stock solution, it was divided in five equal parts and a predetermined amount of NaCl was added to each one in order to reach the desired salt concentration (salinity). The five parts of were then filtered under the laminar with 0.2 μm pore filters Each column after the first, depicts the mass content of each substance within each test solution (referred to as psu solution). This first ensemble of five test solutions, named "batch β", was created to study in depth the effects of salinity around the value of psu 33 which roughly corresponds to the salinity of natural seawater. Studying this area could potentially reveal if the other natural factors (like bacterial content) might be affecting the metabolic activity of the RTgill-W1 cells. Furthermore, the test solution psu 40 as an anchor point to batch α which also features a psu 40. This was done in order to verify the reliability of the batches as their results were expected to be the same or at least similar/relevant.

Batch γ stock solution (Table 12) final volume 100 mL, pH=7.6

Table 12: Batch γ stock solution overview

substances	required (g)	weighted (g)	M (g/mol)	moles (mmols)	C (mmol/mL)
NaCl	0.8000	0.8008	58.44	13.703	0.1370
KCl	0.0400	0.0483	74.55	0.648	0.0065
$CaCl_2 \cdot 2H_2O$	0.0185	0.0148	147.55	0.101	0.0010
$MgCl_2$	0.0094	0.0091	95.21	0.096	0.0010
$MgSO_4 \cdot 7H_2O$	0.0200	0.0214	246.48	0.087	0.0009
KH_2PO_4	0.0060	0.0060	136.09	0.044	0.0004
$Na_2HPO_4 \cdot 2H_2O$	0.0238	0.0204	177.99	0.115	0.0011
D(+)Galactose	0.0900	0.0911	180.16	0.506	0.0051

Listed in this table are the substances which were used to create the stock solution which in turn was used to prepare test solutions of varying salinities. The latter ones were referred to as "psu solutions". The column "required" depicts the masses (g) which were theoretically needed to create the stock solution, whereas the column "weighted" depicts the masses (g) which were actually used. The column "M" depicts the corresponding molar masses, including the molecular weight of water in the cases of $CaCl_2 \cdot 2H_2O$, $MgSO_4 \cdot 7H_2O$ and Na_2HPO_4 $2H_2O$. The column "moles" depicts the content of the corresponding substances in mmol by dividing the actual mass weighted by the corresponding molecular weight. Finally, the column "C" depicts the concentration of each substance in the solution. The stock solution of batch γ had a final volume of 100 mL (after pH adjusting). Consequently, the concentration of each substance was calculated by dividing each mole content by 100 mL. It can be observed that the final concentrations of the substances in the stock solution are exceptionally low, and it might have been a source of errors during the experiments since minor handling errors would be more consequential for such miniscule concentrations.

Batch γ test solutions after division of stock solution, addition of required NaCl and filtration with 0.2 μm pore filters (Table 13):

Table 13: Batch γ psu solutions overview

substances	psu 30	psu 35	psu 40	psu 45	psu 50
NaCl	*0.2837 g	0.5874 g	0.6835 g	0.7246 g	0.8804 g
KCl	0.0097 g	0.0097 g	0.0097 g	0.0097 g	0.0097 g
$CaCl_2 \cdot 2H_2O$	0.0030 g	0.0030 g	0.0030 g	0.0030 g	0.0030 g
$MgCl_2$	0.0018 g	0.0018 g	0.0018 g	0.0018 g	0.0018 g
$MgSO_4 \cdot 7H_2O$	0.0043 g	0.0043 g	0.0043 g	0.0043 g	0.0043 g
KH_2PO_4	0.0012 g	0.0012 g	0.0012 g	0.0012 g	0.0012 g
$Na_2HPO_4 \cdot 2H_2O$	0.0041 g	0.0041 g	0.0041 g	0.0041 g	0.0041 g
D(+)Galactose	0.0182 g	0.0182 g	0.0182 g	0.0182 g	0.0182 g

After creating and filtering the stock solution of batch α with 0.2 μm pore filters, it was divided in five equal parts and a predetermined amount of NaCl was added to each one in order to reach the desired salt concentration (salinity). Each column after the first, depicts the mass content of each substance within each test solution (referred to as psu solution). This series of psu solutions was created in order to broaden the scope of the salinity effects, with psu 50 acting as a stress test solution and others functioning as anchors to both batch α and batch β. The asterisked value denotes a weighing error occurred at psu 30 regarding the mass of NaCl which might be responsible for irregularities in the results.

SEAWATER

Provided by the laboratory as a means of investigating the behavior of RTgill-W1 in more natural water. It originated from the Helgoland Isles (Germany) in Germany and is considered to have a salinity of 33 psu (Wolf, 2021).

4.6 RTgill-W1

Over the last decades there has been a keen interest to move away from animal experiments and toward more ethical alternatives following the “3R Principles”, namely replacement, reduction, and refinement (Bury et al., 2014; Scholz et al., 2013). Whole effluent toxicity (WET) test of effluents from wastewater facilities is a prime

example of experiments which are legally mandated for the protection of the environment and require vast amounts of live fish on a routine basis (Scott et al., 2021). Another prominent example is that under the European Chemical Legislation REACH (Registration, Evaluation, Authorization, and restriction of Chemicals) produced and imported chemicals must by legislation be tested on fish according to established protocols (Fischer et al., 2019). The concerns regarding live animal testing are both ethical and economic and the desire for alternatives is substantial. One such promising alternative is the use of the fish gill cell line "RTgill-W1".

Rainbow trout (*Oncorhynchus mykiss*) gill cells were first isolated and successfully cultivated in permeable supports in the early 90s (Part et al., 1993) and very soon an immortalized permanent cell line was also developed and therefore bypassing the need for constant supply and sacrifice of fishes (Bols et al., 1994). Before the end of the decade, these gill cells could also be reliably grown on permeable supports (Wood and Pärt, 1997). These groundbreaking milestones paved the way for the establishment of the RTgill-W1 as a very reliable and flexible experimental model.

The RTgill-W1 cells have many characteristics which make them prime subjects for *in vitro* toxicologic experiments. These epithelial cells in the gills of fish are ideal sentinel models since they are naturally the first sites of contact with toxins in the environment, can withstand a wide range of salinity, osmotic pressure and pH and even have metabolic activity (Figure 6) and defenses against these toxins like the enzyme cytochrome P4501A (Bury et al., 2014; Lee et al., 2009). As such, environmental samples can be brought in direct contact with these cells and evaluated without the need for extraction or concentration steps (Lee et al., 2009).

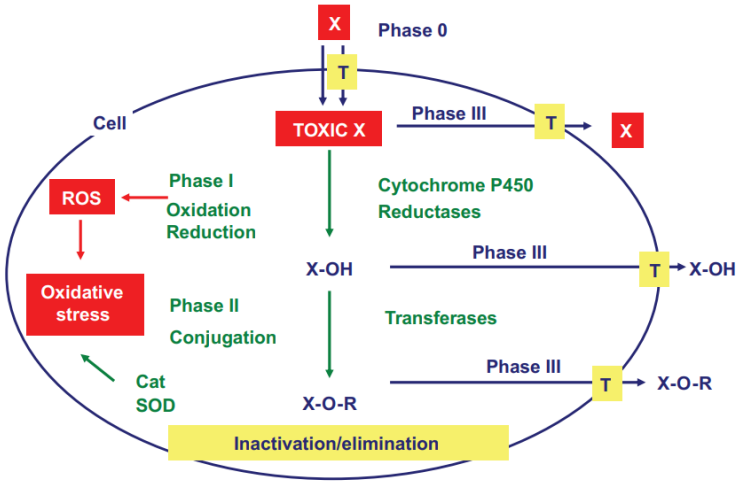

Figure 6: Overview of xenobiotic transformation in a generic cell.
Depicted are phase 0, I, II and III as well as transporters. X denotes xenobiotic, X-OH denotes hydroxylated xenobiotic, X-O-R denotes xenobiotic conjugated with hydrophilic species. Such hydrophilic species might be glutathione, sulfate, glycine, acetyl-group or glucuronic acid. ROS denotes reactive oxygen species, Cat denotes catalase, SOD denotes superoxide dismutase and finally T denotes transporters. RTgill-W1 cells provide the key advantage to behave like the general scheme above so as to be able to be utilized in toxicological studies without reservation regarding the relevance of the results to human/animal health (Bury et al., 2014).

Furthermore, a clear correlation between the EC_{50} factors of the *in vitro* experiments and the LC_{50} factors of the *in vivo* experiments can be drawn (Tanneberger et al., 2013). At confluency these cells adopt a characteristic polygonal shape (Bols et al., 1994) and this was in fact used in this study as an indicator for the healthy growth of the RTgill-W1 cells in the culture flask.

For the experiments conducted in this study RTgill-W1 were kingly provided by Prof. Dr. Kristin Schirmer, Department Environmental Toxicology, EAWAG, Dübendorf, CH. The cells were cultivated in the dark inside an incubator (19 °C) and handled inside in the laminar for the purposes of the experiments.

In general, established cell lines are very advantageous for routine experimental procedures as they, are easily maintained and handled, provide highly reproducible results, and can theoretically be maintained at *infinitum* (Bury et al., 2014) whilst circumventing the constant need for new fish from which they must be extracted (Bols et al., 1994).

On the other hand, *in vitro* experiments on cells, instead of *in vivo* experiments on fish, also come with a range of important limitations. Specifically, one cannot reliably investigate phenomena of bioaccumulation and long-term exposure or identify

endocrine disruptors (Scholz et al., 2013). Considering that these parameters are integral in the research of HABs this blind spot should not be overlooked. Furthermore, Bury *et al.,* (2014) make the key observation that: "that the mechanism behind what kills an organism is not always the same as that killing a cell". Therefore extrapolating *in vitro* results for environmental risk assessment can be challenging as it is hard to derive a standard which can be considered as safe (Bury et al., 2014). In conclusion, the results of such experiments can be extraordinarily rich in information and fruitful, but at the same time need to be part of larger and more pluralistic research effort.

4.7 Autoclaving

Autoclaving took place in the Autoclave systec DX-150 from Bartelt GmbH (Graz, AT). Solid materials like pipette tips and Eppendorf tubes were autoclaved at 134℃ under a pressure of 101.0 kPa for 20 minutes followed by drying in vacuum at 120 ℃ for 30 minutes. Liquis like distilled water and PBS were autoclaved at 134℃ under a pressure of 101.0 kPa for 20 minutes.

4.8 Laminar operation

During the conduct of the experiments, it was vital that stringent sterile conditions could be maintained in order to avoid contaminations of the cell lines and the test samples. Equally important was the unwavering adherence to safety regulations. All experiments were conducted whilst always wearing appropriate laboratory coat and nitrile gloves. To that end, all experiments with the RTgill-W1 cell line were performed under the laminar.

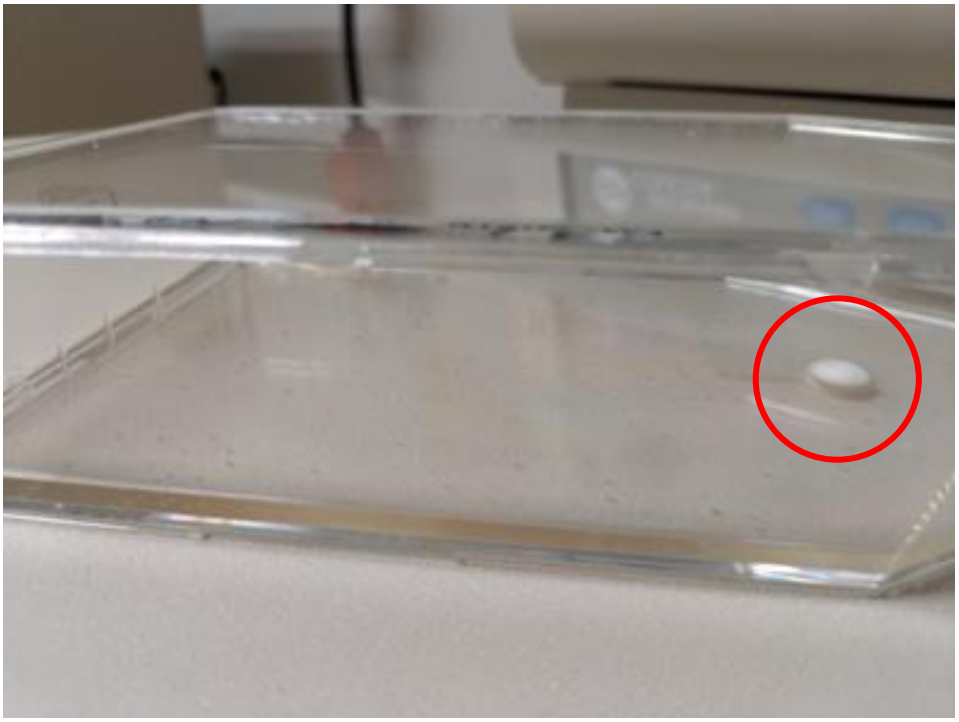

Photograph 1: Example of contaminated flask.
Depicted is a typical T175 which was used during the course of the experimental procedure. The thin line of liquid at the bottom is the L-15 medium which was used to cultivate the RTgill-W1 cells. The white observable particle which is encircled at the right of this picture is in fact a colony of contaminating agents most probably of fungal nature. A possible vector of contamination is the L-15 medium itself if it has touched the bottle cap. This could have facilitated the transfer of fungal spores from the air to the inside of the flask where the contamination would be able to establish itself and flourish. After detection of contamination such a flask must be removed immediately and cautiously so as to not endanger neighboring culture flasks within the incubator. Protocol even dictates that such a contaminated flask be autoclaved (high heating under pressure) before it is discarded.

At the beginning of the work process, the laminar was turned on and the glass retracted. It was left like this for a few minutes, until the airflow inside could be automatically stabilized. After this the working area inside the laminar was cleaned with 70% ethanol. Following that, all materials and test-samples were “imported” into the laminar. “Importing” meant, that a tissue fully soaked in 70% ethanol was used to fully clean and sterilize the surfaces of the items which would enter the laminar. Finally, before working inside the laminar, the own gloves were thoroughly doused in 70% ethanol.

While working under the hood inside the laminar, several key details had to be taken into account in order to minimize the risk of contamination (Photograph 1) and ensure good laboratory praxis. Movements had to be deliberate and constrained. It was advised not to touch the working area with one’s elbows, nor move items which might drip underneath (like pipettes) above others.

After the conclusion of the experiment, the imported materials and test-solutions were removed from the laminar and carefully stored. The working area of the laminar was once again cleaned with 70% ethanol and the hood was closed. An inbuilt UV light source irradiated the inside of the laminar for 30-60 minutes in order to ensure sterilization.

4.9 Cell culture

Cell culture in this body of work is the process of growing a population of cells, specifically RTgill-W1 cells, artificially in a controlled environment. To this end, the cells were grown in special flasks specifically manufactured for this purpose. The bottom of the flask is made according to specifications which help the cells to adhere to it and start proliferating. The cells were grown in L-15 medium along with fetal bovine serum (FBS) which provided the cells with a fluid environment and ample nutrients. The medium also contained penicillin streptomycin (P/S) which is an antibiotic in order to help prevent contaminations. Finally, the flasks containing the cells were kept away from the light within an incubator which maintained stable CO_2 conditions and a temperature of 19 ℃.

Handling a culture flask always took place whilst wearing nitril gloves and opening one was always done within the laminar under the strictest sterile conditions. When taking the flask out of the incubator or transporting it, special care was taken so as to never let the L-15 medium of the cell culture touch the cap of the flask as this would facilitate the entry of fungi from the outside of the flask towards the inside and thus contaminate the cell culture. The cap itself had to never be firmly closed. Instead, the cap had to be semi-closed in order to allow air flow and pressure equilibration following temperature fluctuations. The flask and cap were specifically designed to be able to have this semi-closed position without the fear of external contaminations. Furthermore, handling of the flask had to be done with care so as to avoid harming the cells inside.

Flasks were seeded with a number of cells depending on the size of the flask and the estimated time of collection of the cells. Two sizes of flasks were used: T175 corresponding to 175 cm^2 available culture surface and T75 corresponding to 75 cm^2 respectively. Depending on the size of the flask (T175 or T75) and the projected day of

cell-harvesting, different numbers of cells were seeded to the flask. Typically, a T175 flask was seeded with 4.5 million cells in 20 mL L-15 medium at the beginning of the week so as to be splitted/passaged at the end of the same week. Similarly, the smaller T75 flasks were seeded with 3 million cells in 10 mL L-15 medium. Alternatively, a flask could be seeded at the end of the week and be used at the beginning or middle of the next one.

The most important factor which influenced the decision of when to split or passage the culture was cell confluency. The cells were preferably harvested at nearly 100% confluency or at the very least 90% (Photograph 2). Confluency in this context is the plethora of the cells in the culture and their proximity to each other. In essence a 100% confluent culture would be uninterrupted in its cell density.

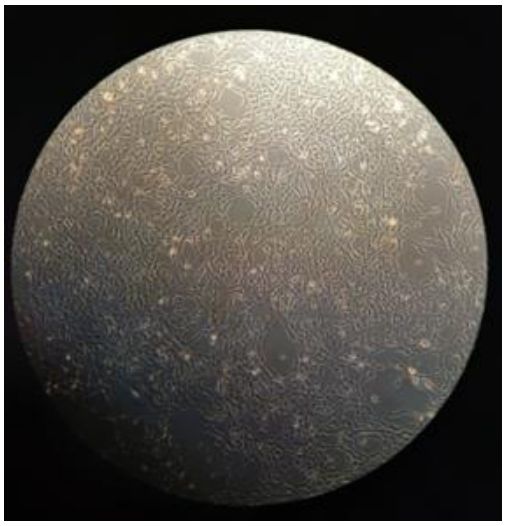

Photograph 2: Characteristic view of RTgill-W1 monolayer.
The RTgill-W1 cell monolayer is adhered to the bottom of a T175 cell culture flask. The observed confluency is above 90% and is the typical stage for splitting and use in an experiment. The dendritic shape of the cells in contrast to a round shape is indicative of the fact that the cells are still adhered to the surface of the flask. Absence of round shapes is indicative of a healthy stratum of RTgill-W1 cells.

A key factor which had to be taken into consideration was that: splitting the cell culture too soon after a seeding could have a negative impact to the cells of the culture. On the other hand, allowing the cell culture to overgrow could also have negative traits. For instance, after covering the entire surface of the bottom of the flask, the cells might start growing in layers above the primary one. This made it harder for the upcoming

trypsinization step and some cells might stay behind in the flask decreasing the amount of collected cells. Over the iterations of splitting and passaging, this had an additive effect severely decreasing the number of cells which were collected and effectively making the flask unusable. To that end a balance between early or late splitting had to be carefully maintained.

4.9.1 Splitting & passaging

Splitting the cell culture in the course of the experiments was the process of collecting the grown cells from the cell culture flask and using them to seed a 96 well plate and the cell culture flask anew. The latter being referred to as "passaging".

Firstly, the cells at the bottom of the cell culture flask were observed under the microscope. This had to be also done as course of routine even if no splitting was planned. Important observations were confluency, consistency, and condition of cells. The shape of the cells was appreciatively observed as this is indicative of living cells which are adhered to the surface of cell culture flask. If the confluency of the cells was in the range of 90-100% (as described above) the cell culture flask was then cautiously placed into the laminar.

Using a glass pipette connected to a pump, the old L-15 medium was removed. Special care had to be taken to consistently place the tip of the glass pipette to the same corner of the cell culture flask in order to minimize losses of cells. In the case of the T175 flask, he cells were washed twice with 1500 μL of Versene using a micropipette in increments of 750 μL (and only once in the case of the T75 flask). Versene was then removed by suction. Versene was kept under cold storage (4 °C) into the laboratory and had to be allowed to reach room temperature before use. This was best facilitated with a simple water bath. After use, Versene was immediately placed back into cold storage (4 °C)

Next, the pre-warmed trypsin was used to sever the adhesion of the cells to the bottom of the cell culture flask, a process referred to as "*trypsinization*". Specifically, 1600 μL of Trypsin was introduced to the cell culture flask using a micropipette in increments of 800 μL. The Trypsin was then left into the flask for nearly 3 minutes at room temperature during which time the cells were observed under the microscope

accompanied by gentle shaking and percussion of the cell culture flask. A successful release of the cells from the cell culture flask could be easily verified under the microscope since currents of cells could be distinctly observed.

Following a successful trypsinization, 5 mL of L-15 medium were swiftly introduced into the flask so as to effectively stop the trypsinization process and the potently toxic effects trypsin has on cells. This was done with a one-use serological pipette.

The cell suspension was then transferred to a falcon tube (15 mL) and centrifuged (50 rcf, 3 minutes, 21 ℃) leading to the formation of a pellet of cells at the bottom of the falcon tube with the mix of L-15 medium and trypsin above it (Photograph 3).

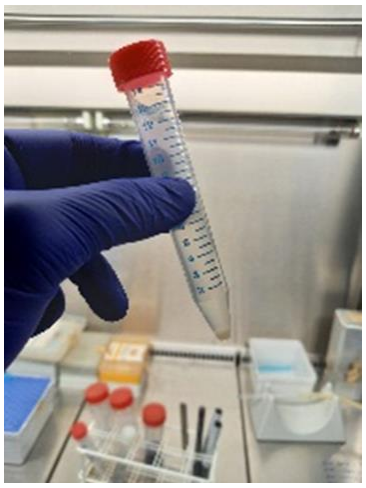

Photograph 3: Flacon tube (15 mL) after centrifugation.
At the bottom of the tube is the pellet of RTgill-W1 cells and above is the supernatant. At this stage of the process the old medium of the supernatant is the 5 mL of L-15 medium which were introduced to swiftly hold the trypsinization process meant to release the cells from the bottom of the flask.

The supernatant was then removed by suction up to 1 mL above the pellet whilst being cautious not to accidentally remove the cells (Photograph 3). The pellet was then resuspended in new 5 mL L-15 medium with the use of a micropipette. Resuspending the pellet with the micropipette had to be done slowly with care so as to not damage the cells by the sheer forces of pipetting. After resuspended the cells, a portion of 20 µL were taken out of the cell suspension and added to 80 µL Trypan Blue solution resulting in a 1:5 dilution of the actual cell suspension. From this solution 10 µL were transferred to each chamber of the Neubauer cell chamber and the cells were manually counted under the microscope.

4.9.2 Cell counting

The Neubauer cell chamber is a reliable tool for the calculation of a representative estimate of the number of cells in a cell suspension. In order to do that, 10 μL of the 1:5 solution (cell solution- trypan blue) are placed in each of the two chambers and then the Neubauer cell chamber is placed under the microscope. Living cells can be distinctly observed white amidst the blue background within a grid whereas dead cells appear as dark blue (Photograph 4).

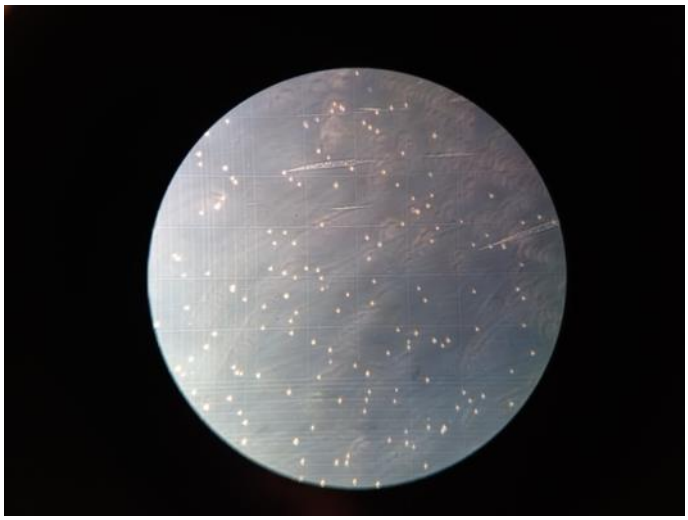

Photograph 4: Example of quadrant of the Neubauer counting cell chamber.
View through the microscope. The photograph depicts a typical view of a Neubauer cell-counting chambers. This particular case also shows a population of cells which for the purposes of the experiments would be considered healthy and plentiful. A good indicator of the health of the culture was the presence/absence of dead cells. These were distinguishable from live cells by their color. Dead cells fail to keep out the dye and show as black or deep blue, while live cells are white/golden.

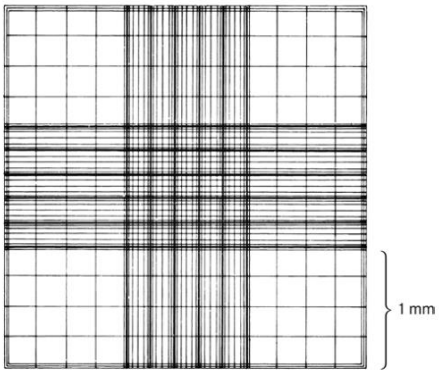

Figure 7: Schematic view of the Neubauer cell chamber.
Counting of cells takes place in the four distinct quadrants which are separated from the thick-lined cross in the middle. The cells are counted separately in each quadrant and an average cell count is then calculated (Gstraunthaler and Lindl, 2021).

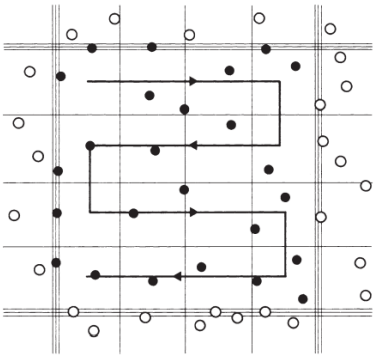

Figure 8: Visualization of Neubauer cell chamber counting method.
Within each of the four quadrants of the Neubauer cell chamber, the cells were counted in the direction which is depicted by the arrow. Black dots represent cells to be counted and white dots represent cells which must be excluded. During counting, two of the four sides were arbitrarily chosen. All the cells which happened to be on the border lines of these chosen two, were included in the cell count and all the cells on the other two border lines were excluded (Gstraunthaler and Lindl, 2021).

Within each of the two chambers are four quadrate grids (Figure 7). The cells are counted in each grid with the use of a hand-held counter and then the average cell count is calculated between the four grids (Figure 8). This is done for both chambers and subsequently the average cell count is found between the two chambers. This corresponds to the number of cells per 0.1 µL of the 1:5 solution. Followingly, the number of cells per mL of the original cell suspension can be readily ascertained with the following formula.

(cells per mL) = (average cell count) * 5 *10000

And followingly

Total number of cells = (cells per mL) * (Volume of cell suspension)

Knowing this information, it is then possible to calculate the necessary volumes which will contain the desired number of cells for CTB, CV and passaging.

(required volume of cell suspension) = (calculated cells per mL) / (desired number of cells)

4.10 Cytotoxic assays

In order to gauge the potency of a substance as a toxin, inescapably test must be performed on living matter. As mentioned, the scientific community strongly desires to move away from the use of live animal experiments according to the three R's principles. To that end animal experiments are being substituted with *in vitro* experiments on cells. This way, the cells act as proxies for toxicity and are therefore ethically clean. Furthermore, these kinds of tests are highly flexible and require relatively small amounts of cells to produce reliable results. It follows that many series of test can be performed on many groups of cells at the same time. Experiments like these are collectively called cytotoxic assays. In these the viability of test cells (e.g., RTgill-W1, HeLa, etc.) is measured using a pre-established test method in well plates (Photograph 5). The cells are seeded in the wells and after an incubation time, test solutions of various concentrations are provided to them. The end results are recorded (usually photometrically) and statistically analyzed.

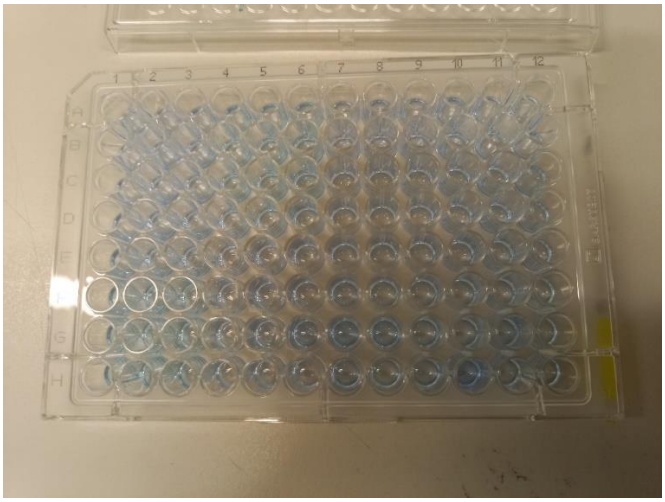

Photograph 5: 96-well plate used in Cell Titer Blue toxicological assay.
During the course of the experiments 96-well plates were at the centre of the research efforts. Their use is intricately linked with the advantages of standardization such as reliability and reproducibility of results. The 96 available wells provide ample space for experimentation with a wide range of test-solutions. These were utilized in triplicates. In essence, three adjacent wells were provided with the same test solution and in the end an average value was calculated out of the three along with their standard deviation. At the bottom right corner is the yellow indication which signifies the specialty of the well floors to adhere with cells. The blue tint in the wells is characteristic of the CellTiter-Blue® (CTB) assay. Seeding the wells with cells and followingly replacing the L-15 medium with the test solutions often proved challenging, since the process had to be done completely uniformly amongst the cells in a very short amount of time so as to not expose the RTgill-W1 cells too long. This step very often introduced pipetting errors which skewed the results and resulted in widened standard deviations and, consequently, reduced reliability of the results.

Other than being ethically clean cytotoxic assays have several advantages over animal testing, like cost-effectiveness, ease of handling, flexibility, and high through-put results. Or as O'Brien *et al.,* 2000 succinctly said: "The ideal test for *in vitro* cell proliferation and cytotoxicity is a simple, rapid, efficient, reliable, sensitive, safe and cost-effective measurement of cell viability" (O'Brien et al., 2000).

Nonetheless, cytotoxic assays have one major blind spot. Specifically, that which kills a cell does not necessarily kill an animal (Bury et al., 2014). As a matter of fact, the dying and replacing of individual cells for various reasons is a sign of healthy organism. More than that, cytotoxic assays are severely limited to studying the long-term toxicological effects or even effects which manifest after the passing of a number of generations.

Even so, whilst it is paramount to not forget the limits of cytotoxic assays, it is undeniable that they are very useful tools for avant-garde studies and their cost-effectiveness makes them ideal for venturing into uncharted territories.

Plate 07
seeded on: 02.06.2021 week: 22
21k cells/well
Assay performed on: 04.06.2021 week 22
RTgill-W1 complete medium
(3h incubation) CH

	Medium	Medium + Triton X C x	Seawater Medium	NES (regular)	NES Cl-fee	Psu 15	Psu 20	Psu 25	Psu 30	Psu 35

	1	2	3	4	5	6	7	8	9	10	11	12
A	Medium	Medium	Medium	Medium +0.1% Triton X above	Medium +0.1% Triton X above	Medium +0.1% Triton X above	Psu 15 α batch	Psu 15 α batch	Psu 15 α batch	Psu 15 α batch	Psu 15 α batch	Psu 15 α batch
B	Medium	Medium	Medium	Medium +0.05% Triton X above	Medium +0.05% Triton X above	Medium +0.05% Triton X above	Psu 20 α batch	Psu 20 α batch	Psu 20 α batch	Psu 20 α batch	Psu 20 α batch	Psu 20 α batch
C	Medium	Medium	Medium	Medium +0.1% Triton X below	Medium +0.1% Triton X below	Medium +0.1% Triton X below	Psu 25 α batch	Psu 25 α batch	Psu 25 α batch	Psu 25 α batch	Psu 25 α batch	Psu 25 α batch
D	Seawater Medium	Seawater Medium	Seawater Medium	Medium +0.05% Triton X below	Medium +0.05% Triton X below	Medium +0.05% Triton X below	Psu 30 α batch	Psu 30 α batch	Psu 30 α batch	Psu 30 α batch	Psu 30 α batch	Psu 30 α batch
E	Seawater Medium	Seawater Medium	Seawater Medium	NES (regular)	NES (regular)	NES (regular)	Psu 32 β batch	Psu 32 β batch	Psu 32 β batch	Psu 32 β batch	Psu 32 β batch	Psu 32 β batch
F	Medium	No cells Medium	Medium	NES (regular)	NES (regular)	NES (regular)	Psu 33 β batch	Psu 33 β batch	Psu 33 β batch	Psu 33 β batch	Psu 33 β batch	Psu 33 β batch
G	Medium	Medium	Medium	NES Cl-fee	NES Cl-fee	NES Cl-fee	Psu 34 β batch	Psu 34 β batch	Psu 34 β batch	Psu 34 β batch	Psu 34 β batch	Psu 34 β batch
H	Medium	Medium	Medium	NES Cl-fee	NES Cl-fee	NES Cl-fee	Psu 35 α batch	Psu 35 α batch	Psu 35 α batch	Psu 35 α batch	Psu 35 α batch	Psu 35 α batch

Figure 9: Example of plate layout for the 96-well plate.
The layout had to be preconceived well before the execution of the experiment. The test solutions were pipetted in triplicates out of which the average value was calculated along with the corresponding standard deviation. In this particular example regarding plate 07 the choice was made to examine the psu test solution in double triplicates in order to further cement the reliability of the results. Another point of note was that the position of the triplicates in the 96-well plates had to be changed for the next assay so as to eliminate local sources of errors. The layouts were similarly prepared for both CTB and CV. Furthermore, in this as well as all other plates, three triplicates were chosen to have only medium L-15 and no cells. These were marked by a red box in the schema and used to determine the background noise during the fluorescence measurement of the plate.

4.10.1 Test over control

After measuring and receiving the data for CTB or CV, a set of calculations had to take place in order to extract meaningful conclusions. The “test over control” method is an astute way of circumventing the absence of commercially available standards and still reach acceptable results (Scott et al., 2021). To that end when setting up the layout for the 96-well plate it was always necessary to fill wells with L-15 medium without cells or test solutions as well as wells with L-15 medium and no test solutions. After receiving the fluorescence measurement, the following calculations took place:

Firstly, the average value for the wells with L-15 medium without cells was calculated (along with the standard deviation as a measure of quality for the experiment). This average value was then subtracted from every separate value of the wells. This step served the purpose of removing the background (L-15 medium) from the signals.

Secondly, the average value of the wells with L-15 medium and cells was also calculated. Every separate well value was then divided with this average value and the result of this division was multiplied with 100. This resulted in the percentile viability rate of the RTgill-W1 cells in each well.

Lastly, since all test solution were given to the cells as triplicates, the values for each test solution were used to calculate their average value and their standard deviation. These results of all the experiments were collected and underwent the Nalimov test in order to exclude outliers. The analysis was performed in Excel while the creation of the graphs was done with the software Origin.

4.10.2 CellTiter-Blue® (CTB)

4. 10.2.1 CTB principles

In this master thesis, the method of choice was the assay CellTiter-Blue® (CTB) due to the high sensitivity and easy calculations it requires. Furthermore, it is a fast, flexible, and cost-effective method to investigate cell viability in the presence of toxins or other chemicals by measuring the metabolic activity of the cells (Dayeh et al., 2013). The method is very practical and suitable for high throughput tests preferably using multiple well plates and automated plate readers (O'Brien et al., 2000; Rampersad, 2012).

CellTiter-Blue® (CTB), also commercially available by other companies as Alamar Blue or Presto Blue, is in fact the chemical known as resazurin which bears the IUPAC name: "7-hydroxy-10-oxidophenoxazin-10-ium-3-one". Resazurin is also known as azoresorcin, diazo-resorcinol. It is water-soluble as well as stable in culture mediums, has a blue color and is non-fluorescent (Figure 10). Most importantly, resazurin is non-toxic to cells and permeable through their cell membranes (Rampersad, 2012).

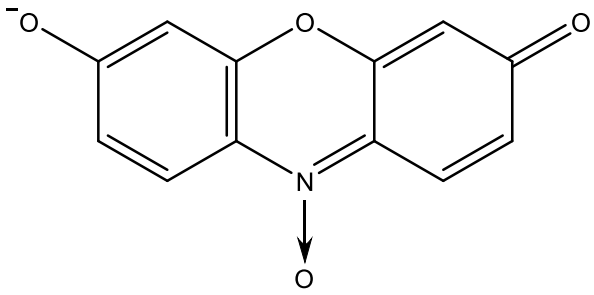

Figure 10: Resazurin.
Pre-reduced state of the key-component in the CellTiter-Blue® (CTB) viability assay. It is theorized that metabolic enzymes inside the cells facilitate oxidation (Riss et al., 2016).

When placed in wells together with live cells, resazurin acts as an intermediate electron acceptor in the electron transfer chain and undergoes reduction to resorufin (Figure 11). Resorufin is a pink, highly fluorescent substance, which can be detected by measuring either absorbance or fluorescence. The latter is usually the recommended way due to the higher sensitivity (Riss et al., 2016). In fact, as few as 80 cells are capable of reproducibly delivering a signal (O'Brien et al., 2000). Fluorescence can be measured at $579_{Ex}/584_{Em}$ (Riss et al., 2016), $570_{Ex}/600_{Em}$ or $540_{Ex}/630_{Em}$ (Rampersad, 2012) or $540_{Ex}/590_{Em}$ (Dorantes-Aranda et al., 2011). Depending on the experiment and the commercial product (CTB, Alamar Blue, etc.) researchers are called upon to optimize their methods and measurements.

Figure 11: Resorufin

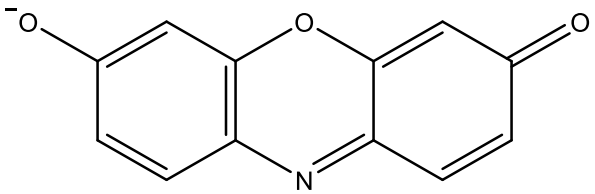

Reduced form of the key-component in the CellTiter-Blue® (CTB) viability assay. Detectable with fluorescence analysis (Riss et al., 2016)

Originally O'Brien *et al.*, 2000 showed with a series of experiments, that the reduction of resazurin resorufin takes place inside the cells. Although they were not able to prove that it does not take place outside the cells as well (O'Brien et al., 2000). More recently, electron microscopy has also verified that the red/ox reaction takes place inside the cells

(Riss et al., 2016). It is hypothesized, that the reduction of resazurin to resorufin happens due to NADPH, FADH, FMNH, NADH, cytochromes and mitochondrial enzymes which can be found inside the cells (Rampersad, 2012; Riss et al., 2016).

The CTB assay rests upon the assumption that cell number and toxicant concentration share a linear and inversely proportional relationship. Although this may seem intuitive and self-evident it does however have exceptions. There are cases of: irregular cell growth; non-responsive cells masking responsive ones; toxins which affect proliferation, cell-cycles or induce apoptosis in non-linear fashions (Rampersad, 2012). Due to cases such as these, investigators should at first try to positively verify the linear relationship between the cell number and the effects of the putative toxins under investigation before the actual experiment.

Another point of caution is that resazurin is photo-sensitive and therefore experiments must be conducted in the dark which raises the risk of human errors. Additionally, too long exposure times may lead to the further reduction of resorufin to a colorless product called dihydroresorufin which quenches the fluorescence (Rampersad, 2012).

The CTB has several advantages which make it a prime tool for laboratory research. It is time efficient and can be conducted easily. It is cost-effective and since it is not toxic it is also safe. It is compatible with many formats, methods of detection and experiment models and thus a very flexible assay which can be used in a wide array of experiments. It has been shown to have a large interlaboratory reproducibility. Lastly, it has a high potential for automation and most importantly for a toxicological assay, it is ethically clean, since it uses cells instead of living animals to test for toxicity and adverse effects (Lee et al., 2009; Rampersad, 2012; Riss et al., 2016).

4.10.2.2 CTB protocol

Firstly, the cells in the cell flask were observed under the microscope and if they were deemed healthy and more than 90 % confluent they were harvested as described in part 4.8.1. Following that, the cells were counted with the Neubauer cell counting chamber as described in part 4.8.2 and the number of cells per mL of cell suspension was determined (cell concentration)

Before the next step it was necessary to calculate the volume (mL) of cell suspension needed so as to seed 21000 cells in each well of the 96-well plate along with 200 μL L-15 medium. For simplicity as well as to provide adequate volume for the reagent reservoir it was a customary practice to calculate as if the plate had 100 places. In essence:

Required number of cells from the cell suspension = 21000 * 100 =2100000
Required volume of the cell suspension (mL) = 2100000 / (cell concentration)

Considering that the desired volume for each well was 200 μL, this led to a total volume of 200 μL * 100 wells = 20000 μL = 20 mL.

Having found the required volume of the cell suspension, 5 mL of fresh L-15 medium were transferred into a reagent reservoir and using a micropipette a volume equal to the calculated required volume of the cell suspension was removed from the reservoir only to be replaced by an equal volume of the actual cell suspension.

The reagent reservoir was then filled with further 15 mL of fresh L-15 medium to a total of 20 mL. Using a multichannel pipette, the contents of the reagent reservoir were softly mixed and finally transferred to the 96-well plate (200 μL per well = 21000 cells per well at this point). The plate was then placed in the incubator (19 °C) and left at rest in the dark for 48 hours.
After the allocated incubation time, the 96-well plate was taken out of the incubator and again placed under the laminar. The L-15 medium was then removed from the cells by siphoning it out with a pump connected to a sterile plastic pipette tip. After that, 100 μL of test solution were placed in each well according to a predetermined plate schema and left to incubate for three hours. During the incubation time, the CTB stock solution was taken out of storage (-20 °C) and left to thaw at room temperature in the dark. At the 2-hour mark, the plate, while still in the incubation phase, was placed in the plate reader and photographs with a magnification of 20X were taken manually (Photograph 6). This was followed up by automatic photography with a 4X magnification (Photograph 7).

Photograph 6: Examples of 20X photographs

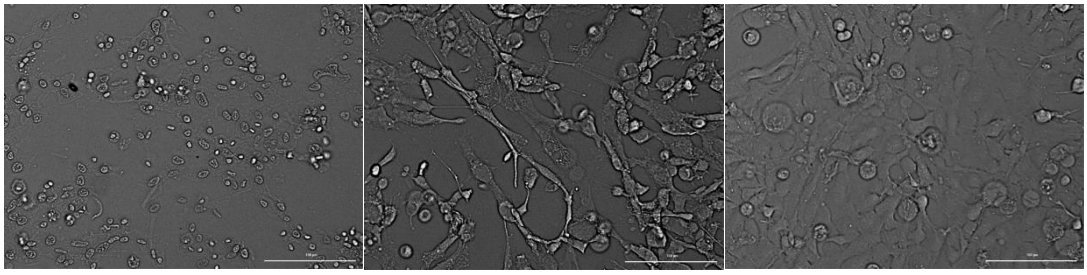

The photographs depict RTgill-W1 cells in three distinct environments during the CellTiter-Blue® (CTB) assay. From left to right: i) Triton-X 100 0.1%, ii) psu 33, iii) chloride-free medium. The magnification is X20 allowing viewing in the μm scale.

Photograph 7: Examples of 4X photographs

The photographs depict RTgill-W1 cells in three distinct environments during the CellTiter-Blue® (CTB) assay. From left to right: i) psu 33, ii) chloride-free medium, iii) Triton-X 100 0.1%. The magnification is X4.

Near the end of the 3-hour incubation period, a 1:10 solution of CTB in L-15 medium was prepared in a reagent reservoir. At exactly the 3-hour mark, the test solutions were aspirated from the plate with the use of sterile plastic pipette tip connected to a pump. The wells were then swiftly filled with 100 μL of the 1:10 CTB solution. After that, the plate was left for 1 hour in the dark. After exactly one hour, 80 μL were transferred from each well with a multichannel pipette from the normal 96-well plate to a black bottom well microtiter in order to prevent fluorescence compromise (Photograph 8). Fluorescence was measured in the plate reader at 560/590 nm and the acquired data were analyzed to determine the viability of the cells in each well after exposure to the test solutions (as described in 4.9.2)

Photograph 8: Black bottom plate
The 96-well black bottom plates were used both during the CellTiter-Blue® (CTB) and Crystal Violet (CV) toxicological assays. Their purpose is to prevent fluorescent compromise of the final measurement in the plate reader.

4.10.4 Crystal violet (CV)

4.10.4.1 CV principles

Complementary to the CTB viability assay, crystal violet (CV) assay was also performed to investigate the impact of Cl^- ion-free medium and different salinities to RTgill-W1 cells. N-[4-[bis[4-dimethyl-amino)-phenyl]-methylene]−2,5-cyclohexadien-1-ylidine]-N-methyl-methanaminiumchloride (Karam et al., 2021) by IUPAC or Crystal Violet as it is commercially known, is a synthetic, basic, cationic dye, which imparts a violet color to aqueous solutions. Cationic dyes can easily interact with negatively charged cell membrane surfaces and can enter cells and concentrate in the cytoplasm (Pourjavadi et al., 2013). It is this exact ability to enter and stay in cells that the assay takes advantage of in order to stain viable cells. As such crystal violet is an excellent and efficient method for *in vitro* cytotoxicity studies because it is simple, accurate, reproducible, and sensitive. Moreover, when conducting this assay, crystal violet must be handled with caution under a hood because it is toxic to mammalian cells, a mutagen, and a mitotic poison (Pourjavadi et al., 2013). Due to this, it must also be discarded responsibly.

Beyond its application as key component in a viability assay, crystal violet, a typical triphenylmethane dye (Karam et al., 2021) is also widely used in textile dyeing industries, as a biological stain, dermatological agent, veterinary medicine, and additive to poultry feed to inhibit propagation of harmful bacteria (Karam et al., 2021).

4.10.4.2 CV protocol

A 96 well plate was seeded with 21000 cells and 200 µL L-15 medium per well and left in the incubator (19 °C) for approximately 48 hours. After this, the L-15 medium was aspirated from the wells and 100 µL of the test solutions were introduced to the wells. The plate was then placed back into the incubator (19 °C) and allowed to incubate for three hours. Within this timeframe, at the two-hour mark, the plate was placed in the plate reader and photos with a magnification of 20X were taken (Photograph 9). This was followed up by automatic photography with a 4X magnification (Photograph 10). After the incubation time of three hours, a premade stock solution of crystal violet (0.1% in 10%EtOH) was taken out of cold storage (4 °C) centrifuged (500 rcf 5 min, 22 °C) and allowed to reach room temperature. The test solutions were aspirated from the wells with the use of a multichannel pipette. The cells were fixated at the bottom of the wells by adding 100 µL 96% EtOH (-20 °C). After 10 minutes, the EtOH was removed from the wells with a multichannel pipette and in its place 50 µL of crystal violet were pipetted to each well at room temperature. This part of the process was referred to as “staining”. After staining for 5 minutes, the crystal violet was carefully removed from the wells, and these were washed 4 times with reverse osmosis water either with a multistep or a multichannel pipette. The plate was then left without a cover so that the water could evaporate. After two days a solution of 1% acetic acid in 96% EtOH would be prepared in a reagent reservoir. 100 µL of this solution were then pipetted into each well of the 96 well plate thereby dissolving the formed crystals. The 96-well plate was then measured in the plate reader at 560/590 nm and the results were analyzed with Excel.

Photograph 9: Examples of 20X photographs

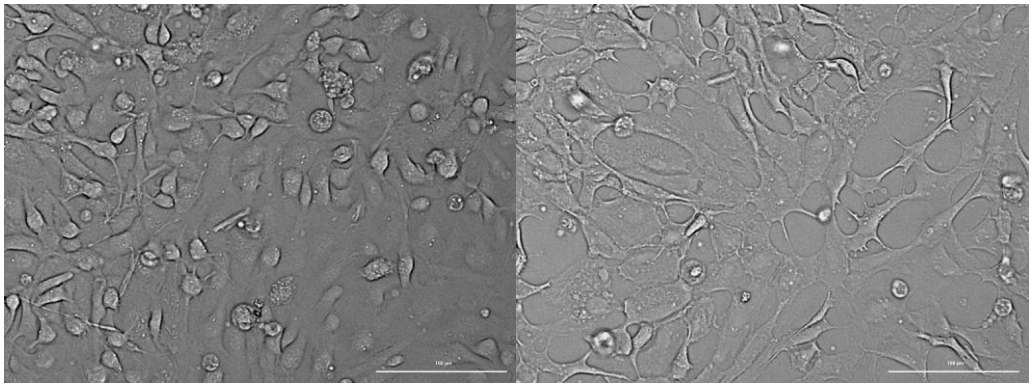

The photographs depict RTgill-W1 cells in three distinct environments during the Crystal Violet assay. From left to right: i) psu 25 ii) psu 31. The magnification is 20X allowing viewing in the μm scale.

Photograph 10: Examples of 4X photographs

The photographs depict RTgill-W1 cells in three distinct environments during the Crystal Violet (CV) assay. From left to right: i) Triton-X-100 0.1% ii) psu 33, iii) chloride-free medium. The magnification is 4X.

4.11 LC-DAD-HRMS: Agilent 6545 QTOF-system

4.11.1 Principles of operation

James Barker in his book Mass Spectrometry defines MS as "an analytical technique in which atoms or molecules from a sample are ionized (usually positively), separated according to their mass-to-charge ratio (*m/z*), and then recorded. The instrument used to conduct this measurement is called a mass spectrometer". Contrary to other methods of analysis, which measure electromagnetic or optical properties, mass spectrometry is a "destructive" method due to the ionization of the sample (Barker, 1999).

4.11.1.1 Electron spray ionization (ESI)

Electron spray ionization (ESI) is probably the most important ionization method used to combine high pressure liquid chromatography (HPLC) and mass spectrometry (MS). The eluent which carries the analyte goes through a thin metallic capillary. A strong electric field is applied, and the process takes place under atmospheric pressure (Figure 12).

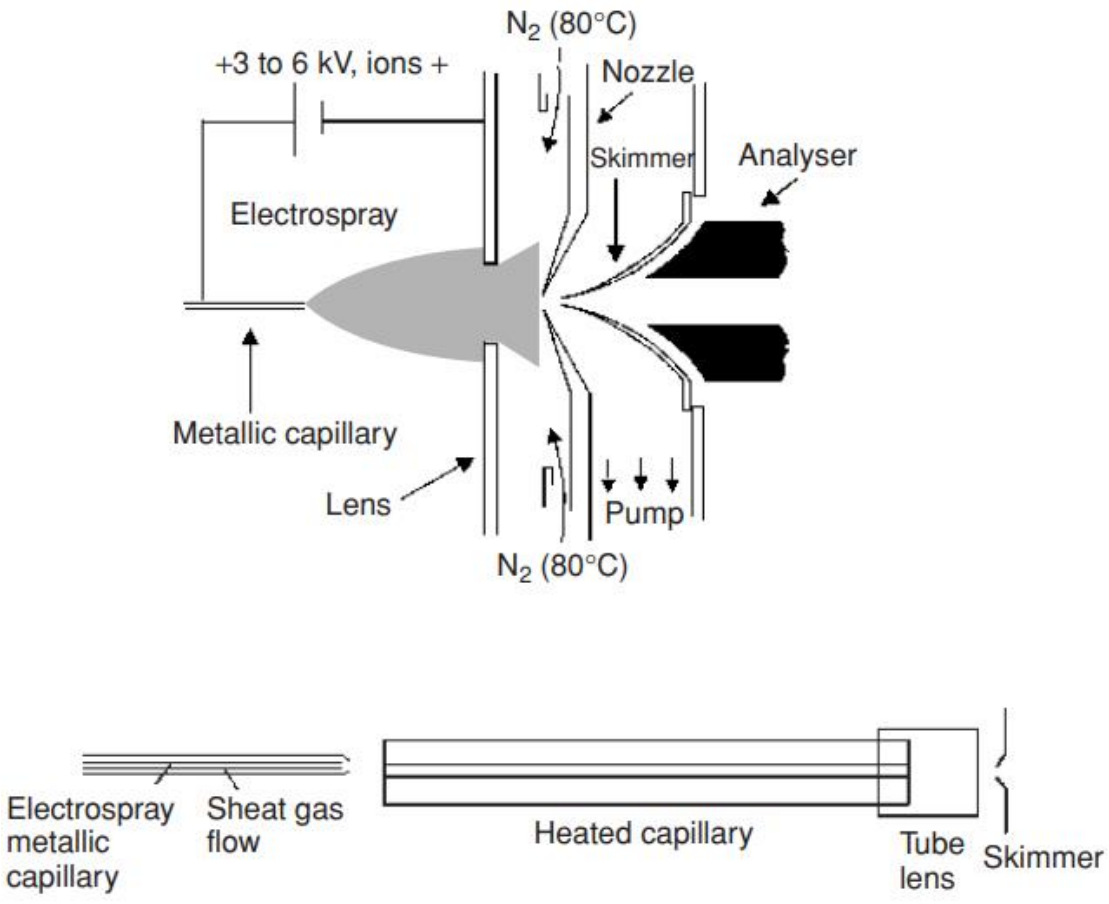

Figure 12: Schematic of electrospray sources.
Ion focalization is achieved through the use of skimmers. Desolvation which will lead to the Coulomb explosion is achieved with a curtain of heated nitrogen gas (top), or with a heated capillary for desolvation (bottom) (Hoffmann and Stroobant, 2007 p.331).

The eluent passes through the capillary with a very weak flux (200-500 µL per min) and forms a droplet at the end of the capillary. The electric field produces a charge accumulation at the liquid surface which form a "Taylor cone" (Figure 13).

Figure 13: Representation of the conformation of the droplet into a Taylor cone (Hoffmann and Stroobant, 2007 p45).

Importantly, the analytes dissolved in the solution are not themselves charged yet. The droplet detaches from the capillary and elongates under the effects of the electric field. A stream of warm N_2 is applied to the next part of the chamber which is also referred to as a "curtain of N_2". The strong electric field is maintained. This helps the solvent evaporate so that the droplet shirks in size while the accumulated charge increases at the surface of the droplet. When the repelling Coulomb forces finally exceed the surface tension, a point which is referred to as Rayleigh-limit, the droplet breaks into a spray. This is referred to as a "Coulomb explosion". There is a cascade of Coulomb explosions as the more solvent evaporates whilst the charge of the smaller droplets increases. At the final stage of the process the accumulated charges are transferred from the solvent to the analyte. Importantly, during this process, the analyte, the molecules of interest, do not as a rule suffer any linkage breaks. It is for this reason that ESI is considered a "soft ionization technique" (Skoog, 2017 p.503) and why it was originally used with great success in investigations of proteins (Barker, 1999, Skoog, 2017; Camman, 2001; Hoffmann and Stroobant, 2007).

4.11.1.2 Quadrupole time of flight (QTOF)

The ions then travel through a quadrupole mass analyzer (Figure 14). This part consists of two pairs of parallel rods with each rod connected to the one opposite to it. A standard DC potential is applied to the rods and the moving ions coming from the ionization chamber and going through the quadrupole will be influenced in their movement by the laws of attraction and repulsion within the electric field differently according to their kinetic energy, or more simply their mass. Additionally, the four poles also have a radiofrequency (RF) component. The latter forces ions into an oscillating movement through the quadrupole. The combination of the two effects has as a result, that only

ions of a particular kinetic energy can pass through this “corridor” and reach the analyzer while all other ions collide with the rods without reaching the other end. Even more, the trajectories of the ions that succeed in passing through are being focused on the center of the quadrupole (Hoffmann and Stroobant, 2007). By keeping the ratio of the DC voltage and the RF field constant whilst at the same time varying their values, different *m/z* ions can reach the analyzer and create the full mass scan. Thanks to the underlying principle behind it, quadrupoles are relatively cheap to build, compact and robust. Computer control of the rod voltage can be very accurate, the mass scale is linear, and the scans are expedient (Barker, 1999 p. 74-80).

Considering that these ions all carry the same charge, and that the differentiation is based on *m/z*, it follows that the time at which they collide with the analyzer after they have travelled through the quadrupole is analogous to their mass. This is then recorded, and the software constructs the spectrum depicting the analyzed sample.

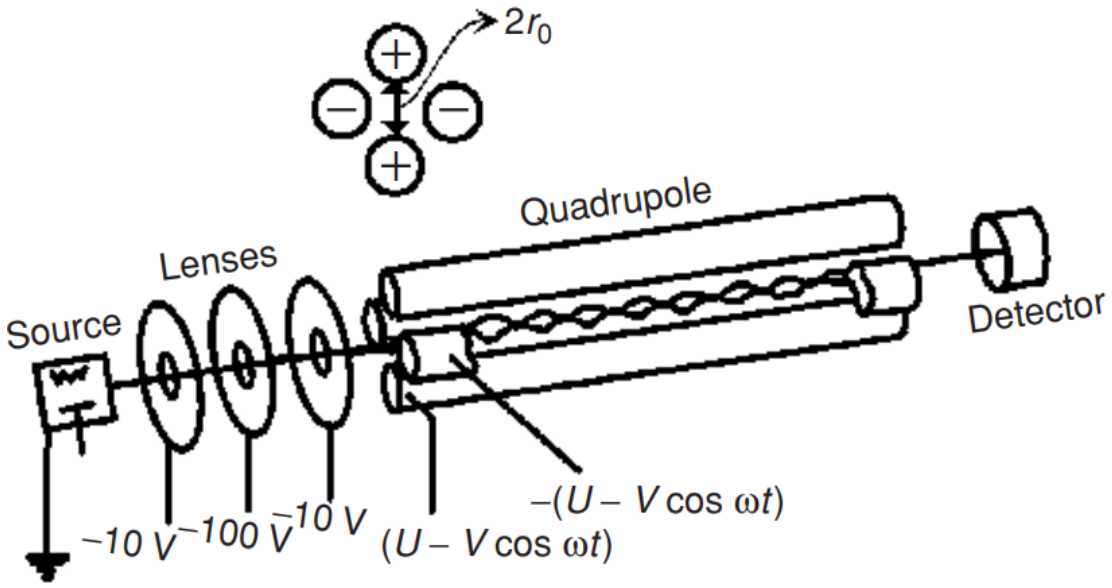

Figure 14: Simple overview of a quadrupole set up.
The apparatus consists of a source, the focusing lenses, the quadrupole cylindrical rods and the detector. Ideally the rods should be hyperbolic (Hoffmann and Stroobant, 2007 p45).

4.11.2 Experimental procedure

4.11.2.1 Stain cultivation and toxin extraction

The research team which authored (Binzer et al., 2019) selected and cultivated six *P. parvum* strains under two different salinity concentrations (9 psu / 30 psu) in triplicates. After a set period of cultivation, the biomass was harvested, and the toxins of the strains were extracted through the use of acetone and methanol. These extracts were then analyzed with HPLC-QTOF-MS from Agilent, utilizing a C18 column. C18 indicates that the stationary phase is composed of atoms with 18 carbons and therefore lipophilic in nature.

4.11.2.2 Manual investigation

The raw data provided by the HPLC-QTOF-MS were then analyzed in a process termed "manual investigation". This refers to the fact that for each possible theoretical prymnesin a researcher has to evaluate the available data from the chromatogram, the MS spectrum and the time of elution without the use of automated software. This drastically increases the possibility for human error (especially in cases of co-elutions) and elongates the required time needed until the data have been fully processed.

4.11.2.3 Theoretical list

In order to conduct the analysis a theoretical list with all the possible combinations of double bonds, Cl and sugar rings was created. This list acted as the backbone for the manual investigation of the raw data provided.

The theoretical list of possible prymnesin-Cs (Index 11.6) was compiled from a): prymnesin-Cs which were successfully detected in previous works, b): prymnesin-Cs which could not be detected completely but whose in-source fragments were detected in the MS analysis and lastly c): prymnesin-Cs which couldn't be detected at all before but which could theoretically be possible. Based on these possibilities, the

isotopic patterns were calculated using an in-house program (IsoPad) and then identified in the samples during the manual investigation of the raw data.

4.11.2.4 Analysis

In order to facilitate a streamlined and work-efficient analysis of the raw data, an excel-sheet encompassing all the possible combinations of prymnesins and their isotopic patterns was prepared. This acted as a platform for the manual investigation of the raw data. In hindsight this simple, practical tool distinctly improved the reliability of the analysis and the time-efficiency of the workflow.

4.11.2.5 Agilent Technologies Mass Hunter

The software with which the raw data were analyzed was Mass Hunter version 10 from Agilent technologies (Figure 15). During the process of the raw data the chromatogram was examined in tandem with the mass spectra. Since the column which was used during the separation phase was a C18 column, which separates substances based on lipophilicity and differences in mass, the prymnesin toxins exited the column at different times which was recorded in the chromatogram as time of elution. This was easily visible by the characteristically large and wide signals in the chromatogram. This characteristic width in the chromatogram stems from the fact that prymnesins as very large polyether ladders which “drag” in the column and are not sharply eluted from the column.

Furthermore, these exceptionally large molecules provided a multitude of stereochemical variations. Even amongst very similar molecular formular it was possible have differences in local lipophilicities and be withheld differently by the C18 column. As a simple example, two prymnesin molecules with near identical molecular formulas could vary in hydrophilicity/lipophilicity simply by adopting slightly different stereochemical confirmations. Further than that, within the same chromatographic entity one could often observe minor peaks separate from each other. These were attributed to different moieties of the sugar rings of the prymnesins (Binzer et al., 2019).

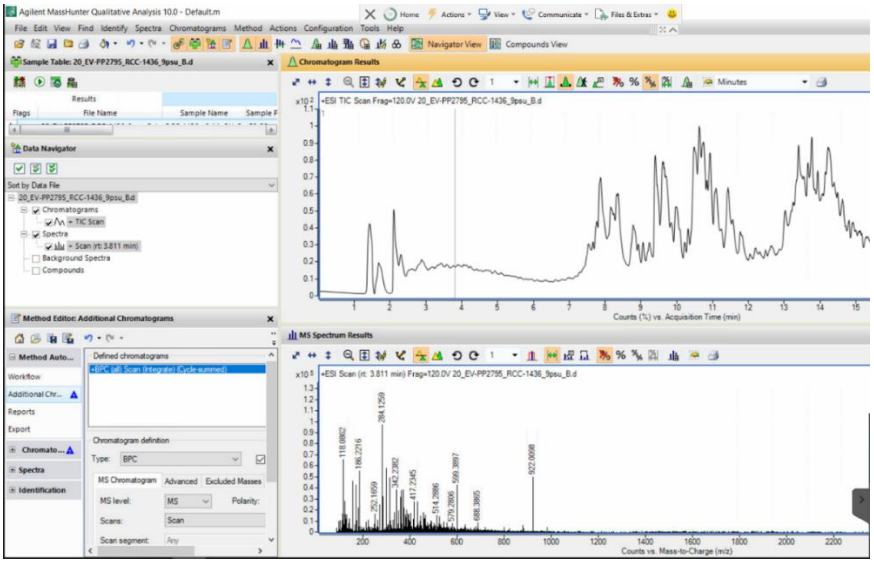

Figure 15: Example of overview of the Mass Hunter Program.
Example overview of the Mass Hunter Program from Agilent Technologies for the manual investigation of raw HPLC-QTOF-MS data. On the top right is the chromatogram and on the bottom the MS spectrum. These two were analyzed in tandem during the analysis in order to detect and identify prymnesin-Cs present in each sample.

In practice, the highest peak of the chromatogram was selected and considered to be the most representative and abundant point of elution of the prymnesin. The time of elution of this point was noted and the corresponding time of the MS spectrum was selected and examined.

In preparation for this investigation a list of all theoretically possible prymnesin Cs was compiled. Additionally, thanks to the "IsoPad" software program, it was possible to calculate the isotope pattern of each prymnesin and even the isotope patterns of their combinations (https://www.researchgate.net/publication/312625688_IsoPat_v111_-_Windows_Application_for_Isotope_Pattern_Simulation_and_13C_Enrichment_Calculator).

As a matter of fact, the cornerstone of this manual investigation was the observation of isotope patterns. In nature atoms can be found with different numbers of neutrons in their cores. This results in atom cores which have the same number of protons and electrons but slightly different masses due to the difference in neutrons. The most notable example is carbon. The most abundant form on earth is carbon-12 (6 protons and 6 neutrons) with an occurrence rate of: 98.93%. Its stable isotope is carbon-13 (6 protons and 7 neutrons) with a natural occurrence rate of: 1.1%.

In the case of prymnesins, which are exceptionally large molecules, the chances isotopes being present in the molecule is near certain, and statistically predictable. At the same time, such differences are detectable by the MS and based on the occurrence rates of the isotopes show up as very specific patterns which are termed “isotope pattern”. The first peak within the isotope pattern is called “monoisotopic peak” and during the manual investigation of the raw data was used as an anchor point. The IsoPad program could thus provide a very reliable calculation and at the same time visualize how the pattern would theoretically look like (Figure 16). Indeed, such a pattern could always be discovered when a specific prymnesin was present in a sample (Figure 17).

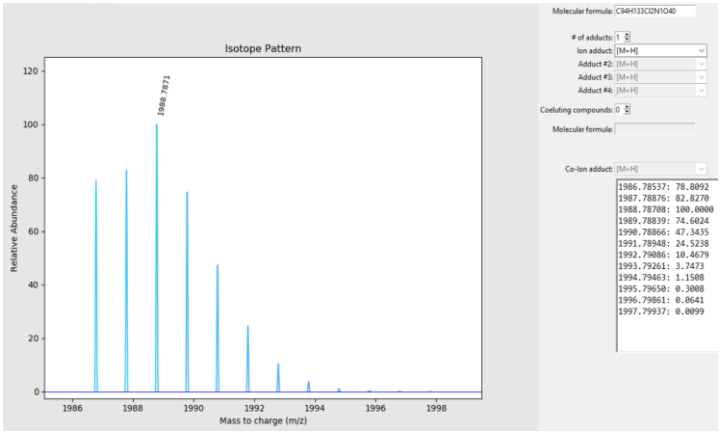

Figure 16: Example of theoretically calculated isotopic pattern of a prymnesin.
In the main panel of the program the isotopic pattern of the prymnesin can be viewed. The isotopic pattern is based on the occurrence ratio of isotopes in the prymnesins. The height of each signal therefore depicts the abundance of each one. The far-left signal is referred to as “monoisotopic peak” and is the most crucial information for the manual investigation. In essence, the monoisotopic peak consists of the prymnesin which only has the most common isotopes, and its value is therefore both unique and indicative. On the right, the exact numerical values of the isotopic peaks are listed. During the manual investigation of the raw HPLC-QTOF-MS data these complemented the identification of each prymnesin-C present in the sample. In this particular case, the prymnesin at hand is PRM-C (2 Cl + 2 DB) + pentose + hexose, $C_{94}H_{133}Cl_2NO_{40}$, $[M+H]^+$.

In summary, The HPLC-MS provided the raw data of the chromatogram and the MS spectra. The investigator would find the characteristic signals in the chromatogram, select their peak, and then go to the corresponding time of elution in the MS spectra. There the pre-calculated isotope pattern was sought after and if ascertained the prymnesin was considered present. At that point the area underneath the chromatogram was calculated by integrating the area underneath the chromatogram (Figure 18). The size of this area was considered representative of the concentration of the prymnesin in the sample. At the end

of the analysis the discovered prymnesins of each sample were depicted as a percentage of the entire sum.

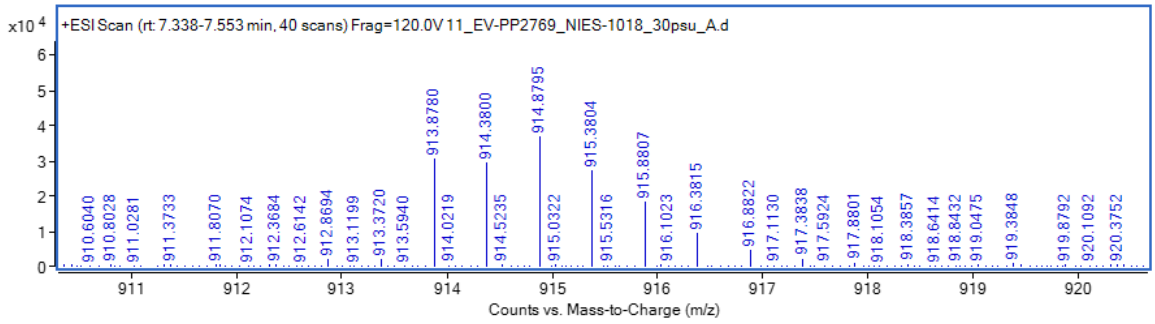

Figure 17: Example of prymnesin-C isotopic MS pattern

The HPLC-QTOF-MS depicted the detected fragments according to their mass to charge ratio (*m/z*). Detecting the isotopic pattern which corresponds to the calculated isotopic distribution was a key step in determining the existence of the prymnesin-C in question. Most notably, the dispersion of the isotopic peaks does not entirely match a gaussian distribution This was then followed by verifying that the *m/z* values matched the expected values calculated by the IsoPad program. In the depicted example, the prymnesin at hand is PRM-C (2 Cl + DB) + pentose, $C_{88}H_{125}Cl_2NO_{35}$.

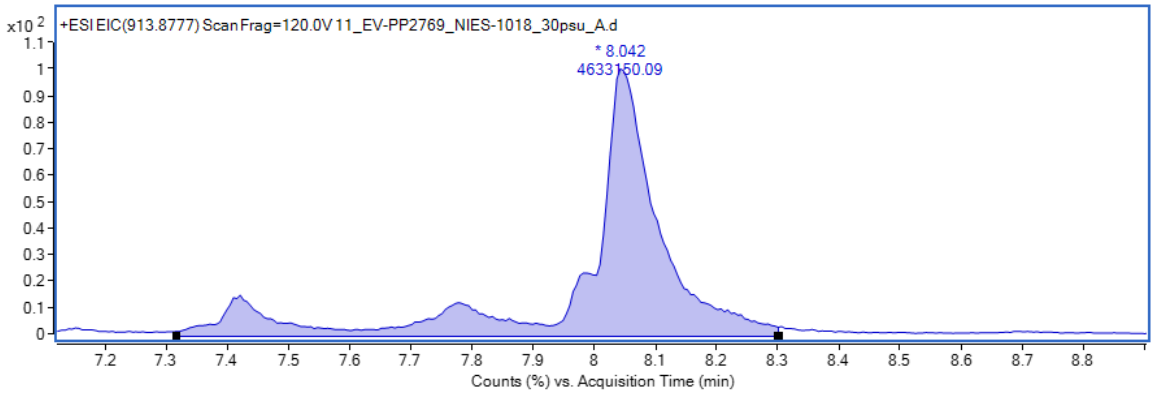

Figure 18: Example of integrated chromatogram of a present prymnesin.

During the HPLC-QTOF-MS technique, the program depicted the flow of mass as it exited the column with the stationary phase in a chromatogram against time of elusion (acquisition time in minutes). The chromatogram was used parallel to the MS spectra to orient the search within the latter, i.e.: the search focused on times of elusion. The chromatogram provided insights into the abundance of the substance and in the cases in which it could be proven that the substance was indeed a prymnesin, then the integration value of the particular part of the chromatogram was analog to the concentration of the prymnesin in the sample. In the depicted example, the prymnesin at hand is PRM-C (2 Cl + DB) + pentose, $C_{88}H_{125}Cl_2NO_{35}$.

This way of calculus is a workaround to the hinderance of not having commercially available standards. The latter is a very prevalent problem (Manning and La Claire, 2013) which all but hinders us from reliably studying prymnesins quantitatively (as well as many other HAB toxins for that matter). Therefore, at the moment we have to work with a “semi-quantitative” and mostly qualitative overview.

The second major problem is the frequent occurrence of co-elutions. Just as different moieties can help slightly separate very similar molecules, similarly, very slight

differences (e.g., of one double bond) of similar prymnesins are very prone to cause these prymnesins to co-elute. This can be debilitating for such a study as it can make it all but impossible to correctly attribute the area under one chromatogram to a single prymnesin in which case it is also uncertain what percentage of this areal belongs to which of the co-eluting prymnesins. Furthermore, it seems that some prymnesins are more prone to co-elute than others. This problem undoubtedly decreases the reliability of the investigation and a solution to this must take priority in future studies.

Additionally, the manual investigation of the raw data had a few more disadvantages which burdened the analysis. Namely that it required from the investigator to have an established understanding of the process and be fairly experienced. This was particularly necessary when identifying false-positives and distinguishing co-elutions. Oftentimes, the presence of a particular prymnesin could only be proven when investigating the chromatogram in detail instead of just the highest peak (Figure 19) and at other times the clear isotopic peak could only become distinguishable after the integration of the chromatogram. This detail-oriented investigation was therefore always labor-intensive and time-consuming.

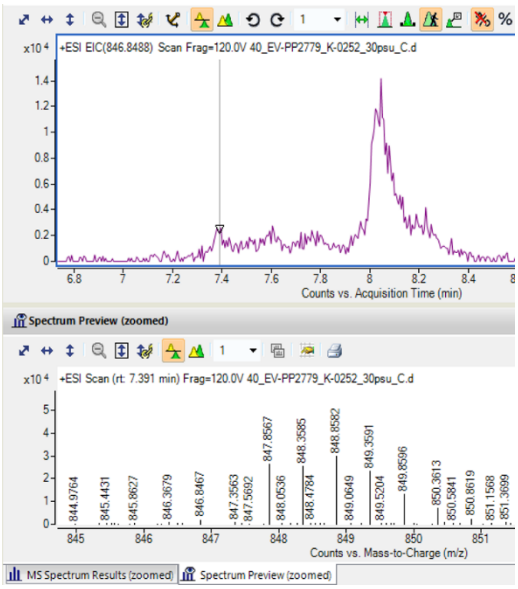

Figure 19: Example of in-depth investigation of the raw data.
In this particular case the presence of the prymnesin could only be positively proven in a minor chromatographic peak instead of the major peak. The prymnesin at hand is PRM-C (2Cl + 2DB), $C_{83}H_{115}Cl_2NO_{31}$, $[M+2H]^+$. This particular prymnesin C had not been detected before and was instead only theoretically conceived. Marking this as the first time which its existence was proven.

On the other hand, the process has a lot of potential. It is exceptionally sensitive even for fingerprint identifications of taxa if employed in chemotaxonomic endeavors. To that end the hindrance of co-elutions must be overcome and standards need to be established. Additionally, more sophisticated software allowed the entire processes to be better streamlined and automated to further exclude human errors and uncertainties and decrease the overall labor/time-intensity.

5 Results & Discussion

5.1 CTB results

Having completed the experimental procedure, the results were analyzed with the software Excel. Test over control was done as described in 4.9.2. The visualization of the results was done with the software Origin. In each plate, the technical triplicates were used to give an average and its standard deviation for each test solution. These average values were then examined with the Nalimov test to identify and exclude the outlier values. The remaining average values were again subject to averaging and their standard deviations were also calculated (without including the standard deviations of the technical triplicates). The average values and their standard deviations were collected in tables and their graphs were plotted and presented in the following parts of this study. In general, the standard deviations proved to be less than ideal and this hindered the drawing of accurate conclusions. However, it was still possible to observe certain trends.

5.1.1 Overview

First it was considered necessary to provide a holistic view of the results regarding the CTB toxicological assays and visualize them (Table 14, Figure 20). The results of L-15 medium were set as 100% metabolic activity of the RTgill-W1 cells, and the rest of the test solutions were viewed in relation to that. Originally, the Triton-X 100 solutions were created in order to act as positive controls, however due to their difficult handling as solutions their results exhibited very high standard deviations and even average values in the negative, which is impossible. Due to this they were not reliable enough to be used as positive controls anymore. Other points of interest, which will also be examined, are the fact that NES had a higher metabolic activity than L-15 medium, the consistent behavior of seawater in relation to its artificial counterparts and the seemingly non-linear decrease of the metabolic activity with increasing salinity concentration.

Table 14: Overview of the CTB assay results

test solution	average value	standard deviation	test solution	average value	standard deviation
Medium	100	11.3	Psu 35α	66.2	28.3
Seawater	60.4	9.6	Psu 35γ	55.5	17.2
NES	114.5	17.9	Psu 37γ	50.9	4.3
NES Cl-	95.7	21.7	Psu 40β	35.9	9.0
old NES Cl-	87.1	14.1	Psu 45γ	50.7	11.5
Psu 15α	100.7	26.6	Tr1 0.0005%	116.7	20.0
Psu 15γ	108.2	15.8	Tr1 0.001%	93.3	28.3
Psu 20α	88.9	21.6	Tr1 0.005%	48.5	17.2
Psu 25α	78.9	17.9	Tr1 0.01%	-0.9	4.3
Psu 30α	61.9	16.4	Tr2 0.005%	85.0	9.0
Psu 30γ	71.7	17.1	Tr2 0.01%	91.4	11.5
Psu 31β	50.1	13.5	Tri2 0.05%	6.5	23.6
Psu 32β	57.7	21.1	Tr2 0.1%	-5.2	15.9
Psu 33β	48.2	9.9	Tr3 0.05%	-6.8	5.5
Psu 34β	51.7	20.0	Tr3 0.1%	-7.5	5.4

Depicted in the table are the values of all test solutions which were produced during CellTiter-Blue® (CTB) viability assay. These values are the averages from all plates which in turn were the averages of the technical triplicates in each plate. In this Figure, NES refers to Normal External Solutions, Psu stands for practical salinity units and refers to the test solutions of varying salinities and Tr refers to the Triton-X 100 solutions. More specifically Tr1: Sigma Lot # BCBN0659V, Tr2: Roth Art.-Nr. 3051.3 and Tr3 Roth Art.-Nr. 3051.4. The standard deviations are only the ones from the various plates while the standard deviations from the technical triplicates were not included. The table was created in Excel while the corresponding graph (Figure 20) was created with the software Origin.

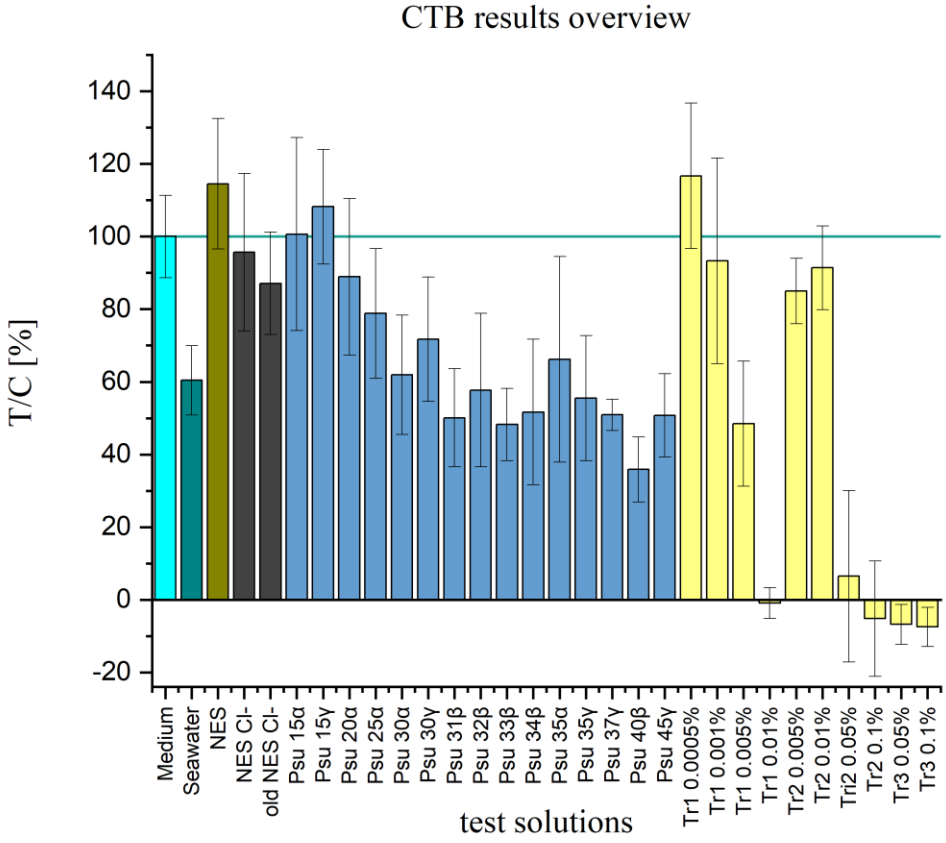

Figure 20: overview of CTB assays

Depicted are the values of all test solutions which were produced during CellTiter-Blue® (CTB) viability assay. These values are the averages from all plates which in turn were the averages of the technical triplicates in each plate. In this Figure, NES refers to Normal External Solutions, Psu stands for practical salinity units and refers to the test solutions of varying salinities and Tr refers to the Triton-X 100 solutions. More specifically Tr1: Sigma Lot # BCBN0659V, Tr2: Roth Art.-Nr. 3051.3 and Tr3 Roth Art.-Nr. 3051.4. The standard deviations are only the ones from the various plates while the standard deviations from the technical triplicates were not included. The choice regarding the inclusion/exclusion of certain values from some plates was informed by the Nalimov outlier test. The values depicted here were calculated as functions of test-over-control (T/C) depicted. The value for L-15 medium is the rule and therefore functions as the 100% standard. A permeating trend is that despite best efforts and disciplined analysis, the standard deviation of most values remains wide. Consequently, the reliability of the results can be called into question. Furthermore, the ability to discern patterns or trends becomes more challenging.

5.1.2 Batch α

The first five test solutions of different salinity concentrations were named “batch α”. These were a simple series in which the salinity was increasing in increments of 5 psu; starting from 15 psu until 35 psu. It can be seen that there is a steady decline in viability with increasing concentrations of salt (Figure 21). The standard deviations from 15 and 20 psu remain under 20% of relative standard deviation, psu 25 has a relative standard deviation of 22.7% and lastly psu 30 and 35 have a relative standard deviation above

30%. It is therefore unclear whether this regression is linear or not. Nonetheless it is clear that higher salt concentrations are less viable for the RTgill-W1 cells.

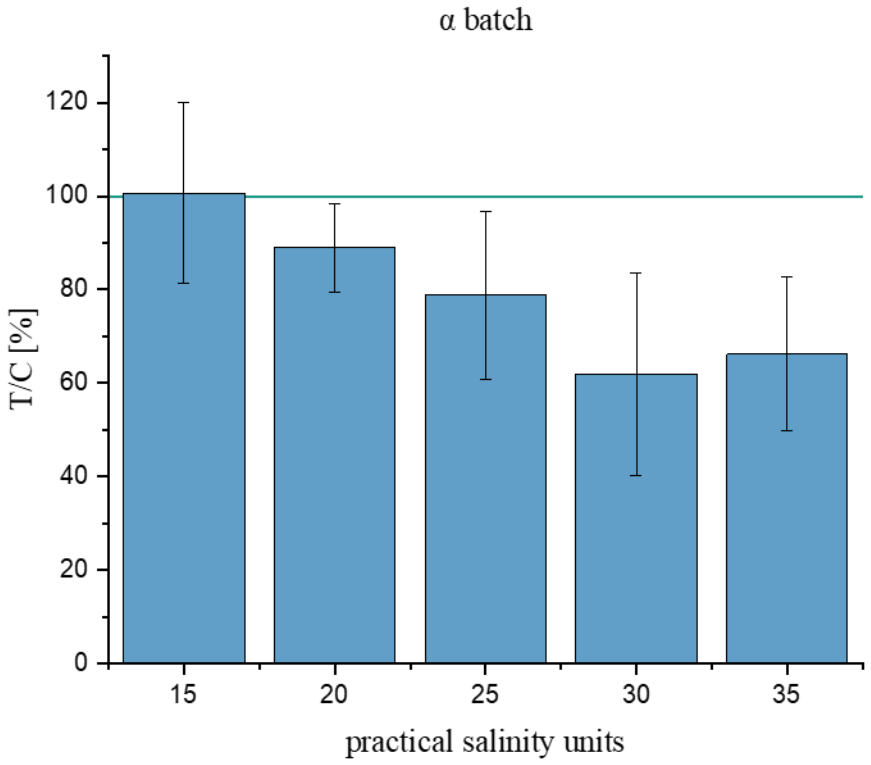

Figure 21: CTB results of batch α
Depicted are the results from all CellTiter-Blue® (CTB) cytotoxicity assays regarding the solutions of batch α. The Y-axis depicts the metabolic activity as a percentile of test-over-control (T/C), in which the L-15 medium with cells but without test solutions functions as the standard for 100% and is depicted as the straight parallel line. The X-axis depicts the concentrations of salinity which were tested in batch α. The trend which can be observed is a decrease in metabolic activity with increase of salinity concentration. The decrease in metabolic activity can be correlated in theory with a decrease in viability of cells. The wide standard deviations, which decrease the reliability of the results, obstruct more insights as to whether this decrease in metabolic activity is linear or non-linear. Non-the less, the decrease of metabolic activity due to higher salinity is clearly visible.

5.1.3 Batch β

The test solutions of batch β were created in order to study the effects of salt on the viability of the RTgill-W1 cells in salt concentrations in the immediate vicinity of seawater which is about 33 (Figure 22). While the average values are close to each other as expected, the standard deviations are large enough to hinder the extraction of meaningful conclusions. It remains unclear why batch β shows such large deviations

especially since it was analyzed together with other test solutions with far smaller deviations. Specifically, the relative standard deviations are all above 20% and the largest of them, psu 40, has a relative standard deviation of 58.9%.

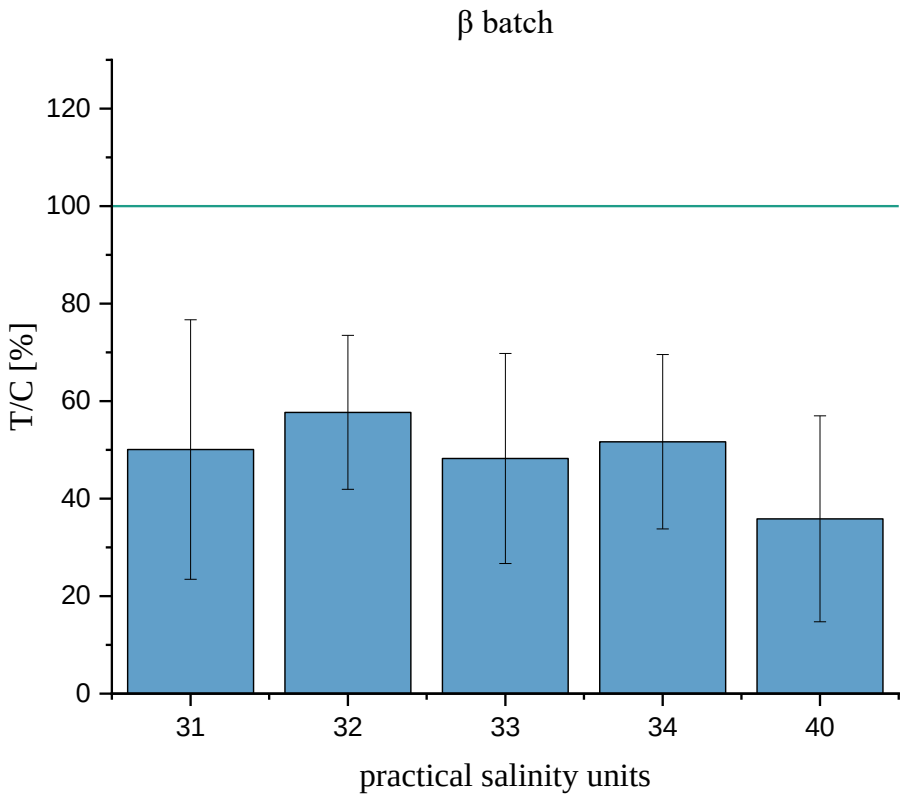

Figure 22: CTB results of batch β
Depicted are the cumulative results of the CellTiter-Blue® (CTB) cytotoxicity assay regarding the test solutions of varying practical salinity units (psu) regarding batch β. On the Y-axis are the test-over-control values for which L-15 medium with cells and without test solution was deemed as the standard (and therefore 100%). On the X-axis are the psu values. Batch β was created with the motive to provide a more detailed view of the area around 33 psu (near seawater values) and provide insights to as the decline of metabolic activity is linear or non-linear. In this case the wide standard deviations obstruct the observation of in-depth motives/trends.

5.1.4 Batch γ

Batch γ has in total the most promising results (Figure 23). This batch was created in part to verify the reliability of the test solutions from the previous batches. It also included a test solution with psu 45. This salinity concentration was considered to be beyond the amount which was optimal and was created as stress test for the RTgill-W1

cells. Interestingly, the drop in viability between psu 35 and psu 45 is far smaller than between psu 15 and psu 30. It would seem that the regression is indeed non-linear. In either case the RTgill-W1 exhibit a clear preference for less saline environments.

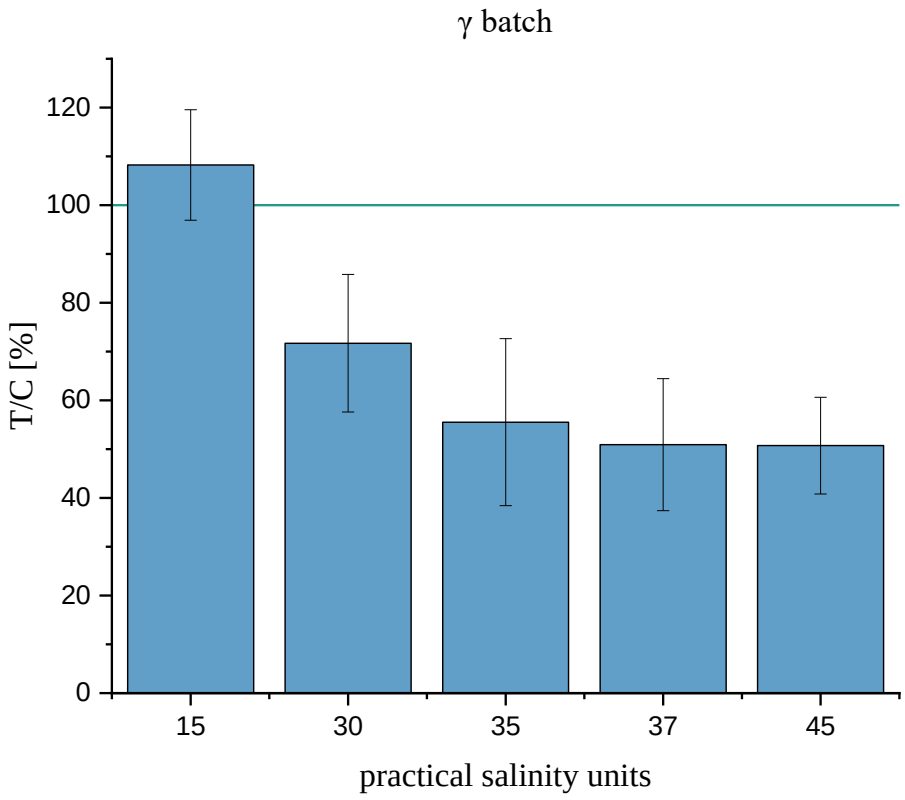

Figure 23: CTB results of batch γ

Depicted are the results of the CellTiter-Blue® (CTB) cytotoxicity assay for batch γ. On the Y-axis are the test-over-control values (T/C) which use L-15 medium with cells in the absence of other test solutions as the standard (100%). This functions as a percentile measurement of the metabolic activity of the cells and followingly of the viability of the cells in test solutions. On the X-axis are the practical salinity units (psu). Batch γ was created to expand the view provided by the other two batches, complement them and also verify them. In this case batch γ managed to provide results with decent standard deviations. It is clear, that increasing concentrations of salinity decrease the metabolic activity of the RTgill-W1 cells and consequently their viability. Furthermore, the pattern which can be observed is closer to a pattern of non-linear rather than linear regression.

5.1.5 NES

Correlating the test solutions of NES, NES Cl^- and NES Cl^- "old" provides interesting insights (Figure 24). Most notably, the viability of the RTgill-W1 cells was above 100% (with Leibovitz L-15 medium set as 100%). This could mean that the conditions of NES are more favorable for the cells, or it could be theorized that a minor stress factor energizes their metabolism. NES Cl^- and NES Cl^- "old" (which was not created but provided) show a similar state of viability. In both cases the viability of the cells is below 100% but still far above higher salinity solutions.

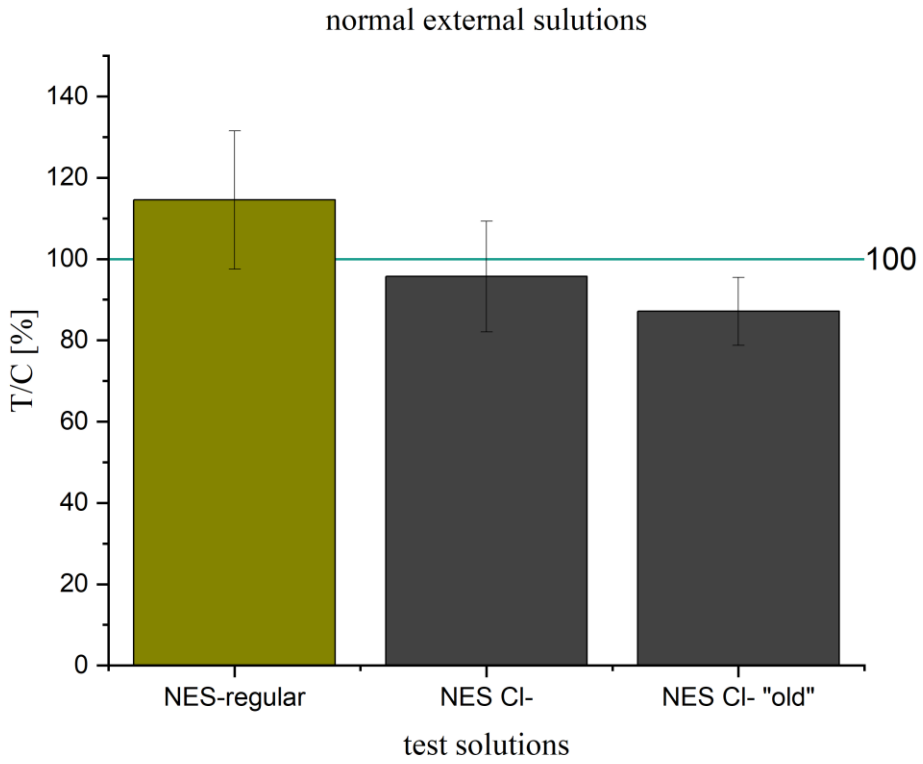

Figure 24: Comparative view of the NES test solutions.
Depicted are the average values from the CellTiter-Blue® (CTB) cytotoxicity assay regarding the test solutions: 1) normal external solution (NES), which was provided by this author's predecessor (Riepl, 2019). 2) chloride-free normal external solution NES Cl^-, 3) normal external solution created by this researcher's predecessor M. Riepl (Riepl, 2019) and provided by the institute (NES Cl^- "old"). The metabolic activity of RTgill-W1 cells in L-15 medium without other test-solutions is considered to be the standard and sets the trendline at 100% (blue line). On the Y-axis are the test-over-control values which depict the percentile metabolic activity of the RTgill-W1 cells for each test solution. It can be observed that the two chloride-free solutions are not dissimilar to each other which verifies the efficacy of their creation as well as their effect on the RTgill-W1 cells.

From this we could theorize that the presence of ions of Cl does indeed factor in in the viability of the cells but does not in itself threaten the cells when absent. Furthermore, as a critique to the experimental procedure, it can be observed that NES “old” which was introduced as a test sample at a later stage clearly has a smaller standard deviation. On the one hand this is a testament to the improvement of the execution of the experimental procedure, but on the other it highlights that the earlier stages of the endeavor were less than perfect.

5.1.6 PSU test solutions comparison

Just like the diagram from batch γ (Figure 23) it seems that the regression of the cell viabilities does not necessarily follow a linear decrease when observing the results wholistically (Figure 25). It was the case that often the standard deviations were disproportionately large which decreases the reliability of many results. It is unclear where the problems were rooted but possible explanations could be a rough handling of the cells, and problematic pipetting of the test solutions in the wells.

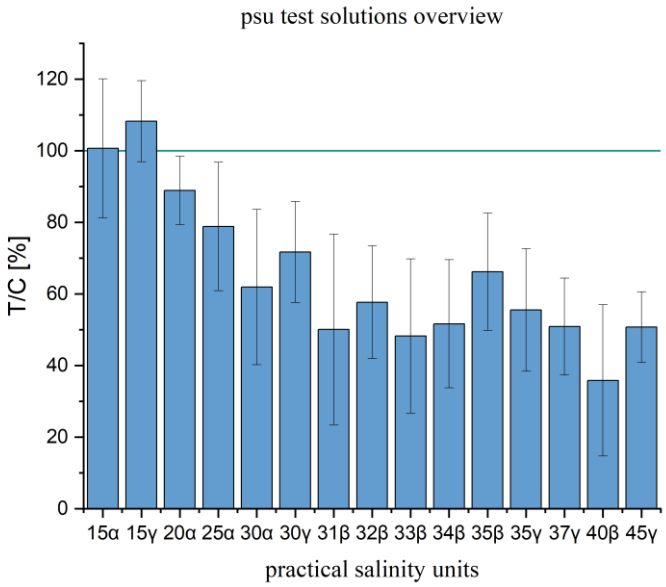

Figure 25: PSU correlations.
Depicted are the result of the CellTiter-Blue® (CTB) cytotoxicity assay regarding the varying salinity test solutions. On the Y-axis is the test-over-control displayed, which uses L-15 medium as the standard (100%) and depicts the percentile metabolic activity of RTgill-W1 cells in contact with the test solutions. On the X-axis are the varying salinity test solutions. The lettering after each number denotes the batch from which each one stems (α, β, γ batch).

5.1.7 Seawater correlation

Seawater is considered to have a salinity of around 33 psu. The standard deviations which can be observed decrease the accuracy with which conclusions can be reliably drawn. Nevertheless, the viability of seawater is consistent to the test solutions with similar salinity concentrations (Figure 26). It could therefore be inferred that the primary factor governing the viability of the RTgill-W1 cells in this experiment is indeed the salinity concentration and no other natural factors found in the seawater like for instance bacterial/viral concentration or other substances. This lends credence to test solutions with different salinities as decent substitutes for natural waters in viability assays.

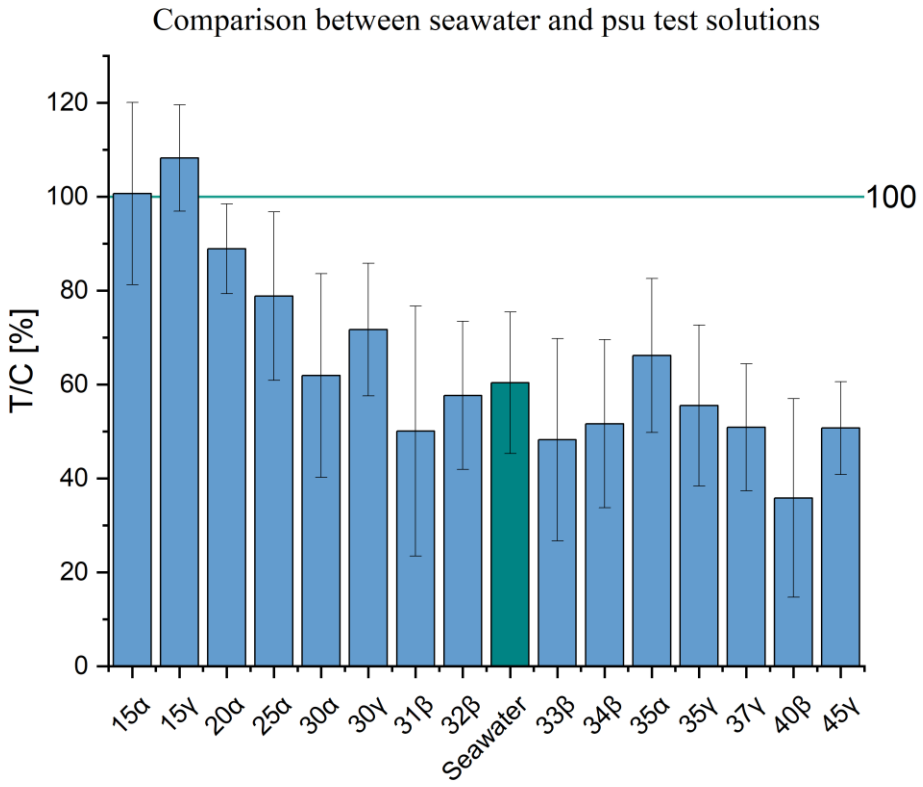

Figure 26: Seawater correlation
Depicted is a correlative ensemble of the varying practical salinity solutions (psu) flanking the test solution "seawater". On the Y-axis is the test-over-control depicted, which uses L-15 medium as the standard for optimum growth (100%) and provides a percentile depiction of the metabolic activity of the RTgill-W1 cells. On the X-axis are the psu test solutions. Seawater is considered to have a psu content of nearly 33% and during the course of the experiments it was considered important to view it relevantly to artificially created psu solutions of the same salinity concentration.

5.1.8 Correlation of batches α and γ

A few of the salinities from previous batches were repeated in batch γ as a means of checking the validity of batch α (Figure 27). In general, the average values are close to each other but the standard deviations of batch γ are smaller than those of batch α. This could indicate that minor errors occurred during the creation of batch α which were present during the experiments but were partly addressed during the creation of batch γ.

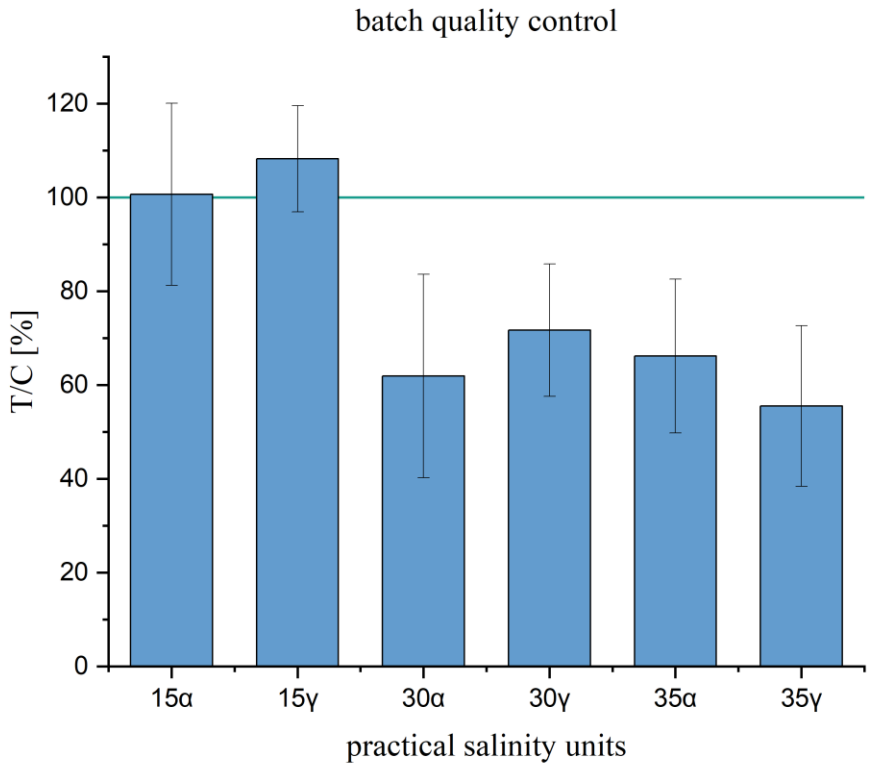

Figure 27: correlation of α and β batch
Depiction of CellTiter-Blue® (CTB) cytotoxicity assay specifically for the practical salinity units (psu) solutions which were in batch α and γ. On the Y-axis is the test-over-control depicted, which uses L-15 medium as the standard for optimum growth (100%) and provides a percentile depiction of the metabolic activity of the RTgill-W1 cells. On the X-axis are the psu test solutions. The recurrent values functioned as means to verify if there were problems in the creation of the solutions or the execution of the experiments. Considering the results have similar average values accompanied with wide standard deviations, it seemed to be the latter.

5.1.9 Triton-X 100

What can be observed from the Triton-X 100 dilutions (Figure 28) is that concentration below 0.01% are much less impactful in their effects. A concentration of 0.1% seems to be completely lethal to cells. Puzzlingly, even though this seems to be the case the very large standard deviations obfuscate the picture. This can most probably be attributed to the very viscous and colloid nature of the substance. In essence the toxic substance did not always reach the cells in the wells the same way.

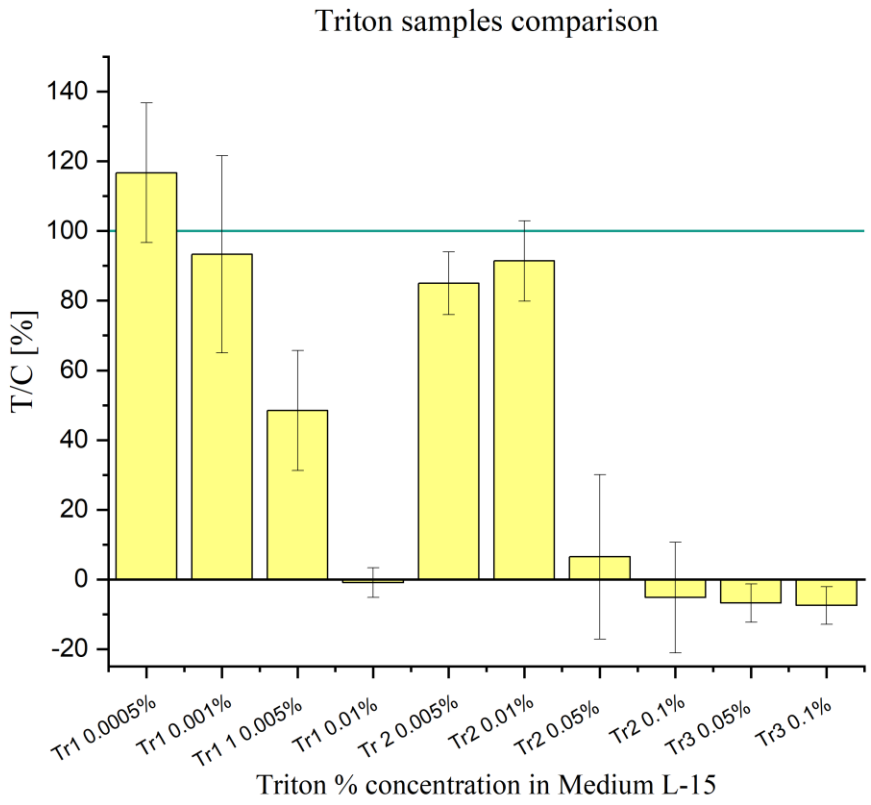

Figure 28: Triton-X 100 correlations
Depiction of CellTiter-Blue® (CTB) cytotoxicity assay specifically for the practical salinity units (psu) solutions which were in batch α and γ. On the Y-axis is the test-over-control depicted, which uses L-15 medium as the standard for optimum growth (100%) and provides a percentile depiction of the metabolic activity of the RTgill-W1 cells. On the X-axis are the concentrations of Triton-X 100 in L-15 medium. Tr1: Sigma Lot # BCBN0659V, Tr2: Roth Art.-Nr. 3051.3 and Tr3 Roth Art.-Nr. 3051.4. It can be observed that the standard deviations (SD) for Triton-X 100 solutions were exceptionally large which can be no doubt linked to the difficult handling of Triton-X 100 as a solution in general.

5.1.10 CTB results under 30% SD

Considering the large relative standard deviations which some test samples exhibited it was termed necessary to be more selective with the results. When considering the test samples with relative standard deviation under 30% observable trends start coming into focus (Figure 29). More specifically, it can be seen that the NES was more supportive of cell viability than the L-15 medium which was used as a basis. Furthermore, it can also be seen that both the NES Cl^- and NES Cl^- "old" allow the RTgill-W1 cells to grow fairly unhindered despite the complete absence of Cl ions, at least in the short term.

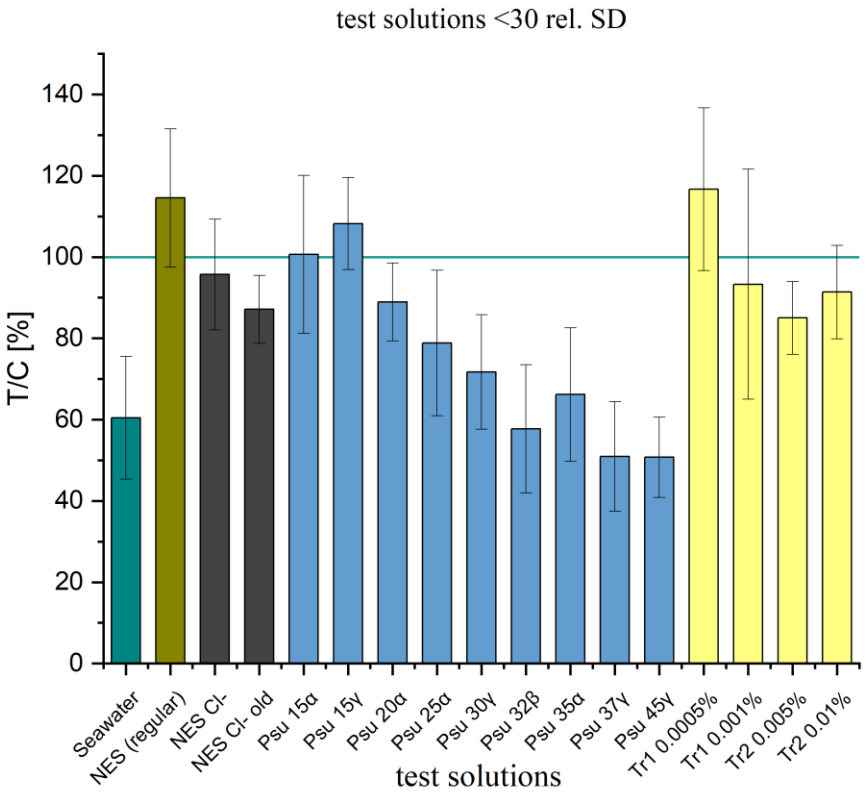

Figure 29: Overview of test solution with under 30% relative standard deviation
Depiction of CellTiter-Blue® (CTB) cytotoxicity assay specifically for the practical salinity units (psu) solutions which were in batch α and γ. On the Y-axis is the test-over-control depicted, which uses L-15 medium as the standard for optimum growth (100%) and provides a percentile depiction of the metabolic activity of the Rtgill-W1 cells. On the X-axis are test solutions which exhibited relative standard deviations (rel. SD) lower than 30%.

The impact of salinities on the viability of the cells is also rather clear to see as viability distinctly decreases with the increase of salt concentration until it reaches a "plateau" after which cell viability, or at least the fluorescent signal, does not decrease

analogically anymore. seawater exhibits values of viability which are consistent with the ones from the neighboring salinities of around 33 psu. This is a good indication, that artificially made salt solutions could indeed be used as substitutes for natural waters of sea and rivers in toxicological studies of HABs and their toxins.

5.2. CTB discussion

The first part of the experimental procedure of the study centered around the use of CTB as the key cytotoxic assay. Just as described in part 5.3.2, the RTgill-W1 cells were seeded into a 96-well plate and left to incubate. The wells were provided with test-solutions after their aspiration and ultimately, after removal of the test solution and addition of the CTB solution, the metabolic activity of the cells was measured fluorometrically following a protocol which is a slight variation from the literature(Lee et al., 2009).

The results of CTB were in large part burdened by large values of standard deviation. Often the relative standard deviation was larger than 30% which makes drawing certain conclusion a tenuous proposition. There could be many possible reasons as to why the standard deviations were as wide, but through observation of the deviations themselves some trends could be observed and therefore have indications about possible problems during the working process. Specifically, the β batch of psu solutions had collectively unreliable values, and it was at some point discovered that an error had taken place during the preparation of these solutions. Namely during the weighing of the chemicals, instead of weighing 0.04 g KCl, 0.40 g were added in their place. This error played a substantial role in the overall problematic behavior of batch β. On the other hand, even though an error, since it took place during preparation of the solutions and not the actual CTB assay, the results should be more reproducible (even if erroneous).

It is highly probable that the large standard deviations can be attributed to pipetting and otherwise handling errors which took place during the experiments. Most notably, performing the experiments in darkness due to the photosensitivity of CTB is probably the main factor which hindered the experimentation procedure.

Additionally, the different exposure times of the RTgill-W1 cells to the air could have contributed to the large standard deviations. During the course of the experiments, the

wells were aspirated one after the other instead of a simultaneous transfer of the well contents into a catch basin as is proposed in other protocols (Dayeh et al., 2013) Keeping the exposure times consistent amongst each well was not possible and this discrepancy must have contributed to the widening of the standard deviation of the results. Furthermore, considering that the aspiration required diligence and caution so as to not harm the RTgill-W1 cell at the bottom of the well, the aspirating cell could not be hastened despite several efforts to that end.

Another point of contention are the results of Triton-X 100. These were originally used as a positive control. However, their results in these experiments made them unsuitable. Their results were extremely irregular, and no reliable conclusions could be drawn from them. The reason for this is most probably the very viscous and colloid nature of the Triton-X 100 itself (Photograph 11). Handling the substance in any repetitive manner was exceptionally challenging. This most probably resulted in non-repetitive errors to be constantly introduced during the experimental procedure. Another point is that Triton-X 100 had a strong tendency to precipitate in solution, requiring constant vortexing and fast pipetting. This could have very well resulted in irregular placement and irregular concentrations in the wells of the 96-well plates resulting in wildly different interactions with the cells. In essence, Triton-X 100 is a poison, and it filled the role of the positive control by killing the RTgill-W1 cells in the well it was introduced. It is highly likely that due to the very viscous, sticky, and concentrated nature of the substance, Triton-X 100 could not reliably and repetitively interact with all the RTgill-W1 cells in the same way when it was introduced to the wells. Despite that, there were results which exhibited relative standard deviation below 30% and through these ones it is more feasible to tentatively draw some conclusions.

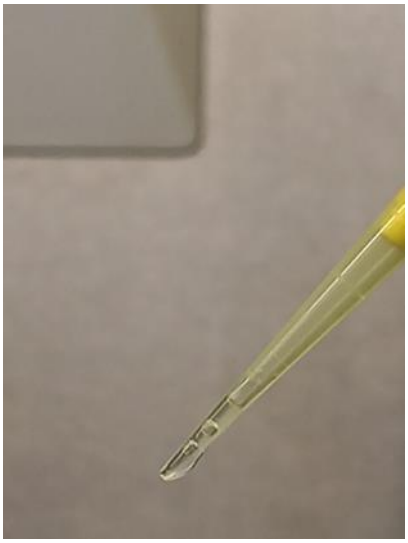

Photograph 11: Micropipette tip carrying Triton-X 100 solution.
The viscous solution was very often imperfectly drawn by the pipette causing bubbles to form inside the tip. Furthermore, the colloid nature of the substance caused it to adhere to exterior of the tip and form a thick layer. In combination, these phenomena drastically inhibited the reliable and measurable use of Triton-X 100 in the experiments.

Most interestingly, the NES solutions seem to exhibit higher viability values than the L-15 medium itself, with 114.5% and 100% metabolic activity respectively (Figure 29). Additionally, considering that the relative standard deviation of these specific results is relatively low, the results are indeed quite reliable. This shows that under certain conditions, the metabolic activity of the cells can be envigored. This is a phenomenon in toxicology known as “Hormesis”. It can be the case toxins or otherwise adverse situations promote the metabolic activity of cells and organisms or their anti-stress responses. The mechanisms behind the Hormesis are not always understood and it has been shown that there are more than one (Calabrese and Baldwin, 2002). Considering that the RTgill-W1 cells are gill cells of fish it is highly likely that they are equipped with anti-stress responses, especially when considering their role for the fish as first-line contacts with the habitat (Bury et al., 2014; Lee et al., 2009).Expanding upon this line of questioning though falls beyond the scope of this study.

The chloride free solutions both current and “old” had narrow standard deviations and viability values which were lower than the L-15 medium (114.5% metabolic activity) but still quite high (95.7% metabolic activity of NES Cl^-, 87.1% metabolic activity of NES Cl^- old). The metabolic activity of the chloride-free mediums was even higher than the value of seawater (metabolic activity 60.4%). This indicates that the absence of Cl ions does not hinder the growth of the RTgill-W1 cells, at least in the short term. In

turn, using Cl-free media in conjunction with HAB-related toxins can indeed help ascertain whether these toxins are Cl ion-mediated and further elucidate the modes/mechanisms of action of these toxins.

The solutions of varying practical salinity units revealed a certain pattern. Namely that the viability of the RTgill-W1 cells decreases with increasing salinity but not in a linear way. It would seem that as the salt concentration increases the viability approaches a plateau at which the effect saturates. There is an interesting possibility that this plateau is in fact the lowest possible level of fluorescence at which the RTgill-W1 cells are no longer viable. CTB is based on the oxidation of resazurin to resorufin in the inside of the cells possibly mediated by enzymes of the cells. Since resazurin enter the cells osmotically, left-over enzymes of dead cells might still be able to oxidize a certain number of resazurin to resorufin enough to produce a signal. This is the point in which a functioning positive control could have provided valuable insights into this line of thinking. Even if it is not the case, the non-linear decrease of viability remains an interesting phenomenon and it could be consistent with the fact that the adverse effects of toxins in general often exhibit sigmoidal behavior. To establish such a pattern and elucidate the full picture of the effects of salinity on RTgill-W1 cells, concentrations on the other end of the spectrum needed to be experimented upon. Namely test solutions with miniscule salinity concentrations, although this would also induce damage to the cells from osmotic stress and skew the sigmoidal curve.

More relevantly, seawater which is considered to have a salinity of around 33 psu (Wolf, 2021) was shown to have been nearly as viable for the RTgill-W1 cells as the artificially created solutions. This might be an indication that the levels of salinity are indeed the main factor effecting the viability of the cells so that considerations of other natural factors like bacterial or viral concentrations are of secondary importance. In other words, simple solutions of L-15 medium and salt can indeed be valuable proxies for such studies. Potentially, it could be very insightful to conduct the same viability experiments with HAB-forming algae instead of RTgill-W1. Considering that bacteria have be shown in the literature to effect algae proliferation and/or HAB toxicity, studying this further could potentially provide valuable insights into HAB formation, HAB sustainability and HAB toxicity (Edvardsen and Paasche, 1998; Granéli et al., 2012).

5.3 CV results

Equally to CTB, CV is also a very practical cytotoxic assay. It is important to note though that other the CTB, CV is toxic and must be handled and dispensed with care. CV was incorporated in this study as tool in order to broaden the approach to the same questions and hopefully elucidate points which the CTB assay was not able to do. To this end, it partially succeeded as it provided results regarding the effects of the Triton-X 100 solutions on the RTgill-W1 cells more clearly (lower standard deviations). However, the results it provided for other test solutions exhibited wider standard deviations then their counterparts in CTB. This is puzzling since poorer execution of the experimental procedure would have resulted in all the results being worse than their counterparts in the CTB assay. This inconsistency was not observed in previous studies(Hochmayr, 2021; Riepl, 2019) and no explanation could be found in the literature. This underlines the importance of multifaceted approaches to research questions, preferably with a battery of test so that each can compensate for the shortcomings of the other.

5.3.1 Overview

After completion of the experiments the results of the CV cytotoxic assays were collected and analyzed with Excel (Table 15). The results were then visualized with Origin (Figure 30). It can be observed that the quality of the results was lower than their counterparts from the CTB assay despite profiting from a more experienced approach. Contrary to that the results of the Triton-X 100 solutions are better with much narrower standard deviations than their counterparts in the CTB assays.

Table 15: CV results overview

Test Solution	**Average value**	**Standard deviation**	**Test Solution**	**Average value**	**Standard deviation**
NES-regular	80.	29.7	Psu 34β	74.1	7.2
NES Cl^-	87.5	18.6	Psu 35α	99.7	15.3
NES Cl^- "old"	85.4	30.5	Psu 35γ	91.0	15.4
Psu 15α	81.8	11.0	Psu 37γ	87.2	6.3

Psu 15γ	103.5	31.4	Psu 40β	87.6	21.4
Psu 20α	112.4	48.6	Psu 45γ	76.7	16.6
Psu 25α	109.6	37.2	Tr1 0.005%	101.7	20.0
Psu 30α	105.4	33.9	Tr1 0.01%	45.7	15.4
Psu 30γ	102.4	22.75573	Tr2 0.05%	15.3	2.0
Psu 31β	92.3	10.1	Tr2 0.1%	17.9	5.1
Psu 32β	87.5	13.6	Tr3 0.05%	19.3	2.1
Psu 33β	53.3	13.4	Tr3 0.1%	16.9	2.3

Depicted are the values of all test solutions which were produced during Crystal Violet (CV) viability assay. These values are the averages from all plates which in turn were the averages of the technical triplicates in each plate. In this Table, NES refers to Normal External Solutions, Psu stands for practical salinity units and refers to the test solutions of varying salinities and Tr refers to the Triton-X 100 solutions. More specifically Tr1: Sigma Lot # BCBN0659V, Tr2: Roth Art.-Nr. 3051.3 and Tr3 Roth Art.-Nr. 3051.4. The standard deviations are only the ones from the various plates while the standard deviations from the technical triplicates were not included.

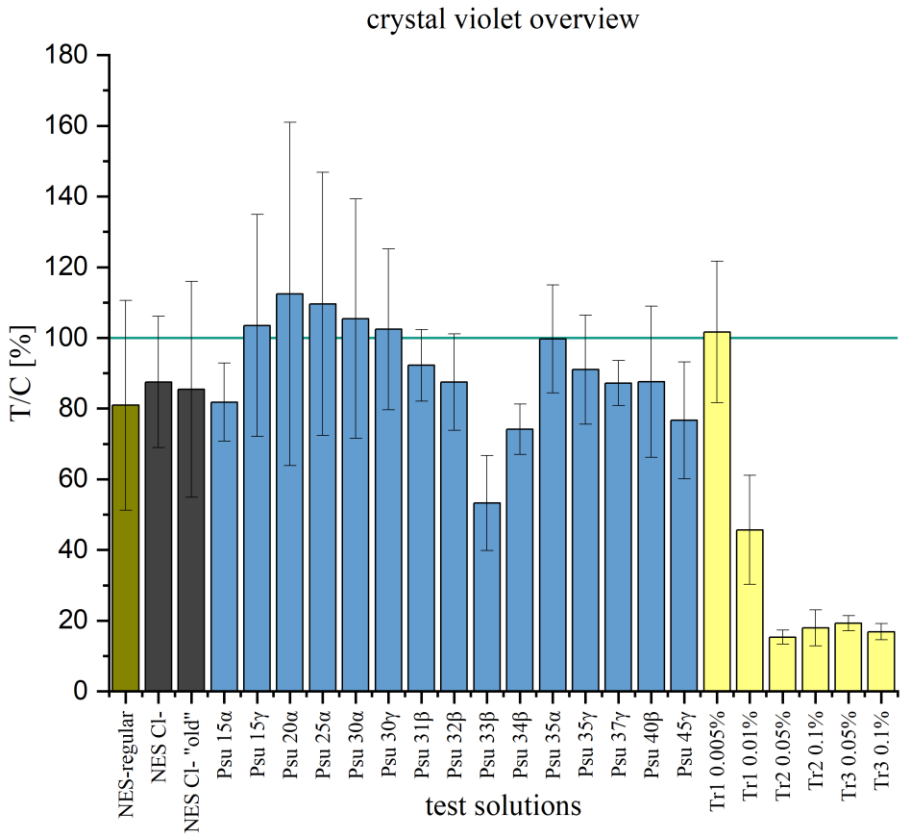

Figure 30: Collective overview of the results of the CV assay
Collective depiction of crystal violet (CV) cytotoxic assay of five biological replicates each having three technical replicates for each test solution. RTgill-W1 cells were incubated for three hours in the presence of the test solutions. On the Y-axis is the test-over-control depicted, which uses L-15 medium as the standard for optimum growth (100%) and provides a percentile depiction of the metabolic activity of the RTgill-W1 cells. On the X-axis are the test solutions. The values for each one is the average value across the test plates, and these were in turn the averages of the triplicates

on each plate. The standard deviations (SD) were only the ones amongst the plates without carrying over the SD of the triplicates themselves.

5.3.2 Correlation of Triton-X 100 solutions

One of the main reasons for using crystal violet was to corroborate the effect of Triton-X 100 on the RTgill-W1 cells. Solutions of Triton-X 100 were used to kill off the cells and thus function as a positive control. However, in practice, the results were excessive and with extraordinary high standard deviations when done with CTB. Predecessors of this study managed to receive more stable results (Hochmayr, 2021). In order to investigate crystal violet was used to provide further data. In this case and despite the fact that crystal violet did not provide better standard deviations for the rest of the test solutions, in regard to the Triton-X 100 solutions, the results were indeed more reliable and repetitive. The results of these experiments were also in line with the results provided by this study's predecessor (Hochmayr, 2021).

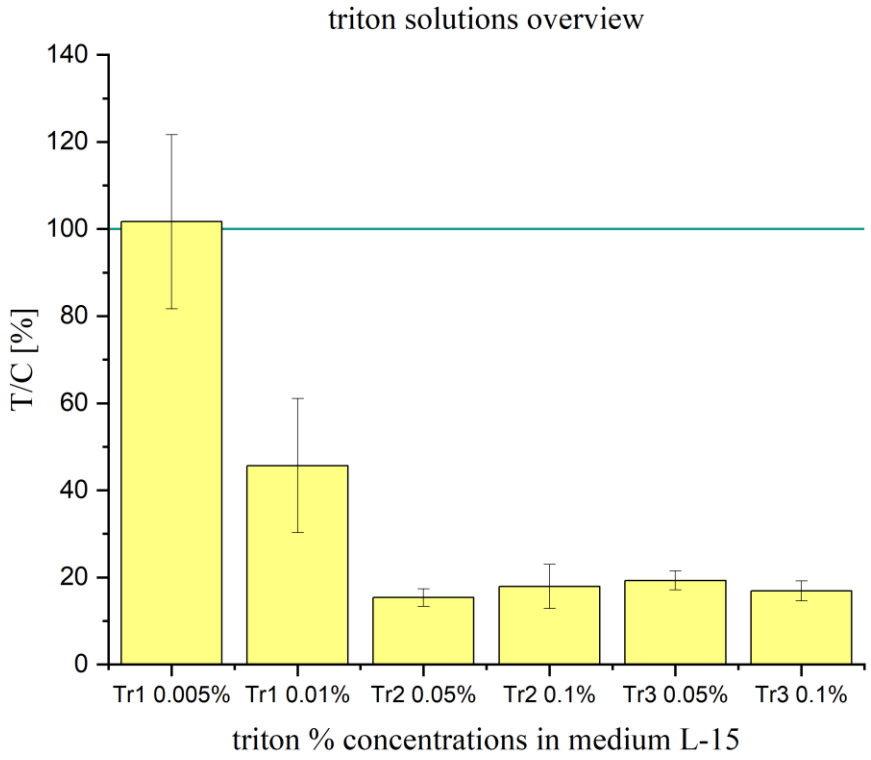

Figure 31: Correlation of Triton-X 100 solutions
Depiction of crystal violet (CV) cytotoxic assay regarding solely the Triton-X 100 solutions. On the Y-axis is the test-over-control depicted, which uses L-15 medium as the standard for optimum growth (100%) and provides a percentile depiction of the metabolic activity of the RTgill-W1 cells. On the X-axis the Triton-X 100 test solutions are provided: Tr1 Sigma Lot # BCBN0659V,

Tr2: Roth Art.-Nr. 3051.3 and Tr3 Roth Art.-Nr. 3051.4. The values for each one is the average value across the test plates, and these were in turn the averages of the triplicates on each plate.

5.3.3 batch α

The test solution of batch α were created with ascending salinity concentration in increments of 5 psu. The CTB assay revealed a gradual decrease in metabolic activity, but this trend cannot be observed here (Figure 32). The high standard deviations (as high as 48.6%) decisively decrease the reliability of the results which are also contrary to what has been established in previous parts of the study (part 5.1.2)

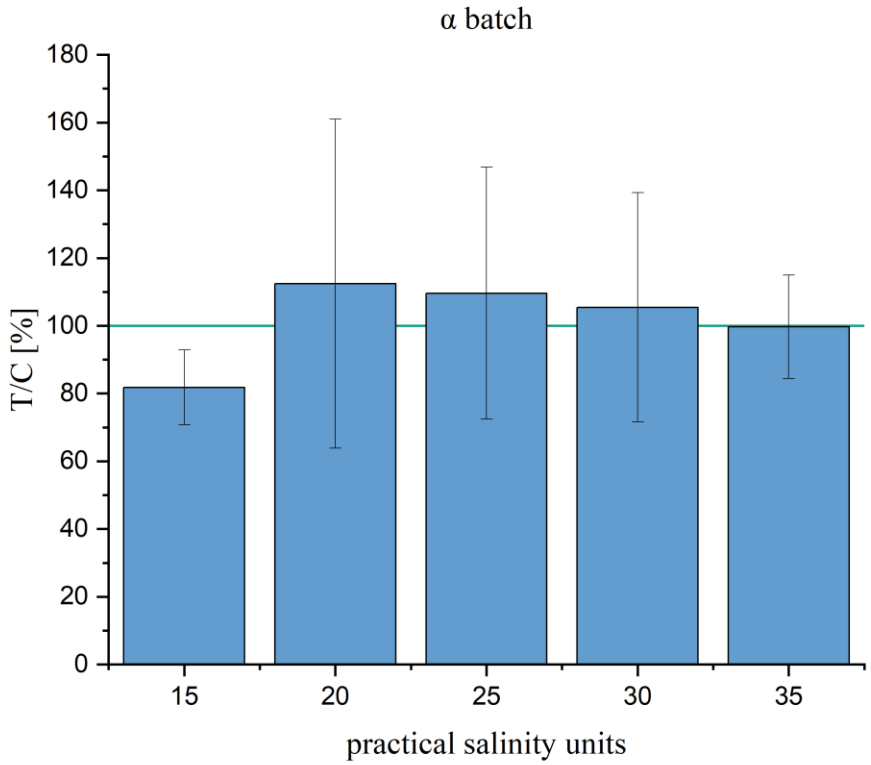

Figure 32: crystal violet results for batch α
Depiction of crystal violet (CV) cytotoxicity assay, specifically for the results concerning batch α. On the Y-axis are the test-over-control (T/C) results displayed and L-15 medium was used as reference for RTgill-W1 cell growth set to 100%. This depicts the percentile metabolic activity of the RTgill-W1 cells in test-solutions. On the X-axis are the practical salinity units (psu). The values for each column results from the average values of all the plates. The standard deviations (SD) concern only the plates without considering the standard deviations of the technical triplicate test solutions in each plate.

5.3.4 batch β

Batch β was created in order to investigate the effects of salinity on the RTgill-W1 cells in detail. The goal was to capture the gradual decline of the metabolic activity with slight increases

in salinity. Additionally, the test solution with 40 psu was meant to provide insights into the effects of salinity beyond psu 35 which was the greatest salinity concentration of batch α. The results of the CV assay for batch β are in contrast to what was expected and also what was established in the CTB assay. It can be seen for instance that psu 40 has a very high metabolic activity (87.6%) (Figure 33) which is highly questionable. Another distinct point of contention is that psu 33 exhibits metabolic activity which is very inconsistent with the values of test solutions which are flanking it.

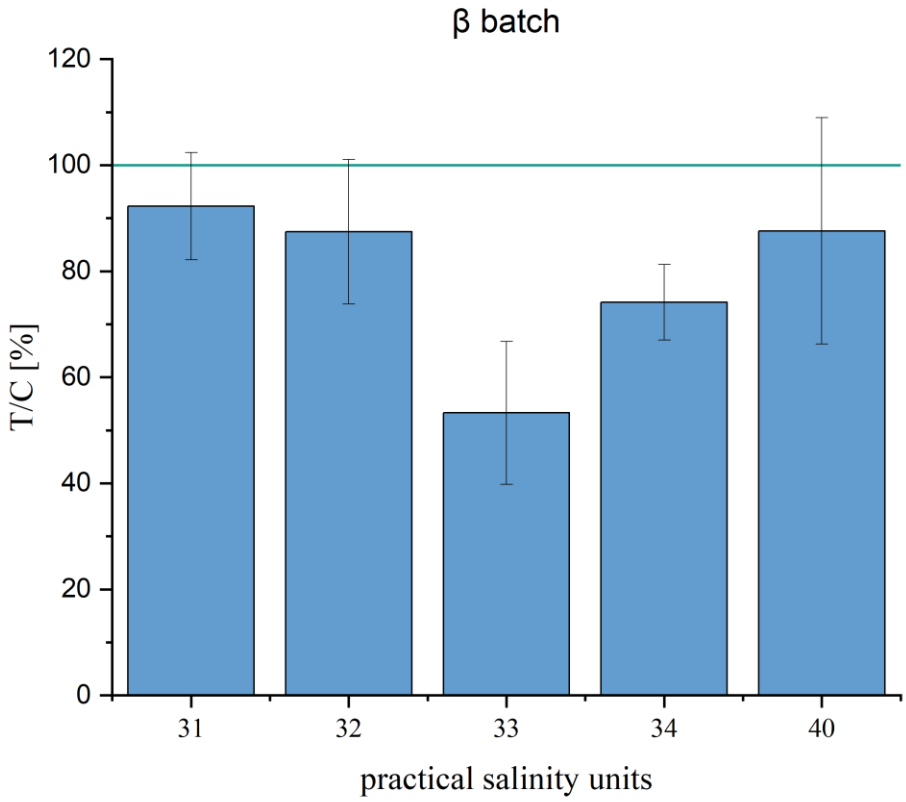

Figure 33: crystal violet results for batch β
Depiction of crystal violet (CV) cytotoxicity assay, specifically for the results concerning batch β. On the Y-axis is test-over-control (T/C) depicted, which uses L-15 medium as the standard for RTgill-W1 cell growth (100%). Depicted is the percentile metabolic activity of the RTgill-W1 cells is test-solutions. On the X-axis are the practical salinity units (psu). The values for each column stem from the average values of all the plates. The standard deviations (SD) concern only the plates without carrying over the standard deviations of the triplicate test solutions in each plate.

5.3.5 Batch γ

Batch γ was created third with the goal of verifying values from the previous two batches. In this case, a gradual decline in metabolic activity can be observed (Figure

34). The standard deviations can call some values into question, particularly psu 15. The observed values of the metabolic activity seem to be fairly high which when compared to the ones from the BTB assay (part 5.2.5).

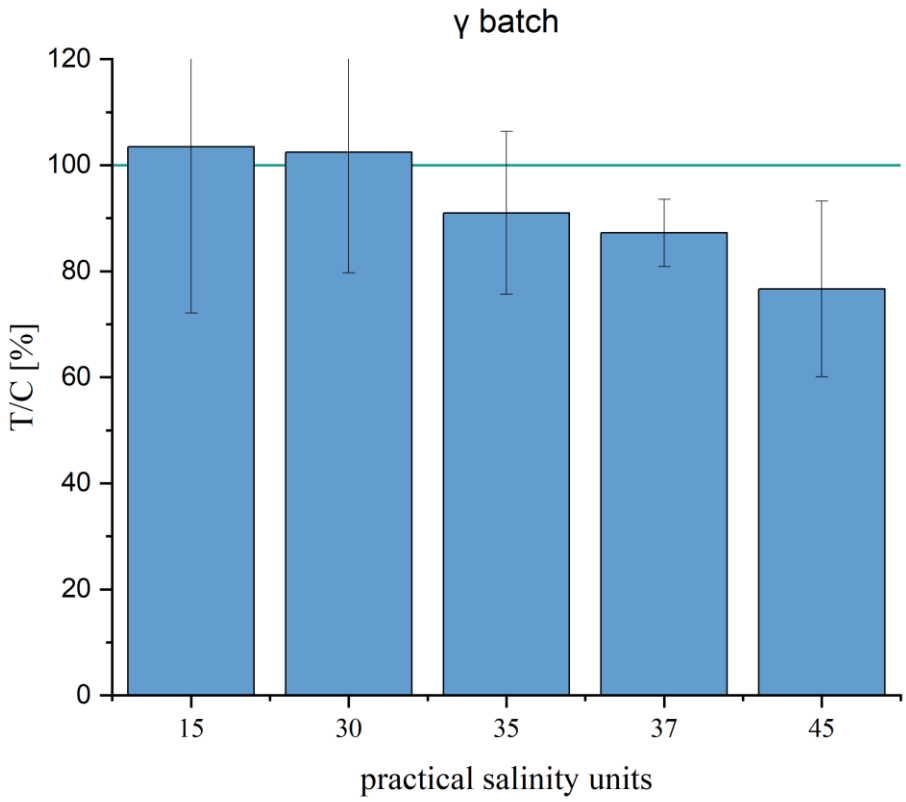

Figure 34: crystal violet results for batch γ

Depiction of crystal violet (CV) cytotoxicity assay, specifically for the results concerning batch γ. On the Y-axis is test-over-control (T/C) depicted, which uses L-15 medium as the standard for RTgill-W1 cell growth (100%). Depicted is the percentile metabolic activity of the RTgill-W1 cells is test-solutions. On the X-axis are the practical salinity units (psu). The values for each column stem from the average values of all the plates. The standard deviations (SD) concern only the plates without carrying over the standard deviations of the triplicate test solutions in each plate.

5.3.6 NES

The correlation of both chloride free NES solution with NES shows that their values are close to each other (Figure 35). The standard deviations though make it hard to observe any trend definitively. Just like in the case of CTB, so too here, it can be seen

that exposure of the RTgill-W1 cells in chloride free medium does not hinder the metabolic activity of the cells, at least not in the short term (3h incubation time). It would be interesting to conduct the same experiments with longer incubation times to see if this would the stay the same.

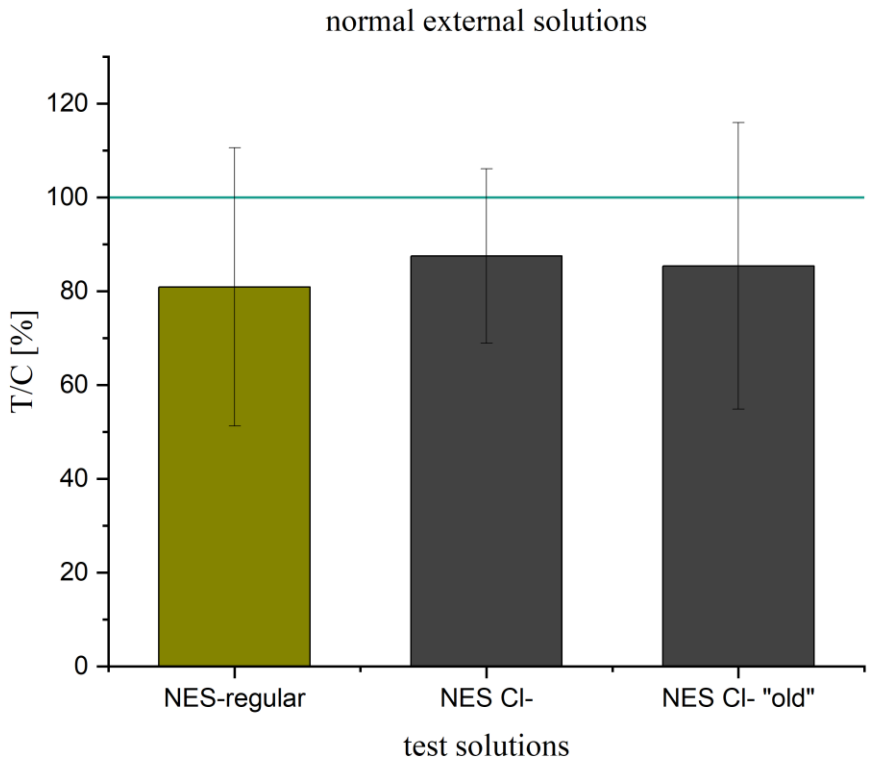

Figure 35: crystal violet results for NES
Depiction of crystal violet (CV) cytotoxicity assay. The test solution in question is the: normal external solution (NES), which was kindly provided by Helene-Christine Prause BSc, MSc, the chloride-free normal external solution (NES Cl^-), which was created by this author, and the equivalent NES Cl^- termed "old" which was created by this author's predecessor M. Riepl (Riepl, 2019). On the Y-axis is test-over-control (T/C) depicted, which uses L-15 medium as the standard for RTgill-W1 cell growth (100%). Depicted is the percentile metabolic activity of the RTgill-W1 cells is test-solutions. On the X-axis are the practical salinity units (psu). The values for each column stem from the average values of all the plates. The standard deviations (SD) concern only the plates without carrying over the standard deviations of the triplicate test solutions in each plate.

5.4 CV discussion

During the course of the CV experiments, RTgill-W1 cells were seeded into 96-well plates and incubated for 48 hours. Test solutions were then be placed into the wells after aspiration of the L-15 medium in which they had been left for three hours.

As described in 4.9.4.2 the test solutions were aspirated from the wells with the use of a multichannel pipette. The cells were fixated to the bottom of the 96-well plate with pre-cooled EtOH. The EtOH was then exchanged in each well with the crystal violet solution. After a short period (5 min) the crystal violet was removed and followed by a washing step. After two days the crystals of CV were dissolved in a solution of 1% acetic acid in 96% EtOH (100 µL per well) (Photograph 12) and were then measured in the plate reader at 560/590 nm.

Working with CV proved to be less challenging due to the ability to conduct the experiments in light in contrast to CTB. This decreased pipetting errors considerably and allowed for a more controlled experimental procedure. On the other hand, the reagents of CV are toxic and had to therefore be handled and disposed with extreme care. Additionally, pattern of displacement of the crystals was observed at the bottom of the wells after use of the multistep pipette during the washing step and it was therefore substituted with the multichannel pipette for a more controlled washing pressure.

Contrary to expectations and despite benefiting from a more practiced and disciplined approach, the standard deviations were holistically less satisfactory than the corresponding ones from the CTB assays. While the trends observed in the CTB experiments can also be observed in the CV assay, they are less clearly visible and are less certain.

These results were surprising due to the fact that as already mentioned the experimental procedure took place with fewer errors and irregularities. A possible explanation could be incompatibility of the assay with the RTgill-W1 cells due to the toxicity of the assay. Another possible explanation, which was proposed by this authors predecessor who faced similar issues, is that the washing steps carry away too many cells to meaningfully measure the impacts of test solutions on them (Hochmayr, 2021). This last explanation was also consistent with the observations of the assay made during this study.

Contrary to the rest of the CV results, the Triton-X 100 solutions in the CV assays are far more consistent than in the CTB assays which gives rise to suspicions of incompatibility between the CTB assay and the Triton-X 100 solutions, although the reason remains unclear. In the CV assays the Triton-X 100 solutions provide the

expected results which are consistent with this Thesis' predecessors (Hochmayr, 2021; Riepl, 2019).

Photograph 12: 96-well plate in crystal violet toxicological assay.
The centerpiece of the cytotoxic assays used in this study were undeniably the 96-well plates. These were used together with an automated plate-reader which was used both in CTB and CV to determine fluorescence. This was in turn used to extrapolate the metabolic activity of the cells when combined with test solutions. The 96-well plates were specifically created to facilitate the growth of cells in the bottoms of their wells. The test solutions were always used in technical triplicates (three wells per test solution) out of which an average value was calculated. In this case, the indicative violet hue in the wells is characteristic of CV assays (Feoktistova et al., 2016; Rampersad, 2012; Riss et al., 2016).

5.5 HPLC-QTOF-MS raw data analysis results

The third and final major part of this study was the manual investigation of raw HPLC-QTOF-MS data which were provided by the institute as part of an overarching research project. Six strains of *P. parvum* (K-0252, PPSR-01, NIES-1017, NIES-1018, RCC-1436, CCAP946) were cultivated in two different salinities (9 psu, 30 psu) in triplicates. The prymnesins were then extracted with methanol and analyzed with HPLC-QTOF-MS (Binzer et al., 2019).

The raw data which were provided, were then analyzed with the software program MassHunter from Agilent Technologies. The C-18 column which was used during the separation phase led to different elution times for the prymnesins. The prymnesins, which are characteristically large polyether ladder-frame molecules, exhibited large and wide chromatograms whose retention times were characteristic of the prymnesins (Binzer et al., 2019). The QTOF-MS analyzer which was coupled to the HPLC created the spectrogram. The key information which was mainly utilized from the spectrum was the isotopic pattern of the prymnesin.

Isotopes have a natural occurrence rate. Consequently, when going through the QTOF-MS prymnesins showed a characteristic isotopic pattern, which was determined by this natural occurrence rate of the isotopes and the sum of their masses. This pattern could be calculated beforehand. The first peak in the pattern, the monoisotopic peak, had to be accounted for, followed by the rest of the isotopic values as well. Use of the monoisotopic peak is advantageous as long as it is possible to distinguish the isotopes experimentally (Barker, 1999 p. 04) which in this case it was. The software program, IsoPad, was used to theoretically calculate the isotopic pattern of each prymnesins as well as its values. The possible prymnesins were summed up in a list and this was used in conjunction with IsoPad. Using the isotopic pattern in MS has the distinct advantage of allowing an analysis without fragment ions and especially fruitful for complex mixtures such as the prymnesins (Barker, 1999 p. 308).

In the cases in which a prymnesin could be definitively shown to be present in the sample, the corresponding area underneath the chromatogram was calculated by integration. The value of the area was consequently analogous to the concentration of the prymnesin within the sample. After analysis of each sample the integrated areas were combined to provide an overview of the percentile presence of each prymnesin.

In this study, for the purposes of depicting the prymnesins succinctly and accurately the proposed systematic name of Binzer et al., (2019) was utilized. The researchers of that study point out that it is not possible to ascribe a chemical name to a molecule which has not been fully elucidated structurally. However the nuanced differences of the discovered prymnesins dictate a need for a systematic approach. In the proposed naming system, PRM-C denotes the 83-carbon backbone of the prymnesin (whose structure is as yet un-elucidated), Cl denotes the number of chlorine atoms, DB denotes

the number of double bonds, O denotes the number of additional oxygen atoms (presumably in OH-group), =O denotes the number of additional keto-groups and hexose/pentose denotes the number of sugar conjugates attached (Binzer et al., 2019).

5.5.1 K-0252 prymnesin C content

The *P. parvum* strain K-0252 had a total of 25 different prymnesins, although not all of them can be found in both 9 and 30 psu (table 16). At 9 psu it could be observed that PRM-C (4Cl + DB) was synthesized predominantly, but at 30 psu no prymnesins was observed to be predominantly synthesized (Figure 36). PRM-C (4 Cl) + 2 hexose was unique for K-0252 and could not be detected in the other strains. Additionally, up until this point, only in-source fragments of this prymnesin had been detected.

Table 16: percentile prymnesin concentrations of K-0252

prymnesin C	9 psu average % presence	standard deviation	30 psu average % presence	standard deviation
PRM-C (2Cl + 2DB)	0.76	0.88	-	-
PRM-C (2 Cl + 2 DB) + pentose	0.59	0.39	-	-
PRM-C (2 Cl + 2 DB) + pentose + hexose	0.13	0.11	-	-
PRM-C (2 Cl + DB)	1.01	2.02	14.79	6.77
PRM-C (2 Cl + DB) + pentose	-	-	9.76	4.68
PRM-C (2 Cl + DB) + 2 pentose	-	-	6.38	2.87
PRM-C (2 Cl)	-	-	10.68	15.10
PRM-C (2 Cl) + 2 pentose	-	-	0.11	0.15
PRM-C (3 Cl + DB)	15.45	3.00	17.32	1.22
PRM-C (3 Cl + DB) + pentose	4.76	4.15	0.45	0.57
PRM-C (3 Cl + DB) + pentose + hexose	0.63	0.73	0.00	0.00
PRM-C (3 Cl + DB) + 2 pentose	1.10	0.98	4.03	3.69
PRM-C (3 Cl + DB) + hexose + 2 pentose	0.17	0.16	0.11	0.02
PRM-C (3Cl)	5.70	11.39	0.06	0.09
PRM-C (3Cl) + pentose	0.09	0.19	-	-
PRM-C (3 Cl) + 2 hexose	-	-	0.07	0.10
PRM-C (4Cl + DB)	51.69	13.97	14.59	3.01

PRM-C (4Cl + DB) + pentose	14.36	4.05	4.48	0.51
PRM-C (4Cl + DB) + pentose + hexose	0.46	0.53	-	-
PRM-C (4Cl + DB) + 2 pentose	2.73	1.87	2.62	3.62
PRM-C (4 Cl + DB) + 2 hexose	-	-	-	0.01
PRM-C (4Cl + DB) + 2 pentose+ hexose	0.24	0.17	0.00	-
PRM-C (4Cl)	-	0.00	14.26	18.56
PRM-C (4 Cl) + 2 pentose	0.12	0.25	-	-
PRM-C (4 Cl) + 2 hexose	-	0.00	0.17	0.24

In the proposed systematic name, PRM-C denotes the 83-carbon backbone of the prymnesin (whose structure is as yet un-elucidated), Cl denotes the number of chlorine atoms, DB denotes the number of double bonds, O denotes the number of additional oxygen atoms (presumably in OH-group), =O denotes the number of additional keto-groups and hexose/pentose denotes the number of sugar conjugates attached (Binzer et al., 2019).

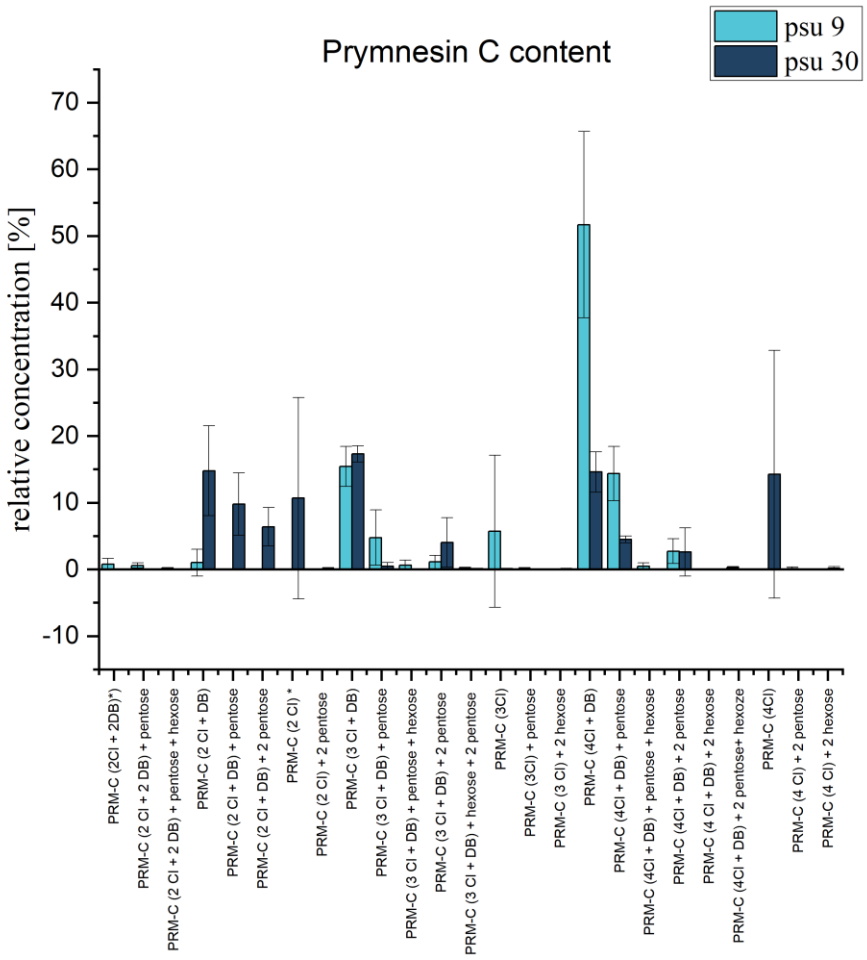

Figure 36: K-0252 prymnesin C content

Depiction of the percentile prymnesin-C content in sample derived from the *P. parvum* strain K-0252. On the Y-axis is the relative concentration. On the X-axis are the prymnesin-Cs which were detected from this specific strain. The strain was cultivated in two different growth cultures with salinities measured in practical salinity units (psu). The columns in light blue depict the results from the 9 psu growth culture and the dark blue depict the results from the 30 psu growth culture. In the proposed systematic name, PRM-C denotes the 83-carbon backbone of the prymnesin (whose structure is as yet un-elucidated), Cl denotes the number of chlorine atoms, DB denotes the number of double bonds, O denotes the number of additional oxygen atoms (presumably in OH-group), =O denotes the number of additional keto-groups and hexose/pentose denotes the number of sugar conjugates attached (Binzer et al., 2019).

5.5.2 PPSR-01 prymnesin C content

The *P. parvum* strain PPSR-01 had a total of 9 prymnesins. Among the six strains which were studied, it is the one with the smallest number of detected prymnesins (Table 17). At 9 psu the prymnesin which is predominant is PRM-C (2Cl) and at 30 psu it is PRM-C (3Cl + DB) (Figure 37). PRM-C (2 Cl) + hexose was a unique prymnesin which could not be found in the other six strains and additionally, this was the first time it could be positively identified apart from in-source fragments. When correlating the two

salinities, no pattern could be established regarding the creation of prymnesins in different salinity concentrations

Table 17: percentile prymnesin concentrations of PPSR-01

prymnesin C	9 psu average % presence	standard deviation	30 psu average % presence	standard deviation
PRM-C (2 Cl + DB)	5.11	8.85	10.73	9.33
PRM-C (2 Cl + DB) + pentose	2.38	4.12	7.26	3.07
PRM-C (2 Cl + DB) + 2 pentose	0.00	0.00	0.57	0.98
PRM-C (2 Cl) + hexose	33.33	57.73	-	-
PRM-C (3 Cl + DB)	18.31	31.72	53.43	3.51
PRM-C (3 Cl + DB) + pentose	7.53	13.04	18.37	7.95
PRM-C (3 Cl + DB) + 2 pentose	-	-	1.34	2.32
PRM-C (4Cl + DB)	-	-	7.96	13.78
PRM-C (4Cl + DB) + pentose	-	-	0.32	0.56

In the proposed systematic name, PRM-C denotes the 83-carbon backbone of the prymnesin (whose structure is as yet un-elucidated), Cl denotes the number of chlorine atoms, DB denotes the number of double bonds, O denotes the number of additional oxygen atoms (presumably in OH-group), =O denotes the number of additional keto-groups and hexose/pentose denotes the number of sugar conjugates attached (Binzer et al., 2019).

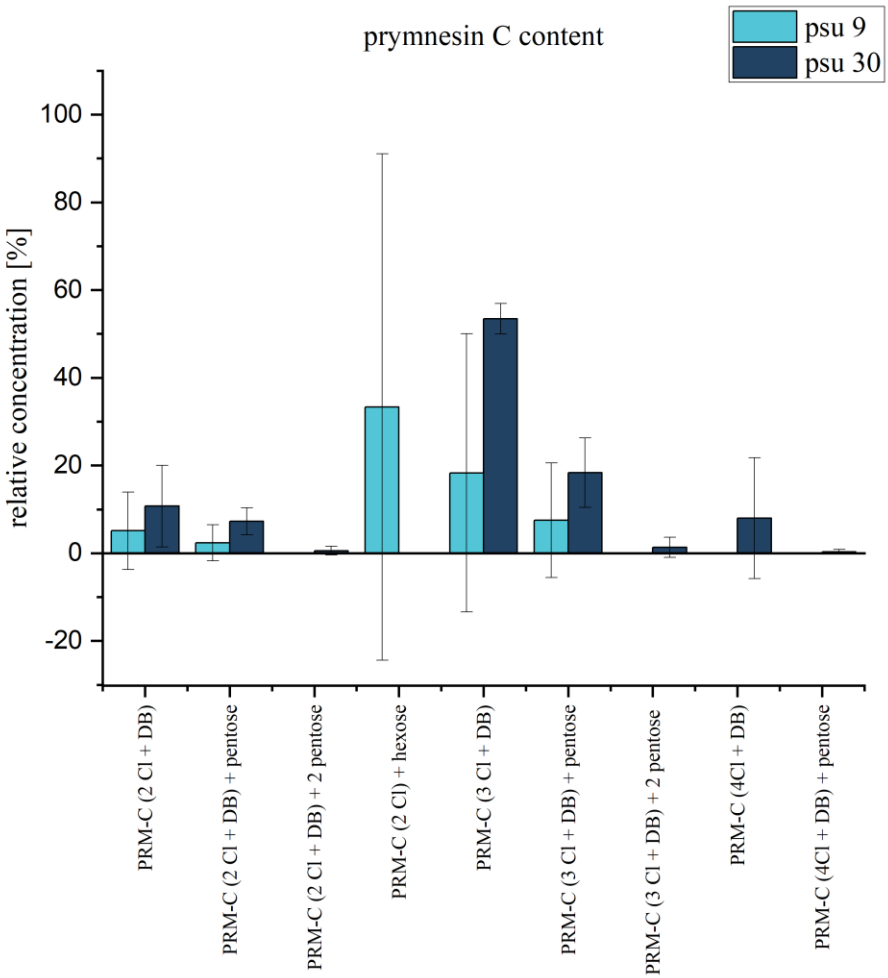

Figure 37: PPSR-01 prymnesin-C content

Depiction of the percentile prymnesin-C content in sample derived from the *P. parvum* strain PPSR-01. On the Y-axis is the relative concentration. On the X-axis are the prymnesin-Cs which were detected from this specific strain. The strain was cultivated in two different growth cultures with salinities measured in practical salinity units (psu). The columns in light blue depict the results from the 9 psu growth culture and the dark blue depict the results from the 30 psu growth culture. In the proposed systematic name, PRM-C denotes the 83-carbon backbone of the prymnesin (whose structure is as yet un-elucidated), Cl denotes the number of chlorine atoms, DB denotes the number of double bonds, O denotes the number of additional oxygen atoms (presumably in OH-group), =O denotes the number of additional keto-groups and hexose/pentose denotes the number of sugar conjugates attached (Binzer et al., 2019).

5.5.3 NIES-1017 prymnesin C content

In the *P. parvum* strain NIES-1017 a total of 26 prymnesins were identified (Table 18). Out of these, PRM-C (2 Cl + 2 DB) + 2 hexose and PRM-C (4 Cl + 3 =O + 3 O) + hexose were unique among the six strains. Additionally they detected for the first time.

Next to them, other prymnesins which were also identified for the first time were PRM-C (2 Cl + 2 DB) + 2 hexose, PRM-C (4 Cl + DB) + 2 hexose, and PRM-C (4 Cl) + 2 pentose. At 9 psu, the prymnesin PRM-C (4Cl + DB) was synthesized by the algae almost predominantly, while at 30 psu no one prymnesin holds such a position (Figure 38). Additionally, similarly to the other strains no pattern could be established regarding the creation of prymnesins in different salinities.

Table 18: percentile prymnesin concentrations of NIES-1017

prymnesin C	9 psu average % presence	standard deviation	30 psu average % presence	standard deviation
PRM-C (2Cl + 2DB)	0.24	0.55	-	-
PRM-C (2 Cl + 2 DB) + pentose	0.08	0.17	-	-
PRM-C (2 Cl + 2 DB) + 2 hexose	1.10	2.46	-	-
PRM-C (2 Cl + 2 DB) + 2 pentose + hexose	-	-	0.10	0.18
PRM-C (2 Cl + DB)	1.38	1.98	9.47	11.65
PRM-C (2 Cl + DB) + pentose	1.23	2.57	15.76	11.05
PRM-C (2 Cl + DB) + pentose + hexose	-	-	-	-
PRM-C (2 Cl + DB) + 2 pentose	-	-	4.58	4.13
PRM-C (3 Cl + DB)	16.63	1.66	27.08	13.97
PRM-C (3 Cl + DB) + pentose	4.59	3.01	4.24	2.19
PRM-C (3 Cl + DB) + pentose + hexose	0.28	0.47	0.51	1.02
PRM-C (3 Cl + DB) + 2 pentose	0.75	0.87	3.90	4.32
PRM-C (3 Cl + DB) + hexose + 2 pentose	-	-	0.17	0.24
PRM-C (3Cl)	4.87	10.89	0.41	0.82
PRM-C (3Cl) + pentose	4.26	2.90	10.93	14.16
PRM-C (3Cl) + 2 pentose	-	-	1.75	3.51
PRM-C (3 Cl) + 2 hexose	-	-	0.06	0.07
PRM-C (3Cl) + 2 pentose + hexose	-	-	0.03	0.05
PRM-C (4Cl + DB)	45.63	10.23	13.61	5.37
PRM-C (4Cl + DB) + pentose	15.24	5.26	2.96	2.36
PRM-C (4Cl + DB) + pentose + hexose	0.18	0.27	0.10	0.19

PRM-C (4Cl + DB) + 2 pentose	3.05	1.51	1.08	1.39
PRM-C (4 Cl + DB) + 2 hexose	-	-	0.03	0.04
PRM-C (4Cl)	0.00	0.00	3.18	6.36
PRM-C (4 Cl) + 2 pentose	0.48	1.08	0.00	0.00
PRM-C (4 Cl + 3 =O + 3 O) + hexose	-	-	0.03	0.05

In the proposed systematic name, PRM-C denotes the 83-carbon backbone of the prymnesin (whose structure is as yet un-elucidated), Cl denotes the number of chlorine atoms, DB denotes the number of double bonds, O denotes the number of additional oxygen atoms (presumably in OH-group), =O denotes the number of additional keto-groups and hexose/pentose denotes the number of sugar conjugates attached (Binzer et al., 2019).

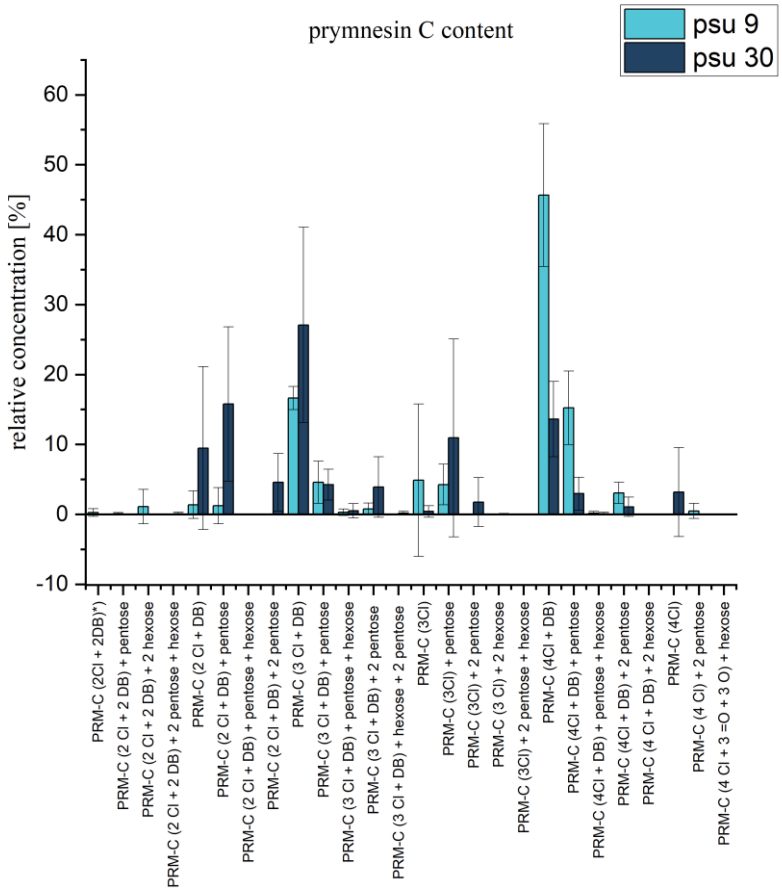

Figure 38: NIES-1017 prymnesin-C content

Depiction of the percentile prymnesin-C content in sample derived from the *P. parvum* strain NIES-1017. On the Y-axis is the relative concentration. On the X-axis are the prymnesin-Cs which were detected from this specific strain. The strain was cultivated in two different growth cultures with salinities measured in practical salinity units (psu). The columns in light blue depict the results from the 9 psu growth culture and the dark blue depict the results from the 30 psu growth culture. In the proposed systematic name, PRM-C denotes the 83-carbon backbone of the prymnesin (whose structure is as yet un-elucidated), Cl denotes the number of chlorine atoms, DB denotes the number of double bonds, O denotes the number of additional oxygen atoms (presumably in OH-group), =O denotes the number of additional keto-groups and hexose/pentose denotes the number of sugar conjugates attached (Binzer et al., 2019).

5.5.4 RCC-1436 prymnesin C content

The RCC-1436 *P. parvum* strain had a total of 28 prymnesins and almost all of them could be detected in both 9 and 30 psu (Table 19). Among these prymnesins, PRM-C (4 Cl + DB) + hexose was unique as it could only be detected in this strain and none of the other five. At 9 psu the prymnesin which was most abundant was PRM-C (4Cl + DB) while at 30 psu it was PRM-C (4 Cl + DB) + hexose (Figure 39). The prymnesins PRM-C (2Cl + 2DB), PRM-C (2 Cl), PRM-C (4 Cl + DB) + hexose and PRM-C (4 Cl + DB) + 2 hexose were detected for the first time (even if present in the other strains as well).

Table 19: percentile prymnesin concentrations of RCC-1436

prymnesin C	9 psu average % presence	standard deviation	30 psu average % presence	standard deviation
PRM-C (2Cl + 2DB)	0.17	0.37	1.75	1.64
PRM-C (2 Cl + 2 DB) + pentose	0.14	0.21	0.07	0.12
PRM-C (2 Cl + 2 DB) + pentose + hexose	0.09	0.12	-	-
PRM-C (2 Cl + DB)	5.65	11.07	4.55	4.30
PRM-C (2 Cl + DB) + pentose	3.40	5.83	2.71	1.93
PRM-C (2 Cl + DB) + 2 pentose	1.28	2.80	1.21	0.62
PRM-C (2 Cl)	-	-	2.24	3.87
PRM-C (2 Cl) + pentose	-	-	0.63	1.09
PRM-C (2 Cl) + 2 pentose	0.01	0.03	0.20	0.34
PRM-C (3 Cl + DB)	11.74	8.11	34.11	32.00
PRM-C (3 Cl + DB) + pentose	3.99	3.07	8.98	8.32
PRM-C (3 Cl + DB) + pentose + hexose	0.38	0.52	0.11	0.20
PRM-C (3 Cl + DB) + 2 pentose	1.31	2.55	0.78	0.68
PRM-C (3 Cl + DB) + hexose + 2 pentose	0.07	0.10	0.02	0.03
PRM-C (3Cl)	10.51	16.02	10.52	18.22
PRM-C (3Cl) + pentose	0.07	0.16	2.34	4.05
PRM-C (3Cl) + 2 pentose	0.03	0.06	0.89	1.55

PRM-C (3Cl) + 2 pentose + hexose	-	-	0.04	0.08
PRM-C (4Cl + DB)	36.30	15.60	17.09	23.63
PRM-C (4Cl + DB) + pentose	6.53	7.47	5.52	4.94
PRM-C (4 Cl + DB) + hexose	-	-	-	-
PRM-C (4Cl + DB) + pentose + hexose	0.63	0.38	0.06	0.10
PRM-C (4Cl + DB) + 2 pentose	0.81	1.34	0.31	0.27
PRM-C (4 Cl + DB) + 2 hexose	-	-	0.05	0.07
PRM-C (4Cl + DB) + 2 pentose+ hexose	0.02	0.05	-	-
PRM-C (4Cl)	11.76	25.69	3.77	6.53
PRM-C (4Cl +3 =O +3O)	4.01	7.09	1.79	3.10
PRM-C (4Cl +3 =O + 3O) + pentose	1.06	2.37	0.26	0.44

In the proposed systematic name, PRM-C denotes the 83-carbon backbone of the prymnesin (whose structure is as yet un-elucidated), Cl denotes the number of chlorine atoms, DB denotes the number of double bonds, O denotes the number of additional oxygen atoms (presumably in OH-group), =O denotes the number of additional keto-groups and hexose/pentose denotes the number of sugar conjugates attached (Binzer et al., 2019).

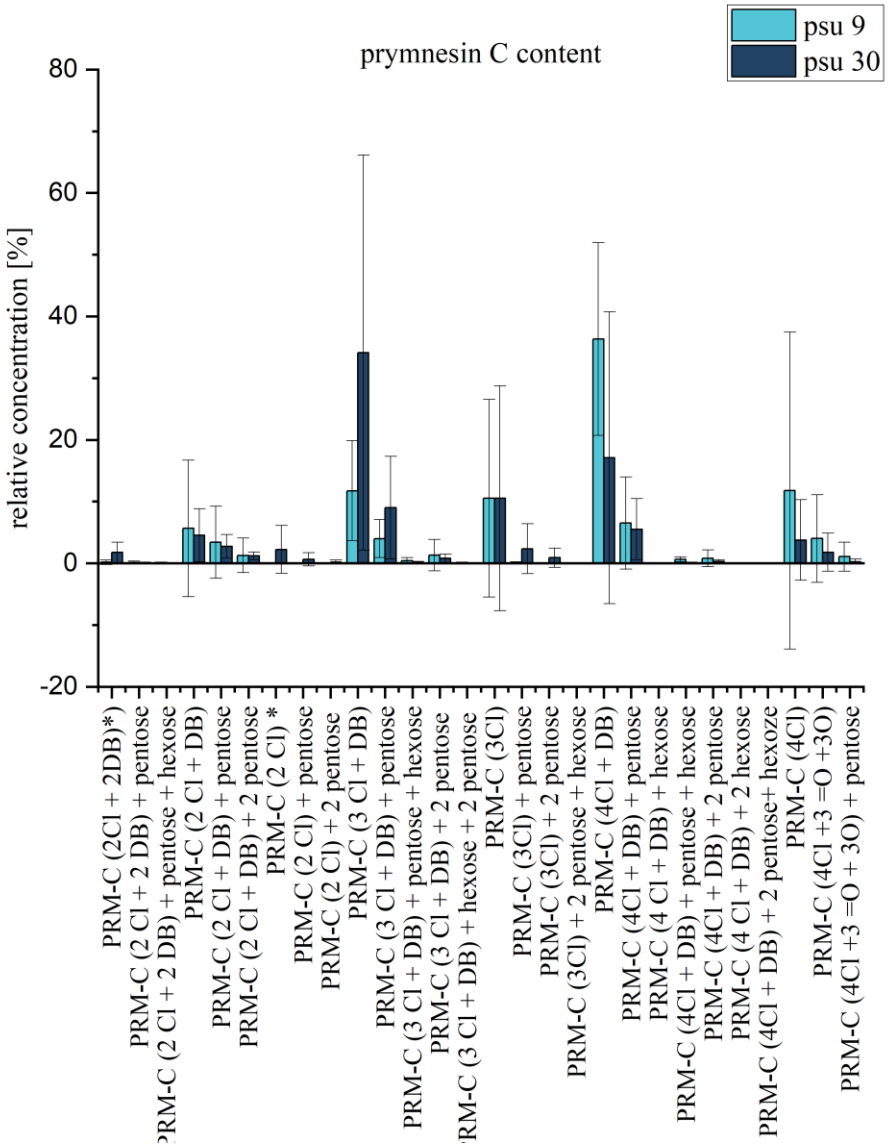

Figure 39: RCC-1436 prymnesin-C content

Depiction of the percentile prymnesin-C content in sample derived from the *P. parvum* strain RCC-1436. On the Y-axis is the relative concentration. On the X-axis are the prymnesin-Cs which were detected from this specific strain. The strain was cultivated in two different growth cultures with salinities measured in practical salinity units (psu). The columns in light blue depict the results from the 9 psu growth culture and the dark blue depict the results from the 30 psu growth culture. In the proposed systematic name, PRM-C denotes the 83-carbon backbone of the prymnesin (whose structure is as yet un-elucidated), Cl denotes the number of chlorine atoms, DB denotes the number of double bonds, O denotes the number of additional oxygen atoms (presumably in OH-group), =O denotes the number of additional keto-groups and hexose/pentose denotes the number of sugar conjugates attached (Binzer et al., 2019).

5.5.5 NIES-1018 prymnesin C content

The *P. parvum* strain NIES-1018 had a total of 24 prymnesins, but not all them could be detected in both 9 and 30 salinities (Table 20). In this case there were no prymnesins which could be characterized as predominantly created although some are certainly more abundant than others like PRM-C (3 Cl + DB) and PRM-C (4Cl + DB) for 9 psu, and PRM-C (2 Cl + DB) and PRM-C (3 Cl + DB) for 30 psu (Figure 40). The stain NIES-1018 had three pymnesins which could not be detected in the other five strains and were therefore unique. These were: PRM-C (2 Cl + DB) + hexose + 2 pentose, PRM-C (2 Cl) + hexose + 2 pentose and PRM-C (4 Cl + 3 =O + 3 O) + pentose + hexose. The last two had not been detected before apart from in-source fragments. The other prymnesin which were also detected for the first time here (as well as in the other strains) were PRM-C (2Cl + 2DB).

Table 20: percentile prymnesin concentrations of NES-1018

prymnesin C	9 psu average % presence	standard deviation	30 psu average % presence	standard deviation
PRM-C (2Cl + 2DB)	-	-	0.4	0.6
PRM-C (2 Cl + 2 DB) + pentose	-	-	0.2	0.4
PRM-C (2 Cl + 2 DB) + pentose + hexose	-	-	0.4	0.6
PRM-C (2 Cl + 2 DB) + 2 pentose + hexose	-	-	-	0.1
PRM-C (2 Cl + DB)	-	-	24.0	7.2
PRM-C (2 Cl + DB) + pentose	-	-	15.0	4.4
PRM-C (2 Cl + DB) + pentose + hexose	-	-	0.6	1.0
PRM-C (2 Cl + DB) + 2 pentose	-	-	1.1	1.2
PRM-C (2 Cl + DB) + hexose + 2 pentose	-	-	-	0.1
PRM-C (2 Cl) + hexose + 2 pentose	-	-	-	0.1
PRM-C (3 Cl + DB)	22.5	7.3	24.5	12.5
PRM-C (3 Cl + DB) + pentose	2.6	2.4	6.5	6.6
PRM-C (3 Cl + DB) + pentose + hexose	-	-	0.6	0.6
PRM-C (3 Cl + DB) + 2 pentose	-	-	0.5	0.6

PRM-C (3 Cl + DB) + hexose + 2 pentose	-	-	0.2	0.2
PRM-C (3Cl)	15.8	27.3	9.4	16.3
PRM-C (3Cl) + pentose	14.0	24.2	4.1	6.3
PRM-C (3Cl) + 2 pentose	-	-	-	-
PRM-C (4Cl + DB)	37.4	15.2	7.0	7.2
PRM-C (4Cl + DB) + pentose	7.7	6.7	3.0	3.4
PRM-C (4Cl + DB) + pentose + hexose	-	-	0.1	0.1
PRM-C (4Cl + DB) + 2 pentose	-	-	0.4	0.7
PRM-C (4Cl + DB) + 2 pentose+ hexose	-	-	0.1	0.1
PRM-C (4 Cl + 3 =O + 3 O) + pentose + hexose	-	-	1.6	2.7

In the proposed systematic name, PRM-C denotes the 83-carbon backbone of the prymnesin (whose structure is as yet un-elucidated), Cl denotes the number of chlorine atoms, DB denotes the number of double bonds, O denotes the number of additional oxygen atoms (presumably in OH-group), =O denotes the number of additional keto-groups and hexose/pentose denotes the number of sugar conjugates attached (Binzer et al., 2019).

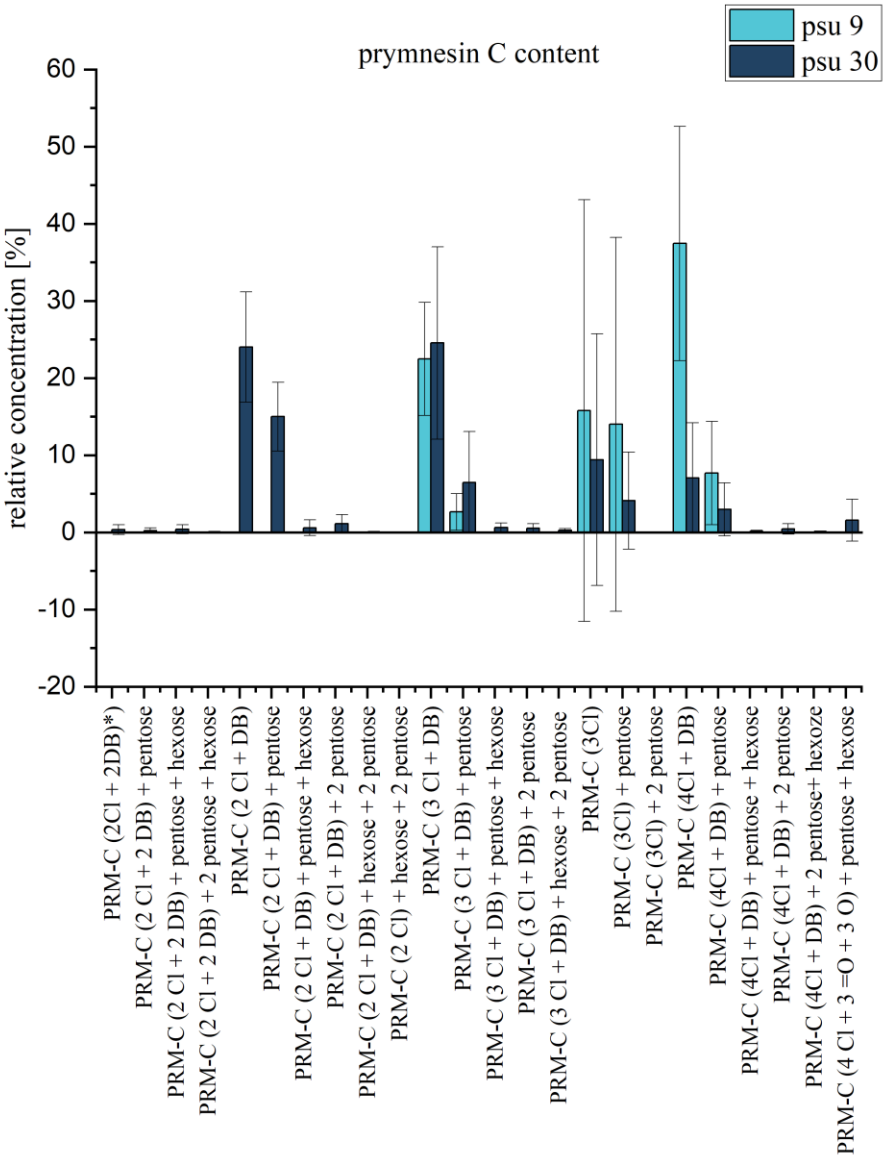

Figure 40: NIES-1018 prymnesin-C content

Depiction of the percentile prymnesin-C content in sample derived from the *P. parvum* strain NIES-1018. On the Y-axis is the relative concentration. On the X-axis are the prymnesin-Cs which were detected from this specific strain. The strain was cultivated in two different growth cultures with salinities measured in practical salinity units (psu). The columns in light blue depict the results from the 9 psu growth culture and the dark blue depict the results from the 30 psu growth culture. In the proposed systematic name, PRM-C denotes the 83-carbon backbone of the prymnesin (whose structure is as yet un-elucidated), Cl denotes the number of chlorine atoms, DB denotes the number of double bonds, O denotes the number of additional oxygen atoms (presumably in OH-group), =O denotes the number of additional keto-groups and hexose/pentose denotes the number of sugar conjugates attached (Binzer et al., 2019).

5.5.6 CCAP946 prymnesin C content

The *P. parvum* strain CCAP946 had a total of 24 prymnesins almost all of which could be detected in both 9 and 30 psu (Table 21). For this strain, one prymnesin: PRM-C (2 Cl + 2 DB) + hexose, could only be detected in this strain and not in the other five strains. It could also be observed, that the prymnesin PRM-C (4Cl + DB) was predominantly synthesized in both 9 and 30 psu, followed by PRM-C (3 Cl + DB) (also in both salinities) (Figure 41). In this strain, the results of the two salinities reverberate each other.

Table 21: percentile prymnesin concentrations of CCAP946

prymnesin C	9 psu average % presence	standard deviation	30 psu average % presence	standard deviation
PRM-C (2Cl + 2DB)	-	-	0.18	0.37
PRM-C (2 Cl + 2 DB) + pentose	0.07	0.09	-	-
PRM-C (2 Cl + 2 DB) + hexose	0.29	0.41	-	-
PRM-C (2 Cl + DB)	0.51	0.72	2.06	2.68
PRM-C (2 Cl + DB) + pentose	0.72	0.32	1.86	2.78
PRM-C (2 Cl + DB) + 2 pentose	-	-	0.04	0.08
PRM-C (2 Cl)	0.55	0.78	6.97	11.88
PRM-C (2 Cl) + pentose	0.00	0.00	0.45	0.90
PRM-C (3 Cl + DB)	19.34	13.21	21.76	16.46
PRM-C (3 Cl + DB) + pentose	5.99	2.34	1.25	1.73
PRM-C (3 Cl + DB) + pentose + hexose	0.76	0.13	-	-
PRM-C (3 Cl + DB) + 2 pentose	0.62	0.88	0.06	0.13
PRM-C (3 Cl + DB) + hexose + 2 pentose	0.05	0.06	-	0.00
PRM-C (3Cl)	-	-	0.05	0.10
PRM-C (3Cl) + pentose	-	-	3.08	6.07
PRM-C (3Cl) + 2 pentose	-	-	0.14	0.28
PRM-C (4Cl + DB)	52.24	5.47	42.02	30.21
PRM-C (4Cl + DB) + pentose	12.03	8.58	10.45	7.09
PRM-C (4Cl + DB) + pentose + hexose	1.01	0.73	0.09	0.18

PRM-C (4Cl + DB) + 2 pentose	0.92	1.30	0.17	0.20
PRM-C (4Cl + DB) + 2 pentose+ hexose	0.33	0.10	-	-
PRM-C (4Cl)	-	-	0.29	0.57
PRM-C (4Cl +3 =O +3O)	3.87	1.49	8.46	10.14
PRM-C (4Cl +3 =O + 3O) + pentose	0.70	0.99	0.61	0.77

In the proposed systematic name, PRM-C denotes the 83-carbon backbone of the prymnesin (whose structure is as yet un-elucidated), Cl denotes the number of chlorine atoms, DB denotes the number of double bonds, O denotes the number of additional oxygen atoms (presumably in OH-group), =O denotes the number of additional keto-groups and hexose/pentose denotes the number of sugar conjugates attached (Binzer et al., 2019).

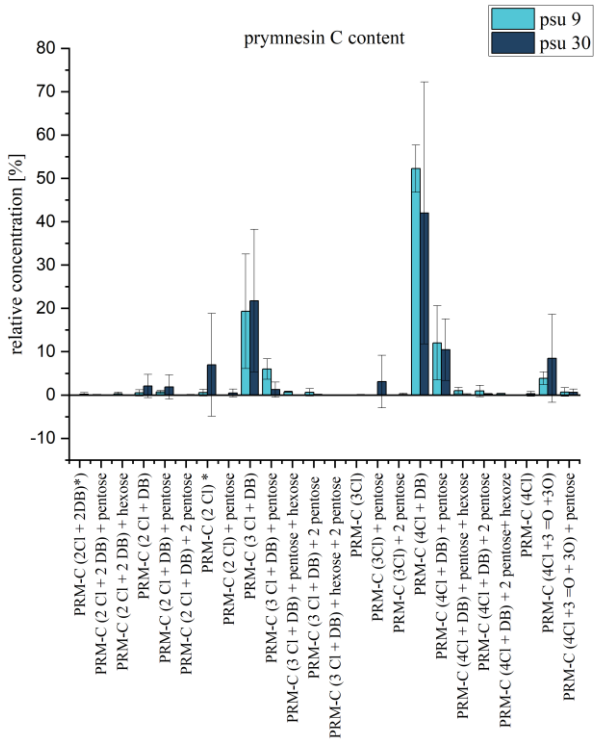

Figure 41: CCAP946 prymnesin-C content

Depiction of the percentile prymnesin-C content in sample derived from the *P. parvum* strain CCAP946. On the Y-axis is the relative concentration. On the X-axis are the prymnesin-Cs which were detected from this specific strain. The strain was cultivated in two different growth cultures with salinities measured in practical salinity units (psu). The columns in light blue depict the results from the 9 psu growth culture and the dark blue depict the results from the 30 psu growth culture. In the proposed systematic name, PRM-C denotes the 83-carbon backbone of the prymnesin (whose structure is as yet un-elucidated), Cl denotes the number of chlorine atoms, DB denotes the number of double bonds, O denotes the number of additional oxygen atoms (presumably in OH-group), =O denotes the number of additional keto-groups and hexose/pentose denotes the number of sugar conjugates attached (Binzer et al., 2019).

5.6 HPLC-QTOF-MS raw data analysis discussion

Due to the lack of commercially available standards the method could only provide relative results and not absolute values. The absence of commercially available standard hinges on the scarcity of these substances in nature and the challenges in isolating them. This obstacle very often hinders studies of prymnesins (Manning and La Claire, 2013).

Another major problem were the frequent co-elutions of similar prymnesins. This was quite possibly the most crucial hindrance since the areas under the chromatograms could not be reliably attributed to a single prymnesin. This was a major problem since it further decreased the reliability of the results.

Consequently, the process of manually investigating the HPLC-QTOF-MS data could become vary labor-intensive, time-consuming, and error-prone. The investigation frequently required efforts to compensate for the afore mentioned problems. Ultimately it was necessary to prove/disprove the presence/absence of each possible prymnesin in each sample.

Despite the hindrances, it was possible to make certain observations and reach conclusions. It was observed by this author's predecessor that each sample predominantly contain a few select prymnesins while the rest of the prymnesins in the sample had much smaller concentrations (Hochmayr, 2021). This observation seems to be supported by the findings of this study as well. Even with the impeding co/elutions the picture is clearly one of a preferential biosynthesis favoring certain prymnesins over others. Additionally, it could be observed by this author that this preferential biosynthesis favored "simpler" prymnesins, which most resembled a basic backbone structure. Prymnesins which had additional pentoses or hexoses were consistently fewer than their simpler versions across all samples. It could be considered that the simpler versions might be parent-structures to which pentoses, and hexoses are added to after biosynthesis by transporters.

The biosynthesis of prymnesins is yet still unclear; but if the ladder-frame of the prymnesins is any indication, the biosynthetic path might include condensation steps and the involvement of the citric cycle similarly to the case of brevetoxins (Yasumoto 2000, Gawley 1995). It stands to reason then that adding sugar-rings is more energy

intensive and lends further credence to the theory that prymnesin formation is a carbon/storing mechanism (Granéli et al., 2012).

Another point which could be observed was that some prymnesins were present in all samples (Table 22) whereas some prymnesins were unique in each sample (Table 23). The presence/absence of specific prymnesins raises interesting questions and further underlines the importance of chemotyping. The question as to which prymnesin can be synthesized by which strain is probably deeply linked to speciation (Binzer et al., 2019). This plural chemical diversity hints to nuanced biosynthetic mechanisms. Elucidating the evolutionary forces which shaped them can in future bear interesting fruits.

Table 22: Ubiquitous prymnesins

prymnesin name	molecular formula
PRM-C (3 Cl + DB) + 2 pentose	$C_{93}H_{132}Cl_3NO_{39}$
PRM-C (2 Cl + DB) + 2 pentose	$C_{93}H_{133}Cl_2NO_{39}$
PRM-C (2 Cl + DB)	$C_{83}H_{117}Cl_2NO_{31}$
PRM-C (2 Cl + DB) + pentose	$C_{88}H_{125}Cl_2NO_{35}$
PRM-C (3 Cl + DB)	$C_{83}H_{116}Cl_3NO_{31}$
PRM-C (3 Cl + DB) + pentose	$C_{88}H_{124}Cl_3NO_{35}$
PRM-C (3Cl) + pentose	$C_{88}H_{126}Cl_3NO_{35}$
PRM-C (4Cl + DB)	$C_{83}H_{117}Cl_4NO_{31}$

The table above list the prymnesin-Cs which could be detected in all six strains of the study (K-0252, PPSR-01, NIES-1017, NIES-1018, RCC-1436, CCAP946). In the proposed systematic name, PRM-C denotes the 83-carbon backbone of the prymnesin (whose structure is as yet un-elucidated), Cl denotes the number of chlorine atoms, DB denotes the number of double bonds, O denotes the number of additional oxygen atoms (presumably in OH-group), =O denotes the number of additional keto-groups and hexose/pentose denotes the number of sugar conjugates attached (Binzer et al., 2019).

Table 23: List of unique prymnesins

P. parvum strain	prymnesin name	molecular formula
K-0252	PRM-C (4 Cl) + 2 hexose	$C_{95}H_{143}Cl_4NO_{43}$
PPSR-01	PRM-C (2 Cl) + hexose	$C_{89}H_{131}Cl_2NO_{37}$
NIES-1017	PRM-C (2 Cl + 2 DB) + 2 hexose	$C_{20}H_{139}Cl_2NO_{43}$
NIES-1017	PRM-C (4 Cl + 3 =O + 3 O) + hexose	$C_{89}H_{125}Cl_4NO_{43}$
RCC-1436	PRM-C (4 Cl + DB) + hexose	$C_{89}H_{129}Cl_4NO_{37}$
CCAP946-1B	PRM-C (2 Cl + 2 DB) + hexose	$C_{89}H_{127}Cl_2NO_{37}$

NIES-1018	PRM-C (2 Cl + DB) + hexose + 2 pentose	$C_{99}H_{143}Cl_2NO_{44}$
NIES-1018	PRM-C (2 Cl) + hexose + 2 pentose	$C_{99}H_{151}Cl_2NO_{47}$
NIES-1018	PRM-C (4 Cl + 3 =O + 3 O) + pentose + hexose	$C_{94}H_{135}Cl_4NO_{48}$

The list depicts the prymnesins which could only be detected in a single strain and are therefore unique. This information has a lot of potential for fingerprint identification in chemotyping studies. The prymnesins in grey are also unique in the fact that this is the first time they were able to be positively identified. In the proposed systematic name, PRM-C denotes the 83-carbon backbone of the prymnesin (whose structure is as yet un-elucidated), Cl denotes the number of chlorine atoms, DB denotes the number of double bonds, O denotes the number of additional oxygen atoms (presumably in OH-group), =O denotes the number of additional keto-groups and hexose/pentose denotes the number of sugar conjugates attached (Binzer et al., 2019).

Possibly the most fruitful conclusion of the Mass Hunter approach was to verify the existence of prymnesins which up until this point were only theoretically perceived and never before verified (Table 17)

Table 24: Newly discovered prymnesins

Name	Molecular Formula
PRM-C (2 Cl)	$C_{83}H_{119}Cl_2NO_{31}$
PRM-C (2Cl + 2DB)	$C_{83}H_{115}Cl_2NO_{31}$
PRM-C (2 Cl + 2 DB) + hexose	$C_{89}H_{127}Cl_2NO_{37}$
PRM-C (2 Cl) + hexose	$C_{89}H_{131}Cl_2NO_{37}$
PRM-C (2 Cl + DB) + hexose + 2 pentose	$C_{99}H_{151}Cl2NO_{47}$
PRM-C (3 Cl) + hexose	$C_{89}H_{130}Cl_3NO_{37}$
PRM-C (3 Cl) + 2 hexose	$C_{95}H_{142}Cl_3NO_{43}$
PRM-C (4 Cl + DB) + 2 hexose	$C_{95}H_{141}Cl_4NO_{43}$
PRM-C (4 Cl) + pentose	$C_{88}H_{129}Cl_4NO_{36}$
PRM-C (4 Cl) + hexose	$C_{89}H_{131}Cl_4NO_{37}$
PRM-C (4 Cl) + 2 pentose	$C_{93}H_{139}Cl_4NO_{41}$
PRM-C (4 Cl) + 2 hexose	$C_{95}H_{143}Cl_4NO_{43}$
PRM-C (4 Cl + 3 =O + 3 O) + hexose	$C_{89}H_{129}Cl_4NO_{37}$
PRM-C (4 Cl + DB) + 2 hexose	$C_{95}H_{141}Cl_4N_1O_{43}$
PRM-C (4 Cl + 3 =O + 3 O) + pentose + hexose	$C_{94}H_{135}Cl_4N_1O_{48}$
PRM-C (4 Cl + DB) + hexose	$C_{89}H_{129}Cl_4N_1O_{37}$
PRM-C (4 Cl + DB) + 2 hexose	$C_{95}H_{141}Cl_4N_1O_{43}$
PRM-C (4 Cl + 3 =O + 3 O) + hexose	$C_{89}H_{125}Cl_4NO_{43}$

Depicted are the prymnesins which were detected for the first time. Depicted in red are the prymnesins for which were solely theoretically expected. Depicted in grey are the prymnesins for which in-source fragments had been detected in the past. In the proposed systematic name, PRM-C denotes the 83-carbon backbone of the prymnesin (whose structure is as yet un-elucidated), Cl denotes the number of chlorine atoms, DB denotes the number of double bonds, O denotes the number of additional oxygen atoms (presumably in OH-group), =O denotes the number of additional keto-groups and hexose/pentose denotes the number of sugar conjugates attached (Binzer et al., 2019).

More specifically, the new prymnesins which were discovered amongst the five strains of *P. parvum* are depicted on table 25.

Table 25: Identified prymnesins

Prymnesin	**K-0252**	**PPSR-01**	**RCC-1436**	**NIES 1018**	**CCAP946**
PRM-C (2Cl + 2DB)	+		+	+	+
PRM-C (2 Cl) + hexose		+			
PRM-C (2 Cl + 2 DB) + hexose	+				+
PRM-C (2 Cl + DB) + hexose + 2 pentose				+	
PRM-C (2 Cl)	+		+		+
PRM-C (3 Cl) + hexose	+				
PRM-C (3 Cl) + 2 hexose	+				
PRM-C (4 Cl + DB) + hexose			+		
PRM-C (4 Cl + DB) + 2 hexose	+	+	+		
PRM-C (4 Cl) + pentose	+		+	+	
PRM-C (4 Cl) + hexose	+				
PRM-C (4 Cl) + 2 pentose	+		+		
PRM-C (4 Cl) + 2 pentose	+				
PRM-C (4 Cl + 3 =O + 3 O) + hexose	+			+	
PRM-C (4 Cl + 3 =O + 3 O) + pentose + hexose		+		+	

Depicted are the new prymnesins which could be definitively identified in the extracts thanks to HPLC-QTOF-MS. In the proposed systematic name, PRM-C denotes the 83-carbon backbone of the prymnesin (whose structure is as yet un-elucidated), Cl denotes the number of chlorine atoms, DB denotes the number of double bonds, O denotes the number of additional oxygen atoms (presumably in OH-group), =O denotes the number of additional keto-groups and hexose/pentose denotes the number of sugar conjugates attached (Binzer et al., 2019). Depicted as red in the left column are the prymnesins for which there were no indications and depicted in grey are the prymnesins for which is-source fragments had been previously detected. The (+) indicate the prymnesins which were detected.

To this authors knowledge no other study exists as of yet which has endeavored to elucidate the percentile presence of prymnesins in these strains which could be used as a reference to corroborate these results.

Looking forward, it will be paramount to better separate co-elutions so as to extract more definitive results from this investigation. Furthermore, at some point the absence

of standards will need to be overcome decisively. This could be possibly achieved with artificial syntheses as was achieved in the case of brevetoxin A and brevetoxin B (Kadota et al., 2005; Nicolaou et al., 1998). Another way would be attaching a fluorescent tag to the primary amine of the prymnesin and use of two other amine containing compounds as proxies for quantification (Svenssen et al., 2019). Lastly a more in-depth analysis of the separate prymnesins regarding their toxicity will help achieve deeper understanding of the mode of action of these unique compounds.

6 Conclusion

In the present study it was undertaken to prepare and test a chloride free medium suitable for cultivating RTgill-W1 cells. This was successfully done, and the results indicate that the chloride free medium can indeed be used for such a purpose. The next step in any future endeavors will be to test the ability of the RTgill-W1 cells to grow in this medium for longer periods of time and hopefully also use this medium in conjunction with HAB toxins like the prymnesins in order to investigate if their mode of action is chloride-dependent.

Mediums of varying salinity concentrations were prepared and tested with the cytotoxic assays CTB and CV. Their results indicate a non-linear relationship between the salinity concentration and the metabolic activity of the RTgill-W1 cells. Specifically, an increase in salinity shows a decrease in metabolic activity, with the cells showing a clear preference for low salinity environments. This relationship however is not analogous. In any case it could also be shown that salinity concentrations of around 33, are similar in their results to natural seawater so as to be able to function as close proxies even if they might lack the natural nutrients or microbiome upon which the algae of interest might have grazed.

The manual investigation of the raw data of the HPLC-QTOF-MS from extracts of *P. parvum* cultures proved to be an involved, time-consuming and labor-intensive effort. Despite this, it managed to secure interesting results and further underline the importance of chemotyping in the study of HABs. It was possible to detect prymnesins which were never discovered before and also provide a semi-quantitative profile of the prymnesin mix associated with the *P. parvum* strains which were studied. Information of this nature will ultimately improve our ability to prevent, combat and mitigate the effects of such toxins. Even more promisingly, information such as this can broaden our understanding of the evolutionary history of species and more definitively answer questions regarding speciation and even correct false assumptions based only on morphology.

The formation of HABs and their associated toxins is, as already stated in this study a very important and consequential phenomenon. Regrettably, the means of removing HABs once they have formed are very limited in their application and a heavy emphasis

must be placed in preventing their occurrence in their first place. It is therefore of vital importance that coordinated research efforts be undertaken in order to provide further insights into the mechanisms of the phenomenon and in turn provide us with the knowledge to create prevention and mitigation strategies.

7. Summary

The influence of the negative effects of harmful algal blooms (HABs) on the environment and on the economy has become more severe in the last years. As a consequence, it has drawn the attention of both local authorities and research institutions, increasing the importance of scientific studies on this problem. Regarding this issue, this master thesis deals with two different aspects of a very specific microalga, called *Prymnesium parvum*. There is the hypothesis that the toxins produced by *P. parvum* interact with the ion canals and arouse their toxic impact through the interference of the salt balance. As a preparation for studies that will investigate this impact of ichthyotoxic compounds *in vitro*, a chloride free medium was produced. This was then tested against the L-15 medium in the cell culture with RTgill-W1 cells. These RTgill-W1 cells are gill cells of the rainbow trout, that have been immortalized and have been cultivated *in vitro*. Additionally, mediums of varying salinities were also prepared and tested with RTgill-W1 cells. The CellTiter-Blue® and Crystal Violet assays have been performed in order to define the viability in the different mediums after an incubation time of 3 hours.

The produced toxins by the different *P. parvum* strains can be classified in three groups on the basis of their carbon frame: the A-type, B-type and C-type prymnesins. Inside the groups there is a large number of variations, for instance: different numbers of chloride atoms or through one or multiple pentose or hexose moieties. The strains which produce C-type prymnesins stand out due to a special diversity and demand therefore a closer examination. That is why in a former investigation six different *P. parvum* strains were cultivated in triplicates under two different salinity conditions (9 psu and 30 psu). Followingly, the prymnesins were collected through centrifugation and then extracted with methanol before being measured by means of HPLC-QTOF-MS. Within the context of this master thesis the available HPLC-QTOF-MS raw data were evaluated.

8 Zusammenfassung

In den letzten Jahren ist der Einfluss der negativen Effekte von sogenannten schädlichen Algenblüten (auf Englisch „harmful algal blooms“ oder kurz HABs) auf die Umwelt und die Wirtschaft stärker geworden, so dass Behörden und Institutionen ein verstärktes Augenmerk darauf legen und Studien darüber an Wichtigkeit gewinnen. Diese Masterarbeit beschäftigte sich im Rahmen dieser Thematik mit zwei verschiedenen Aspekten einer spezifischen Mikroalge, die *Prymnesium parvum* genannt wird: Es gibt die Hypothese, dass die von *P. parvum* produzierten Toxine mit den Ionenkanälen interagieren und durch die Störung des Salzhaushaltes ihre toxische Wirkung hervorrufen. In Vorbereitung von Studien, die diese Wirkung von fischtoxischen Verbindungen *in vitro* untersuchen sollen, wurde im Rahmen der Masterarbeit ein chlorfreies Medium hergestellt. Dieses wurde dann im Vergleich zum Zellkulturmedium in der Zellkultur mit RTgill-W1 Zellen ausgetestet. Bei den RTgill-W1 Zellen handelt es sich um Kiemenzellen der Regenbogenforelle, die unsterblich gemacht wurden, und *in vitro* kultiviert werden können. Weiters wurden auch Medien unterschiedlicher Salinitäten vorbereitet und ebenfalls mit RTgill-W1 ausgetestet. Zur Bestimmung der Viabilität in den unterschiedlichen Medien nach einer Inkubationszeit von 3 h wurden die CellTiter-Blue® und Crystal Violet zytotoxische Assays durchgeführt.

Die von unterschiedlichen *P. parvum* Stämmen produzierten Toxine können basierend auf dem Kohlenstoffgrundgerüst in drei Gruppen, den sogenannten A-Typ, B-Typ und C-Typ Prymnesinen eingeteilt werden. Innerhalb der Gruppen gibt es eine Vielzahl an Variationen, z.B. durch unterschiedliche Anzahl an Chloratomen oder durch ein- oder mehrere Pentose oder Hexose-Einheiten. Jene Stämme, die C-Typ Prymnesine produzieren, zeichnen sich durch eine besondere Vielfalt aus und erforderten eine genauere Betrachtung. Sechs unterschiedliche *P. parvum* Stämme wurden daher in einer früheren Untersuchung unter zwei unterschiedlichen Salinitätsbedingungen (9 psu und 30 psu) in Triplikaten angezüchtet. Die Biomasse wurde anschließend mittels Zentrifugation gewonnen, extrahiert und mittels HPLC-QTOF-MS gemessen. Im Rahmen dieser Masterarbeit sollten die zur Verfügung gestellten HPLC-QTOF-MS Rohdaten ausgewertet werden.

9 Index

9.1 Abbreviations

AOP	adverse outcome pathway
ASP	amnesic shellfish poisoning
BSA	bovine serum albumine
CTB	cell titer blue assay
CV	crystal violet assay
Da	dalton
DAD	diode array detector
DB	double bond
DC	direct current
EC_{50}	half maximal effective concentration
EGTA	ethylene glycol-bis(β-aminoethyl ether)-N,N,N′,N′-tetraacetic acid
ESI	electron spray ionization
FBS	fetal bovine serum
FLD	fluorescence detector
HABs	harmful algal blooms
HeLa cells	immortalized cells named after Henrietta Lacks
HRMS	high resolution mass spectrometry
ITS	internal transcribed spacer
LC	liquid chromatography
LD_{50}	half maximal lethal dose
MIE	molecular initiating event
MS	mass spectrometry
NAD^+/NADH	nicotinamide-adenine dinucleotide oxidized/reduced
NES	normal external solution
Pa	Pascal
PC	positive control
PRM-C	prymnesin C
PSP	paralytic shellfish poisoning
PSU	practical salinity unit

rcf	relative centrifugal force
rpm	rounds per minute
RTgill-W1	rainbow trout gill cell line W1
RF	radio frequency
SD	standard deviation
T/C	test over control
HPLC	high pressure liquid chromatography
QTOF-MS	quadrupole time-of-flight mass spectrometry

9.2 List of Figures

9.3 List of Tables

9.4 List of Photographs

9.5 Theoretical prymnesin-C list

Table 26: Prymnesin C theoretical list

Prymnesin name	molecular formula	$[M + H]^+$	$[M + 2H]^{+2}$
PRM-C (2Cl + 2DB)	$C_{83}H_{115}Cl_2NO_{31}$	1692.69	846.85
PRM-C (2 Cl + 2 DB) + pentose	$C_{88}H_{123}Cl_2NO_{35}$	1824.73	912.87
PRM-C (2 Cl + 2 DB) + hexose	$C_{89}H_{127}Cl_2NO_{37}$	1872.75	936.88
PRM-C (2 Cl + 2 DB) + pentose + hexose	$C_{94}H_{133}Cl_2NO_{40}$	1986.79	993.90
PRM-C (2 Cl + 2 DB) + 2 pentose	$C_{18}H_{135}Cl_2NO_{41}$	1092.80	546.90
PRM-C (2 Cl + 2 DB) + 2 hexose	$C_{20}H_{139}Cl_2NO_{43}$	1152.82	576.91
PRM-C (2 Cl + 2 DB) + 2 pentose + hexose	$C_{99}H_{141}Cl_2NO_{44}$	2118.83	1059.92
PRM-C (2 Cl + 2 DB) + pentose + 2 hexose	$C_{100}H_{147}Cl_2NO_{48}$	2200.85	1100.93
PRM-C (2 Cl + 2 DB) + 2 pentose + 2 hexose	$C_{105}H_{159}Cl_2NO_{53}$	2352.92	1176.96
PRM-C (2 Cl + DB)	$C_{83}H_{117}Cl_2NO_{31}$	1694.71	847.86
PRM-C (2 Cl + DB) + pentose	$C_{88}H_{125}Cl_2NO_{35}$	1826.75	913.88
PRM-C (2 Cl + DB) + hexose	$C_{89}H_{127}Cl_2NO_{37}$	1872.75	936.88
PRM-C (2 Cl + DB) + pentose + hexose	$C_{94}H1_{35}Cl_2NO_{40}$	1988.80	994.90
PRM-C (2 Cl + DB) + 2 pentose	$C_{93}H_{133}Cl_2NO_{39}$	1958.79	979.90
PRM-C (2 Cl + DB) + 2 hexose	$C_{95}H_{141}Cl_2NO_{43}$	2054.83	1027.92
PRM-C (2 Cl + DB) + hexose + 2 pentose	$C_{99}H_{143}Cl_2NO_{44}$	2120.84	1060.93
PRM-C (2 Cl + DB) + pentose + 2 hexose	$C_{100}H_{151}Cl_2NO_{48}$	2204.89	1102.95
PRM-C (2 Cl + DB) + 2 pentose + 2 hexose	$C_{105}H_{161}Cl_2NO_{53}$	2354.94	1177.97
PRM-C (2 Cl)	$C_{83}H_{119}Cl_2NO_{31}$	1696.72	848.86
PRM-C (2 Cl) + pentose	$C_{88}H_{127}Cl_2NO_{35}$	1828.76	914.89
PRM-C (2 Cl) + hexose	$C_{89}H_{131}Cl_2NO_{37}$	1876.78	938.90
PRM-C (2 Cl) + pentose + hexose	$C_{94}H_{141}Cl_2NO_{42}$	2026.84	1013.92
PRM-C (2 Cl) + 2 pentose	$C_{93}H_{135}Cl_2NO_{39}$	1960.81	980.91
PRM-C (2 Cl) + 2 hexose	$C_{95}H_{143}Cl_2NO_{43}$	2056.85	1028.93
PRM-C (2 Cl) + hexose + 2 pentose	$C_{99}H_{151}Cl_2NO_{47}$	2176.89	1088.95
PRM-C (2 Cl) + pentose + 2 hexose	$C_{100}H_{153}Cl_2NO_{48}$	2206.90	1103.95
PRM-C (2 Cl) + 2 pentose + 2 hexose	$C_{105}H_{163}Cl_2NO_{53}$	2356.95	1178.98
PRM-C (3 Cl + DB)	$C_{83}H_{116}Cl_3NO_{31}$	1728.67	864.84
PRM-C (3 Cl + DB) + pentose	$C_{88}H_{124}Cl_3NO_{35}$	1860.71	930.86
PRM-C (3 Cl + DB) + hexose	$C_{89}H_{128}Cl_3NO_{37}$	1908.73	954.87
PRM-C (3 Cl + DB) + pentose + hexose	$C_{94}H_{134}Cl_3NO_{40}$	2022.76	1011.88

PRM-C (3 Cl + DB) + 2 pentose	$C_{93}H_{132}Cl_3NO_{39}$	1992.75	996.88
PRM-C (3 Cl + DB) + 2 hexose	$C_{95}H_{140}Cl_3NO_{37}$	1992.82	996.92
PRM-C (3 Cl + DB) + hexose + 2 pentose	$C_{99}H_{142}Cl_3NO_{44}$	2154.80	1077.91
PRM-C (3 Cl + DB) + pentose + 2 hexose	$C_{100}H_{150}Cl_3NO_{48}$	2238.85	1119.93
PRM-C (3 Cl + DB) + 2 pentose + 2 hexose	$C_{105}H_{160}Cl_3NO_{53}$	2388.90	1194.95
PRM-C (3Cl)	$C_{83}H_{118}Cl_3NO_{31}$	1730.68	865.84
PRM-C (3Cl) + pentose	$C_{88}H_{126}Cl_3NO_{35}$	1862.72	931.87
PRM-C (3 Cl) + hexose	$C_{89}H_{130}Cl_3NO_{37}$	1910.75	955.88
PRM-C (3 Cl) + pentose + hexose	$C_{94}H_{140}Cl_3NO_{42}$	2060.80	1030.90
PRM-C (3Cl) + 2 pentose	$C_{93}H_{134}Cl_3NO_{39}$	1994.77	997.89
PRM-C (3 Cl) + 2 hexose	$C_{95}H_{142}Cl_3NO_{43}$	2090.81	1045.91
PRM-C (3Cl) + 2 pentose + hexose	$C_{99}H_{144}Cl_3NO_{44}$	2156.82	1078.91
PRM-C (3 Cl) + pentose + 2 hexose	$C_{100}H_{152}Cl_3NO_{48}$	2240.86	1120.93
PRM-C (3 Cl) + 2 pentose + 2 hexose	$C_{105}H_{162}Cl_3NO_{53}$	2390.92	1195.96
PRM-C (4Cl + DB)	$C_{83}H_{117}Cl_4NO_{31}$	1764.64	882.83
PRM-C (4Cl + DB) + pentose	$C_{88}H_{125}Cl_4NO_{35}$	1896.69	948.85
PRM-C (4 Cl + DB) + hexose	$C_{89}H_{129}Cl_4NO_{37}$	1944.71	972.86
PRM-C (4Cl + DB) + pentose + hexose	$C_{94}H_{135}Cl_4NO_{40}$	2058.74	1029.87
PRM-C (4Cl + DB) + 2 pentose	$C_{93}H_{133}Cl_4NO_{39}$	2028.73	1014.87
PRM-C (4 Cl + DB) + 2 hexose	$C_{95}H_{141}Cl_4NO_{43}$	2124.77	1062.89
PRM-C (4Cl + DB) + 2 pentose+ hexose	$C_{99}H_{143}Cl_4NO_{44}$	2190.78	1095.89
PRM-C (4 Cl + DB) + pentose + 2 hexose	$C_{100}H_{151}Cl_4NO_{65}$	2546.74	1273.87
PRM-C (4 Cl + DB) + 2 pentose + 2 hexose	$C_{105}H_{161}Cl_4NO_{53}$	2424.88	1212.94
PRM-C (4Cl)	$C_{83}H_{119}Cl_4NO_{31}$	1766.66	883.83
PRM-C (4 Cl) + pentose	$C_{88}H_{129}Cl_4NO_{36}$	1916.71	958.86
PRM-C (4 Cl) + hexose	$C_{89}H_{131}Cl_4NO_{37}$	1946.72	973.86
PRM-C (4 Cl) + pentose + hexose	$C_{94}H_{141}Cl_4NO_{42}$	2096.78	1048.89
PRM-C (4 Cl) + 2 pentose	$C_{93}H_{139}Cl_4NO_{41}$	2066.76	1033.89
PRM-C (4 Cl) + 2 hexose	$C_{95}H_{143}Cl_4NO_{43}$	2126.79	1063.90
PRM-C (4 Cl) + 2 pentose + hexose	$C_{99}H_{151}Cl_4NO_{47}$	2246.83	1123.92
PRM-C (4 Cl) + pentose + 2 hexose	$C_{100}H_{153}Cl_4NO_{48}$	2276.84	1138.92
PRM-C (4 Cl) + 2 pentose + 2 hexose	$C_{105}H_{163}Cl_4NO_{53}$	2426.89	1213.95
PRM-C (4Cl +3 =O)	$C_{83}H_{113}Cl_4NO_{34}$	1808.60	904.80
PRM-C (4Cl +3 =O) + pentose	$C_{88}H_{121}Cl_4NO_{38}$	1940.64	970.82
PRM-C (4 Cl + 3 =O) + hexose	$C_{89}H_{137}Cl_4NO_{46}$	2096.72	1048.87

PRM-C (4Cl +3 =O) + pentose + hexose	$C_{94}H_{131}Cl_4NO_{43}$	2102.69	1051.85
PRM-C (4 Cl + 3 =O) + 2 pentose	$C_{93}H_{133}Cl_4NO_{44}$	2108.70	1054.86
PRM-C (4 Cl + 3 =O) + 2 hexose	$C_{95}H_{137}Cl_4NO_{46}$	2168.72	1084.87
PRM-C (4 Cl + 3 =O) + 2 pentose + hexose	$C_{99}H_{145}Cl_4NO_{50}$	2288.77	1144.89
PRM-C (4 Cl + 3 =O) + pentose + 2 hexose	$C_{100}H_{147}Cl_4NO_{51}$	2318.78	1159.89
PRM-C (4 Cl + 3 =O) + 2 pentose + 2 hexose	$C_{100}H_{157}Cl_4NO_{56}$	2408.83	1204.92
PRM-C (4Cl +3 =O +3O)	$C_{83}H_{113}Cl_4NO_{37}$	1856.58	928.79
PRM-C (4Cl +3 =O + 3O) + pentose	$C_{88}H_{121}Cl_4NO_{41}$	1988.62	994.82
PRM-C (4 Cl + 3 =O + 3 O) + hexose	$C_{89}H_{125}Cl_4NO_{43}$	2036.65	1018.83
PRM-C (4 Cl + 3 =O + 3 O) + pentose + hexose	$C_{94}H_{135}Cl_4NO_{48}$	2186.70	1093.85
PRM-C (4 Cl + 3 =O + 3 O) + 2 pentose	$C_{93}H_{133}Cl_4NO_{47}$	2156.69	1078.85
PRM-C (4 Cl + 3 =O + 3 O) + 2 hexose	$C_{95}H_{137}Cl_4NO_{49}$	2216.71	1108.86
PRM-C (4 Cl + 3 =O + 3 O) + 2 pentose + hexose	$C_{99}H_{145}Cl_4NO_{53}$	2336.75	1168.88
PRM-C (4 Cl + 3 =O + 3 O) + pentose + 2 hexose	$C_{100}H_{147}Cl_4NO_{54}$	2366.76	1183.88
PRM-C (4 Cl + 3 =O + 3 O) + 2 pentose + 2 hexose	$C_{105}H_{157}Cl_4NO_{59}$	2516.81	1258.91

The theoretical prymnesin C list contains all possible variations of the main backbone of the prymnesin C with substitutes. In the nomenclature in the first column PRM-C denotes the prymnesin backbone, Cl the possible number of chlorine atoms, O the number of oxygens in single of double bond, pentose/hexose the sugar conjugates which might be attached. Lastly, DB indicates double bond inside the chemical structure. Depicted in red are the prymnesins which were never detected before and depicted in grey are the prymnesins of which only insource fragments could be detected in the past.

9.6 References

Álvarez G, Díaz PA, Godoy M, Araya M, Ganuza I, Pino R, Álvarez F, Rengel J, Hernández C, Uribe E, Blanco J. 2019. Paralytic shellfish toxins in surf clams *Mesodesma donacium* during a large bloom of *Alexandrium catenella* dinoflagellates associated to an intense shellfish mass mortality. Toxins. 11(4):No 188. https://www.mdpi.com/2072-6651/11/4/188.

Anderson DM, Cembella AD, Hallegraeff GM, editors. 1998. Physiological Ecology of Harmful Algal Blooms. NATO ASI Series G: Ecological Sciences 41. Berlin- Heidelberg: Springer-Verlag. Chapter, Bloom dynamics and physiology of *Prymnesium* and *Chrysochromulina*: p 193-208.

Anderson DM, Cembella AD, Hallegraeff GM. 2012. Progress in understanding harmful algal blooms: Paradigm shifts and new technologies for research, monitoring, and management. Ann Rev Mar Sci. 4:143-176. https://www.annualreviews.org/doi/10.1146/annurev-marine-120308-081121.

Anderson DM, Hoagland P, Kaoru Y, White AW. 2000. Estimated annual economic impacts from harmful algal blooms (HABs) in the United States https://darchive.mblwhoilibrary.org/entities/publication/d60237ab-7c7d-5d39-93f6-0e2b6e63f7b4.

Ankley GT, Bennett RS, Erickson RJ, Hoff DJ, Hornung MW, Johnson RD, Mount DR, Nichols JW, Russom CL, Schmieder PK, Serrano JA, Tietge JE, Villeneuve DL. 2010. Adverse outcome pathways: A conceptual framework to support ecotoxicology research and risk assessment. Environ Toxicol Chem. 29(3):730-741. https://doi.org/10.1002/etc.34.

Ankley GT, Edwards SW. 2018. The adverse outcome pathway: A multifaceted framework supporting 21st century toxicology. Curr Opin Toxicol. 9:1-7. https://doi.org/10.1016/j.cotox.2018.03.004.

Arnich, N., Abadie, E., Amzil, Z., Bottein, M.Y.D., Comte, K., Chaix, E., Delcourt, N., Hort, V., Mattei, C., Molgó, J., Le Garrec, R., 2021. Guidance level for brevetoxins in French shellfish. Mar Drugs 19.https://doi.org/10.3390/md19090520

Barker J. 1999. Mass spectrometry: Analytical chemistry by open learning. Ando DJ, editor. 2nd edition. City (State if in USA): Wiley. 532 p. 4, 74-80, 308, 337

Binford JS, Martin DF, Padilla GM. 1973. Hemolysis induced by *Prymnesium parvum* toxin calorimetric studies. –Biochim Biophys Acta Biomembr. 291(1):156-164. https://doi.org/10.1016/0005-2736(73)90071-0.

Binzer SB, Svenssen DK, Daugbjerg N, Alves-de-Souza C, Pinto E, Hansen PJ, Larsen TO, Varga E. 2019. A-, B- and C-type prymnesins are clade specific compounds and chemotaxonomic markers in *Prymnesium parvum*. Harmful Algae. 81:10-17. https://doi.org/10.1016/j.hal.2018.11.010.

Binzer SB, Varga E, Andersen AJC, Svenssen DK, de Medeiros LS, Rasmussen SA, Larsen TO, Hansen PJ. 2020. Karmitoxin production by *Karlodinium armiger* and the effects of *K. armiger* and karmitoxin towards fish. Harmful Algae. 99: No 101905. https://doi.org/10.1016/j.hal.2020.101905

Bols NC, Barlian A, Chirino-Trejo M, Caldwell SJ, Goegan P, Lee LEJ. 1994. Development of a cell line from primary cultures of rainbow trout, *Oncorhynchus mykiss* (Walbaum), gills. J Fish Dis. 17(6):601-611. https://doi.org/10.1111/j.1365-2761.1994.tb00258.x.

Bradbury SP, Feijtel TCJ, van Leeuwen CJ. 2004. Meeting the scientific needs of ecological risk assessment in a regulatory context. Environ Sci Technol. 38(23):463A-470A. https://doi.org/10.1021/es040675s.

Brooks BW, Grover JP, Roelke DL. 2011. *Prymnesium parvum*: An emerging threat to inland waters. Environ Toxicol Chem. 30(9):1955-1964. https://doi.org/10.1002/etc.613.

Bury NR, Schnell S, Hogstrand C. 2014. Gill cell culture systems as models for aquatic environmental monitoring. J Exp Biol. 217(5):639-650. https://doi.org/10.1242/jeb.095430.

Calabrese, E.J., Baldwin, L.A., 2002. Defining hormesis. Hum Exp Toxicol 21(2):91-97. https://doi.org/10.1191/0960327102ht217oa

Davidson K, Gowen RJ, Tett P, Bresnan E, Harrison PJ, McKinney A, Milligan S, Mills DK, Silke J, Crooks AM. 2012. Harmful algal blooms: How strong is the evidence that nutrient ratios and forms influence their occurrence? Estuar Coast Shelf Sci. 115:399-413. https://doi.org/10.1016/j.ecss.2012.09.019.

Dayeh VR, Bols NC, Tanneberger K, Schirmer K, Lee LEJ. 2013. The use of fish-derived cell lines for investigation of environmental contaminants: An update following OECD's fish toxicity testing framework no. 171. Curr Protoc Toxicol. 56:1.5.1-1.5.20. https://doi.org/10.1002/0471140856.tx0105s56.

Dorantes-Aranda JJ, Waite TD, Godrant A, Rose AL, Tovar CD, Woods GM, Hallegraeff GM. 2011. Novel application of a fish gill cell line assay to assess ichthyotoxicity of harmful marine microalgae. Harmful Algae. 10(4):366-373. https://doi.org/10.1016/j.hal.2011.01.002.

Feoktistova M, Geserick P, Leverkus M. 2016. Crystal violet assay for determining viability of cultured cells. Cold Spring Harb Protoc. 4:343-346. https://doi.org/10.1101/pdb.prot087379.

Fischer M, Belanger SE, Berckmans P, Bernhard MJ, Bláha L, Schmid DEC, Dyer SD, Haupt T, Hermens JLM, Hultman MT, Laue H, Lillicrap A, Mlnaříková M, Natsch A, Novák J, Sinnige TL, Tollefsen KE, von Niederhäusern V, Witters H, Zupanič A, Schirmer K. 2019. Repeatability and reproducibility of the RTgill-W1 cell line assay for predicting fish acute toxicity. Toxicoll Sci. 169(2):353-364. https://doi.org/10.1093/toxsci/kfz057.

Granéli E, Edvardsen B, Roelke DL, Hagström JA. 2012. The ecophysiology and bloom dynamics of *Prymnesium* spp. Harmful Algae. 14:260-270. https://doi.org/10.1016/j.hal.2011.10.024.

Gstraunthaler G, Lindl T. 2021. Zell- und Gewebekultur: Allgemeine Grundlagen und spezielle Anwendungen. City: Springer Spectrum. https://doi.org/10.1007/978-3-662-62606-1.

Hallegraeff GM, Anderson DM, Cembella AD, editors. 2004. Monographs on Oceanographic Methodology: manual on harmful marine microalgae. 2nd edition. Paris: UNESCO Publishing. 793 p. Available from: https://unesdoc.unesco.org/ark:/48223/pf0000131711.

Hochmayr N. 2021. Chemical analysis and toxicological evaluation of potential toxic microalgal compounds (master thesis). Vienna: University of Vienna.

De Hoffmann E, Stroobant V. 2007. Mass spectrometry principles and applications. 3rd edition. City: Wiley. 512 p 45, 331

Hutchinson TH, Lyons BP, Thain JE, Law RJ. 2013. Evaluating legacy contaminants and emerging chemicals in marine environments using adverse outcome pathways and biological effects-directed analysis. Mar Pollut Bull. 74(2):517-525. https://doi.org/10.1016/j.marpolbul.2013.06.012.

Igarashi T, Satake M, Yasumoto T. 1999. Structures and partial stereochemical assignments for prymnesin-1 and prymnesin-2: Potent hemolytic and ichthyotoxic glycosides isolated from the red tide alga *Prymnesium parvum*. J Am Chem Soc. 121(37):8499-8511. https://doi.org/10.1021/ja991740e.

Igarashi T, Satake M, Yasumoto T. 1996. Prymnesin-2: A potent ichthyotoxic and hemolytic glycoside isolated from the red tide alga *Prymnesium parvum*. J Am Chem Soc. 118(2):479-480. https://doi.org/10.1021/ja9534112.

Ignatiades L, Gotsis-Skretas O. 2010. A review on toxic and harmful algae in Greek coastal waters (E. Mediterranean Sea). Toxins. 2(5):1019-1037. https://doi.org/10.3390/toxins2051019.

James SV, Valenti TW, Prosser KN, Grover JP, Roelke, DL, Brooks BW. 2011. Sunlight amelioration of *Prymnesium parvum* acute toxicity to fish. J Plankton Res. 33(2):265-272. https://doi.org/10.1093/plankt/fbq082.

Karam FF, Hassan FF, Hessoon HM. 2021. Adsorption of toxic crystal violet dye using (Chitosan-OMWCNTs) from aqueous solution. J Phys Conf Ser. https://doi.org/10.1088/1742-6596/1999/1/012015.

Kramer VJ, Etterson MA, Hecker M, Murphy CA, Roesijadi G, Spade DJ, Spromberg JA, Wang M, Ankley GT. 2011. Adverse outcome pathways and ecological risk assessment: Bridging to population-level effects. Environ Toxicol Chem. 30(1):64-76. https://doi.org/10.1002/etc.375.

La Claire JW, Manning SR, Talarski AE. 2015. Semi-quantitative assay for polyketide prymnesins isolated from *Prymnesium parvum* (Haptophyta) cultures. Toxicon. 102 :74-80. https://doi.org/10.1016/j.toxicon.2015.06.002.

Larsen A, Medlin LK. 1997. Inter- and intraspecific genetic variation in twelve *Prymnesium* (Haptophyceae) clones. J Phycol. 33(6): 1007-1015. https://doi.org/10.1111/j.0022-3646.1997.01007.x

Lassus P, Chaumérat N, Hess P, Nézan E. 2016. Toxic and harmful microalgae of the world ocean. 1st edition. Paris: International society for the study of harmful algae and the United Nations educational, scientific and cultural organization. 523 p. 128-130 https://unesdoc.unesco.org/ark:/48223/pf0000247767.

Lee LEJ, Dayeh VR, Schirmer K, Bols NC. 2009. Applications and potential uses of fish gill cell lines: Examples with RTgill-W1. In Vitro Cell Dev Biol Anim. 45:127-134. https://doi.org/10.1007/s11626-008-9173-2.

Lindehoff E, Granéli E, Granéli W. 2009. Effect of tertiary sewage effluent additions on *Prymnesium parvum* cell toxicity and stable isotope ratios. Harmful Algae. 8(2):247-253. https://doi.org/10.1016/j.hal.2008.06.004.

Lutz-Carrillo DJ, Southard GM, Fries LT. 2010. Global genetic relationships among isolates of golden alga (*Prymnesium parvum*). J Am Water Resour Assoc. 46(1):24-32. https://doi.org/10.1111/j.1752-1688.2009.00388.x.

Manganelli,M.,2016. Blooms of toxic microorganisms in aquatic environments: marine microalgae and freshwater cyanobacteria. A brief review with a particular focus on the Italian situation: Diffusion and health effects of toxic marine microalgae and freshwater cyanobacteria in Italy. Rend Lincei. 27 :135-143. https://doi.org/10.1007/s12210-015-0488-0.

Manning SR, la Claire JW. 2013. Isolation of polyketides from *Prymnesium parvum* (Haptophyta) and their detection by liquid chromatography/mass spectrometry metabolic fingerprint analysis. Anal Biochem. 442(2):189-195. https://doi.org/10.1016/j.ab.2013.07.034.

Marampouti C, Buma AGJ, de Boer MK. 2021. Mediterranean alien harmful algal blooms: origins and impacts. Environ Sci Pollut Res. 28:3837-3851. https://doi.org/10.1007/s11356-020-10383-1.

Medić N, Varga E, Van de Waal DB, Larsen TO, Hansen PJ. 2022. The coupling between irradiance, growth, photosynthesis and prymnesin cell quota and production in two strains of the bloom-forming haptophyte, *Prymnesium parvum*. Harmful Algae. 112. https://doi.org/10.1016/j.hal.2022.102173.

Nikolaidis G, Koukaras K, Aligizaki K, Heracleus A, Kalopesa E, Moschandreou K, Tsolaki E, 2005. Harmful microalgal episodes in Greek coastal waters. J Biol Res. 3:77–85. Available from: https://elnais.hcmr.gr/wp-content/uploads/2015/01/Nikolaidis-et-al-2005.pdf.

O'Brien J, Wilson I, Orton T, Pognan F. 2000. Investigation of the Alamar Blue (resazurin) fluorescent dye for the assessment of mammalian cell cytotoxicity. Eur J Biochem. 267(17):5421-5426. https://doi.org/10.1046/j.1432-1327.2000.01606.x.

Pärt P, Norrgren L, Bergström E, Sjöberg P. 1993. Primary cultures of epithelial cells from rainbow trout gills. J Exp Biol. 175(1):219-232. https://doi.org/10.1242/jeb.175.1.219.

Pierce RH, Henry MS, Blum PC, Hamel SL, Kirkpatrick B, Cheng YS, Zhou Y, Irvin CM, Naar J, Weidner A, Fleming LE, Backer LC, Baden DG. 2005. Brevetoxin composition in water and marine aerosol along a Florida beach: Assessing potential human exposure to marine biotoxins. Harmful Algae. 4(6):965-972. https://doi.org/10.1016/j.hal.2004.11.004.

Pourjavadi A, Hosseini SH, Seidi F, Soleyman R. 2013. Magnetic removal of crystal violet from aqueous solutions using polysaccharide-based magnetic nanocomposite hydrogels. Polym Int. 62(7): 1038–1044. https://doi.org/10.1002/pi.4389.

Rampersad SN. 2012. Multiple applications of alamar blue as an indicator of metabolic function and cellular health in cell viability bioassays. Sensors. 12(9):12347-12360. https://doi.org/10.3390/s120912347.

Rasmussen SA, Meier S, Andersen NG, Blossom HE, Duus JØ, Nielsen KF, Hansen PJ, Larsen TO. 2016. Chemodiversity of Ladder-Frame Prymnesin Polyethers in *Prymnesium parvum*. J Nat Prod. 79(9):2250-2256. https://doi.org/10.1021/acs.jnatprod.6b00345.

Riepl M. 2019. Determination of prymnesins and toxicological evaluation of *Prymnesium parvum* extracts on human colon epithelial cells (HCEC-1CT) (master thesis). Vienna: University of Vienna.

Markossian S, Grossman A, Brimacombe K, et al., editors. 2016. Assay Guidance Manual. Bethesda(MD): Eli Lilly and Company and the National Center for Advancing Translational Sciences. Chapter, Cell Viability Assays. Available from: https://www.ncbi.nlm.nih.gov/books/NBK144065/#top.

Roelke DL, Barkoh A, Brooks BW, Grover JP, Hambright KD, Laclaire JW, Moeller PDR, Patino R. 2016. A chronicle of a killer alga in the west: Ecology, assessment, and management of *Prymnesium parvum* blooms. Hydrobiologia. 764:29-50. https://doi.org/10.1007/s10750-015-2273-6.

Scholz S, Sela E, Blaha L, Braunbeck T, Galay-Burgos M, García-Franco M, Guinea J, Klüver N, Schirmer K, Tanneberger K, Tobor-Kapłon M, Witters H, Belanger S, Benfenati E, Creton S, Cronin MTD, Eggen RIL, Embry M, Ekman D, Gourmelon A, Halder M, Hardy B, Hartung T, Hubesch B, Jungmann D, Lampi MA, Lee L, Léonard M, Küster E, Lillicrap A, Luckenbach T, Murk AJ, Navas JM, Peijnenburg W, Repetto G, Salinas E, Schüürmann G, Spielmann H, Tollefsen KE, Walter-Rohde S, Whale G, Wheeler JR, Winter MJ. 2013. A European perspective on alternatives to animal testing for environmental hazard identification and risk assessment. Regul Toxicol Pharmacol. 67(3):506-530. https://doi.org/10.1016/j.yrtph.2013.10.003.

Scott, J., Belden, J.B., Minghetti, M., 2021. Applications of the RTgill-W1 cell line for acute whole-effluent toxicity testing: *In vitro–in vivo* correlation and optimization of exposure conditions. Environ Toxicol Chem. 40(4):1050-1061. https://doi.org/10.1002/etc.4947.

Skoog, DA, Holler, FJ, Crouch, SR. 2017. Principles of instrumental analysis. 7th edition. Cengage Learning. P. 503

Svendsen MBS, Andersen NR, Hansen PJ, Steffensen JF. 2018. Effects of harmful algal blooms on fish: Insights from *Prymnesium parvum*. Fishes. 3(1): No 11. https://doi.org/10.3390/fishes3010011.

Svenssen DK, Binzer SB, Medić N, Hansen PJ, Larsen TO, Varga E. 2019. Development of an indirect quantitation method to assess ichthyotoxic b-type prymnesins from *Prymnesium parvum*. Toxins. 11(5): No 251. https://doi.org/10.3390/toxins11050251.

Tang YZ, Kang Y, Berry D, Gobler CJ. 2015. The ability of the red macroalga, *Porphyra purpurea* (Rhodophyceae) to inhibit the proliferation of seven common harmful microalgae. J Appl Phycol. 27:531-544. https://doi.org/10.1007/s10811-014-0338-y.

Tanneberger K, Knöbel M, Busser FJM, Sinnige TL, Hermens JLM, Schirmer K. 2013. Predicting fish acute toxicity using a fish gill cell line-based toxicity assay. Environ Sci Technol. 47(2):1110-1119. https://doi.org/10.1021/es303505z.

Taylor RB, Hill BN, Langan LM, Chambliss CK, Brooks BW. 2021. Sunlight concurrently reduces *Prymnesium parvum* elicited acute toxicity to fish and prymnesins. Chemosphere. 263: No 127927. https://doi.org/10.1016/j.chemosphere.2020.127927.

Theodorou JA, Moutopoulos DK, Tzovenis I. 2020. Semi-quantitative risk assessment of Mediterranean mussel (*Mytilus galloprovincialis L.*) harvesting bans due to harmful algal bloom (HAB) incidents in Greece. Aquac Econ Manag. 24(3):273-293. https://doi.org/10.1080/13657305.2019.1708994.

Ulitzur S. 1973. The amphiphatic nature of *Prymnesium parvum* hemolysin. Biochim Biophys Acta Biomembr. 298(3):673-679. https://doi.org/10.1016/0005-2736(73)90083-7.

Ulitzur S, Shilo M. 1966. Mode of action of *Prymnesium parvum* Ichthyotoxin. J Protozool. 13(2):332-226. https://doi.org/10.1111/j.1550-7408.1966.tb01915.x.

Vinken M. 2013. The adverse outcome pathway concept: A pragmatic tool in toxicology. Toxicology. 312:158-165. https://doi.org/10.1016/j.tox.2013.08.011.

Wang J, Chen J, He X, Hao S, Wang Y, Zheng X, Wang B. 2021. Simple determination of six groups of lipophilic marine algal toxins in seawater by automated on-line solid phase extraction coupled to liquid chromatography-tandem mass spectrometry. Chemosphere. 262: No 128374. https://doi.org/10.1016/j.chemosphere.2020.128374.

Wood CM, Pärt P. 1997. Cultured branchial epithelia from freshwater fish gills. J Exp Biol. 200(6):1047-1059. https://doi.org/10.1242/jeb.200.6.1047.

Yariv J, Hestrin S. 1961. Toxicity of the extracellular phase of *Prymnesium parvum* cultures. J Gen Microbiol. 24(2):165-175. https://doi.org/10.1099/00221287-24-2-165.